SEAWORTHINESS ANALOG COMPUTER

by

John N. Andrews

and

Sheng-Lun Chuang

August 1965 Report 1829

TABLE OF CONTENTS

LIST OF FIGURES

Page

LIST OF TABLES

NOTATION

Symbol	Definition	Unit
A	Cross-sectional area of submerged portion of ship	ft^2
$A(j\omega)$	Transfer function of electrical filter	
$\overline{A}$	Cross-sectional area due to nonlinear portion of the buoyancy force	ft^2
A_0	Cross-sectional area for still waterline	ft^2
a_1, a_2, a_3	Arbitrary constants	
$B(p)$	Laplace transform of buoyancy force coefficient	
$B(j\omega)$	Laplace transform of buoyancy force coefficient	
b_1	Equivalent ship beam at still waterline for analog computer	ft
b_{1_n}	Ship beam at nth station at still waterline	ft
b_2, b_3	Arbitrary constants	
C	Ship structural damping coefficient	
c	Celerity of wave propagation	ft/sec
$C(\omega)$	Real part of hydrodynamic damping coefficient	
C	Capacitance	farads
c_1, c_2, c_3	Arbitrary constants	
$D(\omega)$	Imaginary part of hydrodynamic damping coefficient	
E	Modulus of elasticity	$lb/in.^2$
EI	Bending rigidity	$ton\text{-}ft^2$
e	Voltage	volts
F_a	Portion of hydrodynamic force generated by active analog elements	tons
F_p	Portion of hydrodynamic force generated by passive analog elements	tons

F_{a_n}	Replacement of F_a for finite difference approximation	tons
F_{p_n}	Replacement of F_p for finite difference approximation	tons
F'_B	Buoyancy force per unit length due to displaced fluid	
G	Modulus of rigidity	lb/in.^{2}
g	Acceleration due to gravity	ft/sec^2
h	Double amplitude of wave	ft
I	Area moment of inertia	
i_μ	Mass moment of inertia	
i	Current	amp
K	Potentiometer	
K_b	Buoyancy spring = $\rho g b \Delta \xi$	tons/ft
KAG	Shear stiffness	tons
L	Inductance	henries
M	Bending moment	ft-tons
m_s, m	Ship mass	
m_v	Added mass of fluid (hydrodynamic mass)	
m_0	Added mass associated with still waterline	
m_1	Added mass during ship immergence	
m_2	Added mass during ship emergence	
$\overline{m}$	Time varying portion of added mass	
m'_v	Unit mass of fluid	
m'_{0_n}	Added mass of ship half section associated with still waterline at nth station	
N	Bow station of ship	

n	Station number of ship	
P	Total hydrodynamic force	tons/ft
P_1	Inertia force acting on a mass of fluid	tons/ft
P_2	Dynamic portion of the buoyancy force	tons/ft
P_2'	Total buoyancy force	tons/ft
P_3	Hydrodynamic damping force	tons/ft
$\bar{P}_3$	Laplace transform of P_3	
P_a	Force per ship unit length generated by active analog elements	tons/ft
P_p	Force per ship unit length generated by passive analog elements	tons/ft
P_w	Fluid pressure	tons/ft^2
p	Laplace operator ($i\omega$)	
R	Resistance	ohms
R_0	Output resistance	ohms
rms	Root mean squared	
T	Wave period	sec
T	Transformer-turns ratio	
T_d	Time required for wave to travel a given distance	sec
t'	Time coordinate in the fluid lamina	sec
t	Time coordinate on the ship	sec
U	Forward velocity of ship	ft/sec
u	Forward velocity of fluid	ft/sec
V	Voltage	
V	Shear force	tons

V_h	Relative horizontal velocity between ship and wave	ft/sec
V_r	Relative vertical velocity	ft/sec
$\bar{V}_r$	Laplace transform of V_r	
v	Vertical velocity of sea surface	ft/sec
y	Waterline distance from baseline	ft
Y_h	Vertical translation of ship	ft
Y_r	Relative vertical translation between ship and sea surface = $Y_h - Y_w$	ft
Y_w	Translation of sea surface	ft
Y_{MWL}	Mean waterline	ft
Y_{AWL}	Actual waterline	ft
$\bar{Y}_w$	RMS of wave height	ft
γ	Angular dispiacement	rad
ζ	Space coordinate fixed in fluid	ft
λ	Length of wave	ft
μ	Mass per unit leng th	
ξ	Space coordinate fixed in ship	ft
ρ	Fluid density	
τ_1, τ_2	Electrical time constant	sec
Ψ	Pitch angle	rad
$\Phi(\omega)$	Power spectral density function	
$\Phi_0(\omega)$	Power spectral density of cutput	
$\Phi_i(\omega)$	Power spectral density of input	
ω	Wave frequency	rad/sec

ω'	Relative frequency between wave and ship	rad./sec
ω_0	Natural frequency of electrical filter	rad./sec
χ	Angle between ship heading and wave propagation	

ABSTRACT

A Seaworthiness Analog Computer has been developed to simulate the structural response of the ship hull to the hydrodynamic forces of the sea, and computations have been made to verify the feasibility, flexibility, and capability of the computer. The analog computer consists of a sea generator to generate sinusoidal seas, discrete wave trains, or random seas; a ship analog divided into 20 equally spaced segments which represent the mass-elastic characteristics along the ship; and a hydrodynamic force generator divided into nine sections, four of which are capable of introducing nonlinear hydrodynamic forces. The output of the ship analog is fed back into the hydrodynamic force generator to produce the dynamic interaction between the ship and the sea. Computations made to determine the response of an aircraft carrier to a specific wave train agreed very well with the actual measurements made on the ship. It is believed, therefore, that the computer can be of great assistance in ship structure design.

ADMINISTRATIVE INFORMATION

To aid in design evaluation, a Seaworthiness Analog Computer was developed to simulate the structural response of a ship hull to the hydrodynamic forces of the sea. This work was authorized by Bureau of Ships letter F013 03 01 serial 442-109 of 8 July 1963 under Subproject S-F013 03 01, Task 1973.

After a theoretical analysis was developed at the David Taylor Model Basin for investigating whipping response phenomena, Computer Engineering Associates, Pasadena, California, was awarded a contract to set up an analog computer method to investigate, primarily, the whipping response of an aircraft carrier due to bow flare slamming and also the bending stress due to wave load.

INTRODUCTION

An analog computer has been developed to simulate the motions and hull stresses of a ship in various seaways. It consists of three essential parts, a sea generator, a ship analog, and a hydrodynamic force generator.

The ship is represented on the analog computer as a beam, which is divided into 20 sections to represent the ship's mass-elastic parameters. Mass and bending and shear flexibilities are represented by lumped quantities at specific points along the length of the analog model; at selected points along these sections, hydrodynamic forces are applied. The hydrodynamic forces are obtained from the equations representing relative motions of the ship and seaway. The computed ship responses include both rigid-body and elastic motions.

The flexibility of the analog computer allows for changes in ship and seaway characteristics to be made easily and their effects on the ship motions and hull stresses to be evaluated. The effects of ship and seaway characteristics on the ship design can be of great value to the designer in immediately assessing consequences of changes in hull parameters on hull strength.

In this report, the fundamentals of the Seaworthiness Analog Computer are presented. An aircraft carrier was chosen as an example. The ship parameters were converted to a computer model for experimental investigation, and the comparisons between the computer results and the measurements obtained from sea trials are discussed and evaluated. Detailed presentations on the seaworthiness analog computer are included in the appendixes.

BACKGROUND

A ship can develop appreciable hull stresses associated with the vibration or "whipping" of the ship in heavy or moderate seas when operating at high speed. This whipping may be generated by emersion of the bottom and subsequent impact or by the nonlinear buoyancy and momentum forces associated with bow flare immersion. The bottom impact forces have been investigated by Dr. Szebehely, Dr. Ochi, and others. The substantial contributions of bow flare that induced whipping stresses in the hull were vividly demonstrated during rough sea trials of an aircraft carrier.[1]

A theoretical analysis was developed at the David Taylor Model Basin for investigating this whipping response phenomenon. This analysis in essence utilized the measured or calculated rigid-body motion at each transverse section of the ship to compute the instantaneous waterline at each section as well as the velocity of the section relative to the water. Next, the added mass for each section at each waterline was computed. Then, the added mass force at each section was computed as the time rate of change of the momentum imparted by the water and was added to the buoyancy and gravity forces to give the total hydrodynamic force. Finally, the response of the elastic ship was computed, thus giving the desired bending moments and shear forces.

Using this procedure, a detailed analysis of the whipping response of USS ESSEX (CVA 9) was made by using a digital computer.[2] Although there are some discrepancies in detail, the maximum stresses are predicted with reasonable accuracy and the general agreement is good, thus providing confidence in the mathematical model developed. However, changes in hull and sea parameters could not be made easily, and the requirement to hand-compute the hydrodynamic forces prior to computer solution was undesirable because of length of time to make these calculations. In particular, the requirement for a prior knowledge of

---

[1]References are listed on page 99.

ship motions severely limited the model for the purposes of design evaluation. These considerations prompted further development of the mathematical model and of computer applications as presented in this report.

It was believed that an analog computer would be more suitable than a digital computer for the solution of problems of ship response because of its greater flexibility in changing values of parameters and other variables.

Therefore, Computer Engineering Associates (CEA), under contract to the Model Basin, set up an analog computer method to investigate primarily the whipping response of an aircraft carrier due to bow flare slamming.[3] The bending stress due to wave load was included in the study. Approximations and the separation of linear and nonlinear terms were made on the computer setup.

At present, the analog computer set up by CEA to perform the response calculations is still in the preliminary stage of development. The original concept of this computer was to supply a new ship design, specifying the lines and mass-elastic parameters of a ship, which would be simulated on the computer for various environmental conditions. The hydrodynamic and buoyancy forces would then be computed automatically and supplied to various positions along the ship. Because of the lack of available equipment, portions of the hydrodynamic and buoyancy forces were supplied by the Model Basin in the form of curves.

Descriptions of the seaworthiness analog computer are also given in References 4, 5, and 6.

ANALOG MODELING

A schematic of the seaworthiness analog computer is shown in Figure 1. The three principal elements that constitute the ship and sea system are the hydrodynamic force generator, the ship analog, and the sea generator.

The time-delay unit shown in Figure 1 is employed to delay the signal from the sea generator along the ship length; i.e., a signal applied at the first station is applied sometime later at the next station depending upon the relative velocity of the ship and wave. The sea generator is capable of simulating random seas, sinusoidal seas, and a wave train of definite shape dependent upon the locations of Positions 1, 2, and 3 shown in Figure 1. The response of the ship (i.e., output of the ship analog) also feeds back to the hydrodynamic force generator to produce the dynamic interaction between the ship and the hydrodynamic forces.

The theoretical representations of the hydrodynamic force, the ship, and the sea for the analog modeling are presented in the following sections.

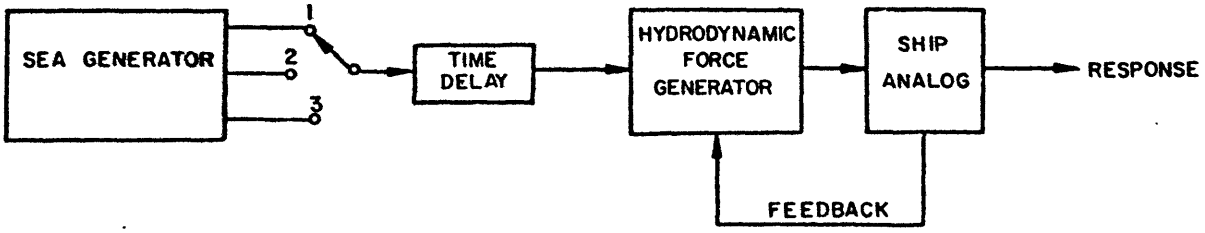

Figure 1 – Schematic Diagram of Seaworthiness Analog Computer

HYDRODYNAMIC FORCE GENERATOR

Hydrodynamic forces simulated by the hydrodynamic force generator of the analog computer are considered to consist of three types: added mass forces; buoyancy forces, including an approximation to the Smith correction; and damping force. The theoretical expression of these three types of forces can be represented by the following equation:

$$P = P_1 + P_2 + \overline{P}_3 \qquad [1]$$

where P is the total hydrodynamic force,

$$P_1 = \frac{d}{dt'}\,(m_v V_r) \qquad [2]$$

is the added mass term,

$$P_2 = \rho A \left(g + \frac{dv}{dt'}\right) - \rho g A_0 \qquad [3]$$

is the dynamic buoyancy force, and

$$\overline{P}_3 = -B(p)\,\overline{V}_r \qquad [4]$$

is the Laplace transform of the hydrodynamic damping term. $B(p)$ is the hydrodynamic damping coefficient.

For the relative vertical velocity between the ship and the sea surface, we have

$$V_r = \frac{d}{dt'}(Y_h - Y_w) = \frac{d}{dt'}(Y_r) \qquad [5]$$

where Y_h is the vertical displacement of the ship and Y_w is the vertical displacement of the sea surface (see Figure A-2, Appendix A), where Y_h and Y_w are positive if they move upward.

The force P_1 and the velocity V_r in the above equations are expressed in terms of a coordinate system (Equation [6]) moving longitudinally with a fixed point in the fluid lamina. This force is expressed in terms of a coordinate system (Equation [7]) fixed in the ship by the following transformation:

$$\begin{aligned} \zeta &= (U - u)\, t + \xi \\ t' &= t \end{aligned} \qquad [6]$$

$$\begin{aligned} \xi &= \zeta - (U - u)\, t' \\ t &= t' \end{aligned} \qquad [7]$$

where U and u are the horizontal velocities of the ship and sea surface, respectively.

Transforming and rewriting Equations [1] through [5] yields, neglecting the horizontal component of the fluid velocity (see Appendix A):

$$P_1 = -\frac{\partial}{\partial t}(m_v V_r) + U \frac{\partial}{\partial \xi}(m_v V_r) \qquad [8]$$

$$P_2 = \rho g(A - A_0) + \rho A_0 \left(\frac{c}{c + U}\right)^2 \frac{\partial^2 Y_w}{\partial t^2} \qquad [9]$$

$$\bar{P}_3 = -[C(w) + iD(w)]\, \bar{V}_r \qquad [10]$$

$$V_r = \frac{\partial Y_r}{\partial t} - U \frac{\partial Y_r}{\partial \xi} \qquad [11]$$

where m_v is the added mass per unit length,

A is the cross-sectional area of the submerged portion of the ship,

A_0 is the cross-sectional area of the ship at the still waterline, and

c is the wave celerity of the sea surface.

In the analog simulation, the force represented by Equations [8] through [10] is represented by two terms. One term, P_p, is generated by passive elements; the other, P_a, is generated by active elements. (An element is said to be passive if it contains no internal-energy sources, e.g., resistor or capacitor; an element is said to be active if internal energy sources are present, e.g., a vacuum-tube amplifier.) These two terms, derived in Appendix A, are

$$P_p = -m_0 \left\{ \frac{\partial^2 Y_h}{\partial t^2} - \left[1 + \frac{\rho A_0}{m_0} \left(\frac{c}{c+U} \right)^2 \right] \frac{\partial^2 Y_w}{\partial t^2} \right\} \qquad [12]$$

$$P_a = m_0 U \frac{\partial^2 Y_r}{\partial \xi \partial t} - \frac{\partial}{\partial t} (\bar{m} V_r) + U \frac{\partial}{\partial \xi} (m_0 V_r + \bar{m} V_r)$$

$$+ \rho g(-b_1 Y_r + \bar{A}) - B(p)\, \bar{V}_r \qquad [13]$$

In these two equations the added mass and area terms have been separated into linear and nonlinear terms so that the effects of the nonlinearities may be examined to assess the importances of hull form variations. These terms are

$$m_v = m_0 + \bar{m} \qquad [14]$$

$$A = A_0 - b_1 Y_r + \bar{A} \qquad [15]$$

where m_0 is the added mass associated with the still waterline and m is the time-varying portion of the added mass. The term $b_1 Y_r$ is the rectangular area measured from the still waterline to the actual waterline, where Y_r is the distance from the still waterline to the actual waterline. $\bar{A}$ is the nonlinear portion of cross-sectional area and produces the dynamic or nonlinear portion of the buoyancy force.

The term m is defined by the following relationships:

$$\bar{m} = m_1 \quad \text{for} \quad V_r > 0 \qquad \text{(emersion)} \qquad [16]$$

$$\bar{m} = m_2 \quad \text{for} \quad V_r < 0 \qquad \text{(immersion)} \qquad [17]$$

The two relationships are the result of the added mass being different, depending upon whether the ship is immerging or emerging. (See Appendix B.)

Thus, with this representation, it is possible to examine the effects of nonlinearity on the slip response. This is readily accomplished on the analog by throwing the proper switch.

Equations [11] through [13] are approximated by finite difference equations (see Appendix A), and these equations are then simulated by the computer as described in Appendix C. The force, which is analogous to current on the computer, is applied to the ship analog simulator to obtain ship response.

When the force function $P(\xi, t)$ acts on the ship, the equations governing the response comprise the following set:

Equation of Motion:

$$m \frac{\partial^2 Y_h}{\partial t^2} + C \frac{\partial Y_h}{\partial t} + \frac{\partial V}{\partial \xi} = P \qquad [18]$$

Inertia + damping + shearing = excitation

Moment Equation:

$$\frac{\partial M}{\partial \xi} = V + I_\mu \frac{\partial \dot{\gamma}}{\partial t} \qquad [19]$$

Spatial change of moment = shearing force + rotary inertia

Elastic Equation:

$$\frac{\partial \gamma}{\partial \xi} = \frac{M}{EI} \qquad [20]$$

Curvature = bending moment/flexural rigidity

Equation of Bending and Shear Effects:

$$\frac{\partial \dot{Y}_h}{\partial \xi} = - \frac{\dot{V}}{KAG} + \dot{\gamma} \qquad [21]$$

$$\text{Space derivitive of vertical velocity} = \frac{\text{Shearing rate}}{\text{Shear rigidity}} + \text{Angular velocity}$$

These equations are put into finite difference equations for simulation by the computer. The term $\dot{Y}_h$ is fed back to the force generator together with the wave input to compute the hydrodynamic force P.

SHIP ANALOG

The electric analog of the ship structure is a finite-difference beam analog including shear deformation and rotary inertia; see Appendix D. Inputs for the ship analog are the mass-elastic properties lumped at appropriate points along the ship length. Figure 2a represents the ship divided into 20 equally spaced sections. Figure 2b shows how the hydrodynamic terms are lumped and distributed along the ship (see Appendix D), and Figure 2c shows how the buoyancy forces are lumped and distributed along the ship. The shape or geometry of the ship employed to determine the hydrodynamic forces is identified by the station numbers in the upper portion of the sections shown in Figures 2b and 2c.

The input quantities used to obtain the analog response of ESSEX are shown in Table 1 and Figures 3 through 5; also see Appendix B. For reference, the hull characteristics of ESSEX are given in Table 2. Each figure shows the actual function and the approximated function used on the computer. The hydrodynamic damping coefficients were obtained from model results. The buoyancy curves and the added mass curves for each of the appropriate stations were plotted from the equations shown in Table 3 (see Appendix B). The original curves were obtained from the calculation employed to obtain the ESSEX response[2] on the TMB digital computer. A more detailed description of the added mass formulation is presented in Reference 2.

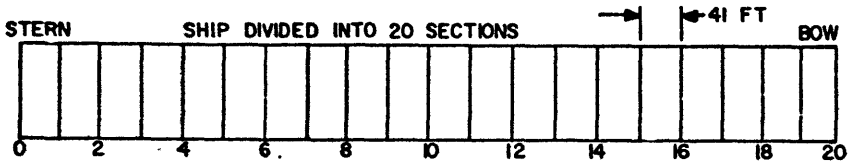

Figure 2a

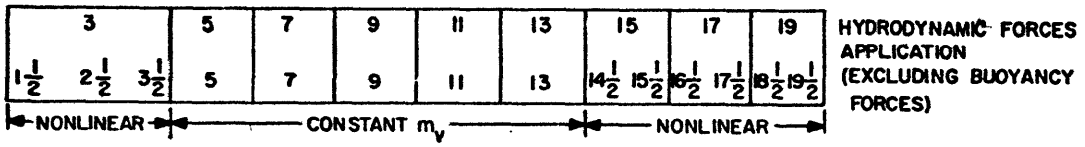

Figure 2b

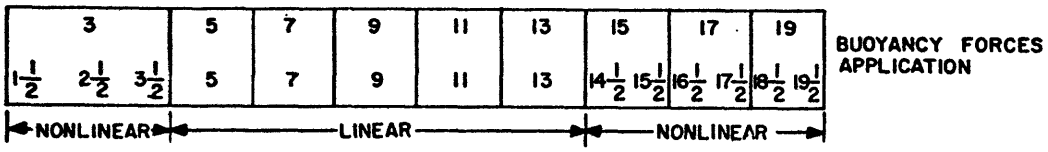

Figure 2c

Figure 2 – Ship Stations Used in Analysis

Note: 1. Curves of nonlinear added mass and buoyancy for Stations 3, 15, 17, and 19 are shown in Figures 3 and 4.

2. At the stern, hydrodynamic forces distributed equally to Stations 1.5, 2.5, and 3.5.

3. At Station 15, hydrodynamic forces distributed equally to Stations 14.5 and 15.5, etc.

Table 4 lists the constant terms in Equations [12] and [13]. The values have been derived for the case when the ship is in calm water at a draft of 28.5 ft.

Table 5 is a summary of inputs and outputs used in the analog computation.

SEA GENERATOR

Three types of seas are capable of generation by the sea generator of the analog computer. They are sinusoidal seas, specific discrete wave trains, and random seas (see Appendix E). Sinusoidal seas are generated by means of a variable-frequency oscillator. A wave train is generated by means of a photoformer which converts the light energy from the mask of the wave train into an electrical signal. Random seas are generated by means of a random noise generator which produces a voltage signal having a constant spectral density over a broad spectrum from 20 cps to 20,000 cps. The required spectrum is then produced by connecting the noise generator to an electrical filter. The spectral density of the output of the filter is related to the spectral density of the input by

$$\Phi_0(\omega) = |A(j\omega)|^2 \Phi_i(\omega) \qquad [22]$$

where $|A(j\omega)|$ is the absolute value of the transfer function of the filter.

Figures 6 through 8 show the spectral density for various sea conditions. Figure 6 is the spectrum of the sea taken from full-scale data obtained on ESSEX, and Figures 7 and 8 show Neumann spectra for idealized seas.

The sea waves were considered to pass from bow to stern along the ship length without change in form at a constant propagation velocity. This was approximated by a delay line that caused the signal to appear at points along the ship with a time delay equal to the distance from the bow divided by the wave velocity.

DISCUSSION OF RESULTS OF ANALOG METHOD

To verify the feasibility and accuracy of the seaworthiness analog computer method, the computer model was driven by simple harmonic excitation forces and the three different types of sea excitation forces previously mentioned.

The conditions under which these forces were applied are tabulated in Table 6.

The simple harmonic excitation is employed mainly for checking the computer setup with the vibration mode of the computer model.

The steady-state sinusoidal wave excitation is employed mainly for collecting the computer test results. These results will be used to compare with the tank test results of a physical model of ESSEX which is currently being tested under regular head sea. Regular head sea is defined such that the sea wave propagates in the onward direction with only one wave frequency, one wave length, one wave height, and one wave profile. This type of wave is identical to the steady-state sinusoidal wave generated by the sea generator.

For descrete wave train excitation, a shape of the wave was traced from a portion of the wave-height record obtained from full-scale trials on ESSEX[3] (see Figure 11a of this report), and was utilized as an excitation force for the computer. Accordingly, measurements procured from the computer were compared directly with data obtained from full-scale ESSEX sea trials.

The random sea wave excitation of the computer is a tool to examine, based solely on statistics, the characteristics of the response of a ship during her usable years with many different combinations of the parameters that describe the state of seas and hull characteristics of the ship.

Once the validity of the computer method has been established by the comparison of the results with those obtained from full-scale sea trials and also those from laboratory experiments with a physical model, the computer model may be used to run a lifetime sea experience of a ship in a very short time. The computer in its present form is confined to the study of ship response in head seas or in following seas and to the study of the slamming problem with bow flare type of impact. Further improvement and development of the seaworthiness computer to increase its flexibility in application would be the next desirable step.

SIMPLE HARMONIC EXCITATION

The vibration modes of the hull of ESSEX were observed during sea trials. Thus it is possible to check the computer setup by comparing the vertical bending modes obtained from simple harmonic excitations of the computer model with the full-scale modes. These modes are obtained by placing the computer model in a calm sea with a zero forward ship speed and driving it by a simple harmonic force of varying frequency from zero to different resonant frequencies. The vertical bending modes for the computer model are tabulated in Table 7. A vibrating system in a simple harmonic motion can be expressed so that the mean values of the total kinetic and potential strain energies are equal[7] or

$$\int_0^l \frac{M^2}{2EI}\, d\xi = \frac{1}{2}\int_0^l m\left(\frac{dy}{dt}\right)^2 d\xi$$

This expression may be used to check the accuracy of computed bending mode frequencies. The accuracy of the method was found to be 1 percent. However, the computer results when compared to full-scale sea trials showed a difference of 10 percent. This discrepancy in frequency may account for some of the differences in transient response found between the computer results and the measured ship data.

Three different representations of hydrodynamic forces are investigated. Case 1 includes only the added mass; Case 2 includes the added mass as well as the buoyancy; and Case 3 includes the added mass, the buoyancy, and also the hydrodynamic damping. (The

damping values actually recorded in Table 7 for Cases 1 and 2 are due to the inherent damping in the computer.) The recorded 2-percent critical damping for the lowest bending mode is about twice the damping evidenced during the sea trials. By means of a "negative damper," the damping for some cases of transient excitation was reduced to about 1 percent of critical damping.

In comparing Case 1 and Case 2, the inclusion of buoyancy forces causes very little change in the lowest bending mode but produces rigid-body heave and pitch. One of the properties of significance in the normal mode treatment is the orthogonality of the heave and pitch modes. This is checked by both kinetic energy and potential energy methods.[3] In comparing Case 2 and Case 3, the inclusion of hydrodynamic damping has little effect in the bending mode and the damping; even the rigid-body heave and pitch modes are substantially damped.

STEADY-STATE SINUSOIDAL WAVE EXCITATION

The steady-state sinusoidal wave excitation includes linear and nonlinear terms of the hydrodynamic forces. The nonlinear terms can be included or excluded in the computer simply by throwing a set of switches. The linear analyses were used to check out the electrical equipment involved in the computer experimentation, particularly the delay line, and to inspect the mechanisms by which large bow immersion may occur.

The results of linear analysis obtained from a steady-state sinusoidal wave excitation are given in Table 8. They show that at a ship speed of 16 knots, the delay line functions well for wave frequencies in sea-fixed coordinates, i.e., a coordinate system moving longitudinally with the fluid lamina, up to about 0.70 rad/sec.

The immersion amplification factor (ratio of peak immersion to peak wave height, $\left|\frac{Y_r}{Y_w}\right|$ is plotted in Figure 9 as a function of position along the ship for different values of wave frequency ω and for a ship speed of 16 knots. At a wave frequency of 0.50 rad/sec, the length of the sinusoidal wave is 812 ft,* which is about equal to the 820-ft hull length of ESSEX. At a wave frequency of 0.46 rad/sec, the wave length is 1.17 of the ship length. As expected, the immersion amplification factors at these wave frequencies are quite large at the bow, quite small amidships, and the stern tends to follow the wave profile. This phenomenon has been evidenced from the physical model tests for various types of ships.[8,9]

A plot, such as shown in Figure 9, also provides invaluable information for various ship design problems, that is, the determination of location for equipment which is sensitive

---

* ω = wave frequency = 0.50 rad/sec
T = wave period = $2\pi/\omega$ = 12.6 sec/cycle
c = wave velocity = g/ω = 32.23/ω = 64.46 fps
L = wave length = cT = 812 ft

to motion, the determination of location for stabilizer which profits with least hydrodynamic attacking force, the propeller racing problem that requires minimum stern emersion, and a study of supercritical speed of ship, water shipping, etc.

A small portion of the results of nonlinear analysis is shown in Figure 10. The bending moment amidships (Station 10) is plotted against the peak-to-peak wave height for a wave frequency of 0.50 rad/sec and a ship speed of 16 knots. The increase in the nonlinear results over the linear results is due mainly to the nonlinear hydrodynamic forces which excite the lowest bending mode of a ship.* For a ship speed of 30 knots (50.6 fps), the frequency of encounter ω' is approximately equal to the natural pitch frequency of the ship.** Ship responses with larger bow immersion cause much higher bending moments at 30 knots than at 16 knots. A curve is included in Figure 10 to show the effect of removing the mass-transport terms (terms proportional to the forward velocity of the ship U in Equation [A-35]), from the total hydrodynamic force. The effect seems to be small for 16 knots.

Regular sea waves can be represented to a close approximation by sinusoidal waves, which are much easier to handle than the usual trochoidal form. Therefore, the sinusoidal wave excitation will be used for the study of ship behavior in regular sea waves (such as sea swell).

The foregoing general discussion may be summarized by stating that the magnitude of objectionable ship motions, bending stress, and the factors affecting sea speed–wetness of decks and likelihood of slamming–are largely governed by the ratio of wave length to ship length and the frequency of encounter to the natural pitch frequency of the ship. A similar summary is contained in Reference 8.

DISCRETE WAVE TRAIN EXCITATION

The advantage of feeding an actual discrete wave train to the computer is that the computer results provide a simple means of comparison with the actual recorded data; see Figure 11. A wave height of 33.4 ft was used in Case 17 versus 23 ft for the actual measurement at sea. Assuming motions and also bending moment are roughly proportional to wave height,[3] computer results were multiplied by a factor of 0.70. The wave height of 33.4 ft was selected in lieu of the measured 25 ft in order to reach agreement between magnitudes of the computer and the full-scale pitch angles. Comparison shows that the character of sea trial records was satisfactorily duplicated by the computer. In particular, the simulated bending moment amidships showed a large contribution of the lowest bending mode of the ship with

---

*The effects of nonlinear hydrodynamic force will be discussed in detail on the triplet pulse.

**Ship natural pitch frequency is 0.158 cps. Frequency of wave encounter is $\omega' = \omega + \frac{\omega^2 V}{g} = 0.50 + 0.25 \cdot \left(\frac{50.6}{32.2}\right) = 0.894$ rad/sec = 0.143 cps. Tuning factor = ratio of frequency of encounter to the natural pitch frequency = 0.143/0.158 ≈ 1.

approximately the same magnitude as for the prototype.

Photographs of ship responses for Case 17 are reproduced in Figures 12, 13, 14, 16, and 17. In this case, the ship speed is 16 knots. As shown in Figure 12, the shift of about 3 1/2 divisions of wave height trace between Station 3 and Station 11 (amidships) is due to the time delay for the wave to cross the intermediate distance.

The bending moment at three amidship stations is shown in Figure 13. The high-frequency component is the lowest bending mode of the ship due to a "slamming event" occurring at the first large peak of bow immersion shown in Figure 14. Reasons for the above may be explained as follows.

As shown previously, the expression for added mass force is

$$P_1 = -\frac{\partial}{\partial t'} m_v \dot{Y}_r = -\frac{\partial}{\partial t'} m_v \dot{Y}_r \qquad [23]$$

Due to the pronounced bow flare and the form of this equation, the added mass force (experienced on the peak of a large wave) at the bow has the shape of a "triplet" pulse. The frequency spectrum of this pulse contains components sufficiently close to the lowest bending mode to produce large excitation of that mode.

The "triplet" pulse is illustrated in Figure 15. As may be seen, the velocity $\dot{Y}_r$ of bow immersion is the time derivative of immersion Y_r. The nonlinear portion of the added mass m_v is represented as shown. The discontinuity indicates that the added mass term used herein depends on the direction of flow as well as on the ship form. This reflects the rise of water on the hull accompanying immersion. The added momentum $m_v \dot{Y}_r$ is the product of the velocity $\dot{Y}_r$ and the mass m_v. Finally, the time derivative of the momentum $\frac{\partial}{\partial t} m_v \dot{Y}_r$ yields a force which reflects the nonlinear portion of the added mass, and has a triplet pulse shape. If two triplet pulses are identical in magnitude but different in period (period measured between two peaks of triplet pulse) then the one with a period closer to the lowest bending mode of the ship is expected to produce a higher magnitude of ship excitation in whipping. This triplet, however, is not a necessary condition to induce whipping. (A similar triplet pulse is illustrated from long-hand computations shown in Figure 11, Reference 2.)

The bending moment traces for a ship speed of 30 knots (Figure 16) show a much stronger excitation of the lowest bending mode of the ship than do corresponding bending moment traces at 16 knots (Figure 17). Their differences may be explained thus:

1. At 30-knot head seas, ship speed is near synchronism (frequency of encounter synchronizing with natural pitch frequency of ship) to produce higher bow immersion, thus to produce a higher triplet pulse whipping excitation in magnitude.

2. Since frequency of encounter increases with the ship speed in head seas, the period of the triplet pulse becomes less; thus it is closer to the period of the lowest bending mode of the ship for 30 knots than for 16 knots.

Some adjustments and a smoothing process were made on the wave trace, as obtained from the ESSEX sea trials, before it could be used in the computer analysis. The wavemeter installed on ESSEX for wave height traces was developed by the British Institute of Oceanography. The meter consists of a pressure transducer mounted on each side of the hull amidships to measure the height of the water surface above it and an accelerometer to measure the vertical motion of the pressure transducer. Their combined output gives a signal proportional to the wave height. The wave distortion due to wavemaking of ship bow moving in the sea restricts the accuracy of measurements and, also, the response due to the vibratory displacement of the ship inherently shown on the wave height record. For these reasons, it is necessary to smooth out the high-frequency component in the wave height record before it can be applied to the computer. Otherwise, this extraneous high-frequency wave component would resonate the computer model, resulting in excessively large excitation of the lowest bending mode. For statistically random excitation, it is found necessary to reduce the magnitude of frequency components near the lowest bending mode to a reasonably low level in order not to interfere with the actual input.

Some of the results for a discrete wave train excitation are plotted in Figures 18 to 26. Figure 18 shows that the peak immersion decreases rapidly toward amidships from the bow but that the stern tends to follow the wave profile. The phenomenon has been noted and discussed in the results from the steady-state sinusoidal wave excitation. These results (Figure 9) agree well with the plot shown in Figure 18 for wave frequency ω of 0.46 rad/sec shown in Figure 9.

Figure 19 shows the effect of speed on the motion of bow; Figure 20, the effect of speed on the bending moment amidships. Both motion and bending moment increase with ship speed and reach their peaks near ship synchronous speed in pitching, then reduce their magnitudes as ship speed is increased further. This again concurs with the conclusion drawn for the sinusoidal wave excitation, and it may be stated that when the ship length and wave length are approximately equal and when the ship speed is near synchronism between period of wave encounter and ship natural pitch period, both bow immersion and bending moment amidships are at their peak in magnitudes.

Figure 21 indicates that including nonlinearities in the analysis results in a small change in bow movement relative to the surface of the wave profile but gives more chances for the bow to ride out of the water. Figure 22 shows that the inclusion of nonlinearities means that the bending moment amidships is much less for a rigid-body ship than for an elastic ship. This indicates that the rise in bending moment is due principally to the excitation of the lowest bending mode of the elastic ship.

The variation of wave height with peak hydrodynamic force at Station 19 is shown in Figure 23, and the variation of peak nonlinear forces at Station 19 with bow immersion is given in Figure 24. Figure 25 shows the effect of structural damping on the peak heave acceleration and bending moment amidships; this effect is small over the range of damping

investigated. Figure 26 indicates the manner in which the peak hydrodynamic force at the bow and the nonlinear components of hydrodynamic force are to be varied with ship speed. The negative peak in the nonlinear inertia force is larger than the negative peak in the total hydrodynamic force because the negative peaks occur at a time when the upward buoyancy force is a maximum.

The David Taylor Model Basin is currently performing a further comparison with computer results by testing a structurally scaled elastic physical model in a towing tank. The model will be used to study the effects of slamming on elastic motions and bending stress as well as on rigid-body motions. Nevertheless, such a study might not permit a complete prediction of the dynamic stresses in a ship hull because:

1. It is difficult to secure similarity in model shear rigidity (of the physical model) hence this will affect the fundamental mode of model.
2. Structural damping is dependent on the vibratory modes for the same reason.
3. It is difficult to simulate sea waves in the towing tank.

RANDOM SEA EXCITATION

Random seas were simulated by means of a "white noise" generator and a peaking filter (see Appendix E). Three random wave inputs were used in the computer. The power spectral density functions had the same shape as those shown in Figures 6, 7, and 8. As mentioned previously, one input represented the spectrum of the sea taken from ESSEX sea trials data and the other two represented Neumann power spectra for 30-knot and 50-knot winds, respectively.

Data for random sea analysis are listed in Table 6. Typical results are shown in Figures 27 to 30 for Case 35, for which a 6-ft rms of wave height and a 30-knot ship speed are employed.

Figure 27 shows a typical 4-min record of wave height. In Figure 28 are three 4-min records of bending moment amidships taken at random times. Each picture contains one slamming "event." Three 1-min records of the bending moment amidships are shown in Figure 29 where the time scale is sufficiently expanded to show the detailed character of the slamming event. The records closely resemble the strain gage traces in Reference 1.

Figure 30 shows three 4-min records of the nonlinear buoyancy force at the bow station. In a given time interval, the trace of the nonlinear buoyancy force pulses can be used for counting the number of slamming events, which are defined as the occurrence of a peak bow immersion greater than a predetermined value.

Because the primary interest of the present analysis is concentrated on the usefulness of the computer, the study of random sea excitation is given for illustration only. Different statistical properties can be measured with analog devices such as rms value (see Reference 1) power spectral density, auto-correlation function, cross-correlation function, zero crossings,

frequency of occurrence of various events, etc. The future analyses of the statistical measurements, however, should be planned with a view toward the requirements of ship design and the significance of various types of information.

SUMMARY AND CONCLUSIONS

The degree of correlation between the computer results and the sea trials of an aircraft carrier demonstrates that the analog computer has definite features suitable for design studies of ships. It provides a means for measuring applied forces, displacements, and structural responses at many points along a ship length. This computer method gives a more complete analytical representation than any computations made by other methods used heretofore, theoretical or empirical. Because of its ability to compress time, the computer may be used to run a lifetime of sea experiences in a very few hours in the laboratory. Refinements for the computer analysis as presented in this report would be necessary only if an increase in accuracy is desired. To some extent, two minor deficiencies affect the accuracy of analysis; i.e.,

1. Course representation of hydrodynamic forces at the bow: This defect can be refined by subdividing ship sections of the analog model at the bow.

2. Nondispersive character of the delay line used in the simulation: This defect is relatively unimportant because the sea spectrum is presumed to be concentrated in a fairly narrow frequency band.

From the computer experimental investigation, some of the findings are:

1. At certain ship speeds, the peak bow immersion is in the neighborhood where the wave lengths are roughly equal to the ship lengths (Figure 9). The stern, on the other hand, tends to follow the wave profiles (Figures 9 and 18).

2. When wave lengths are roughly equal to ship lengths, the peak bow immersion is in the environs of the synchronous pitching speed (Figure 19).

3. If the bow immersion is high, a pronounced bow flare may cause ship slamming followed by ship whipping. Ship whipping caused by slamming may be regarded as the result of a double resonance phenomenon. The first resonance occurs between the motions of sea wave and the immersion of the bow (Figures 9 and 18). The second resonance occurs between a "triplet" pulse of the nonlinear inertia force at the bow (Figure 15). If the frequency spectrum of this pulse remains sufficiently close to the lowest bending mode of the ship, it produces large excitation of that mode. This triplet pulse is not a requirement for inducing ship whipping; for example, the impact of ship bottom may induce ship whipping also.

4. With an increase of ship speed, the peak-to-peak bending moment amidships shows a greater than proportional increase in bow immersion (Figure 20a). This additional increase is due to two factors:

a. An increase in magnitude of the bow inertia force pulse.

b. An increase in the characteristic frequency of this pulse which tends to resonate with the lowest bending mode of the ship.

5. With respect to increased wave height, peak bow immersion shows a less than proportional increase, but peak bow emersion shows more than proportional increase (Figure 21).

6. The hydrodynamic forces at the bow increase sharply with increased wave height, thus resulting in a more than proportional increase in peak bending moment amidships (Figures 22 and 23).

7. Structural damping is relatively unimportant in regard to the peak bending moment amidships experienced in transient excitation (Figure 25); however, this might not be true for steady-state excitation.

8. For the cases studied, the mass transport terms (i.e., added mass terms proportional to ship speed) are relatively unimportant at higher speeds.

9. The nonlinear terms included in the analysis for the slamming problem are probably unimportant except for the forward 20 percent of the ship because the immersion of the ship at the bow is relatively large as compared with that at other sections along the ship. At the bow, large immersion results in a rapid change in the added mass due to bow flare, which results in slamming (Figures 9, 15, and 18).

The main purpose of this study is to check the feasibility and workability of the seaworthiness analog computer, which combines the well-known beam analog with means for generating interaction with waves. These aforementioned findings lead us to conclude confidently that this seaworthiness analog computer developed by the David Taylor Model Basin will be an extremely useful tool for advanced ship research and design.

ACKNOWLEDGMENTS

The authors wish to thank Dr. N.H. Jasper of the U.S. Navy Mine Defense Laboratory for initiating the work given in this report. Thanks are extended to Dr. MacNeal of Computer Engineering Associates for his part in providing the computer facilities and his development of the analog computer program.

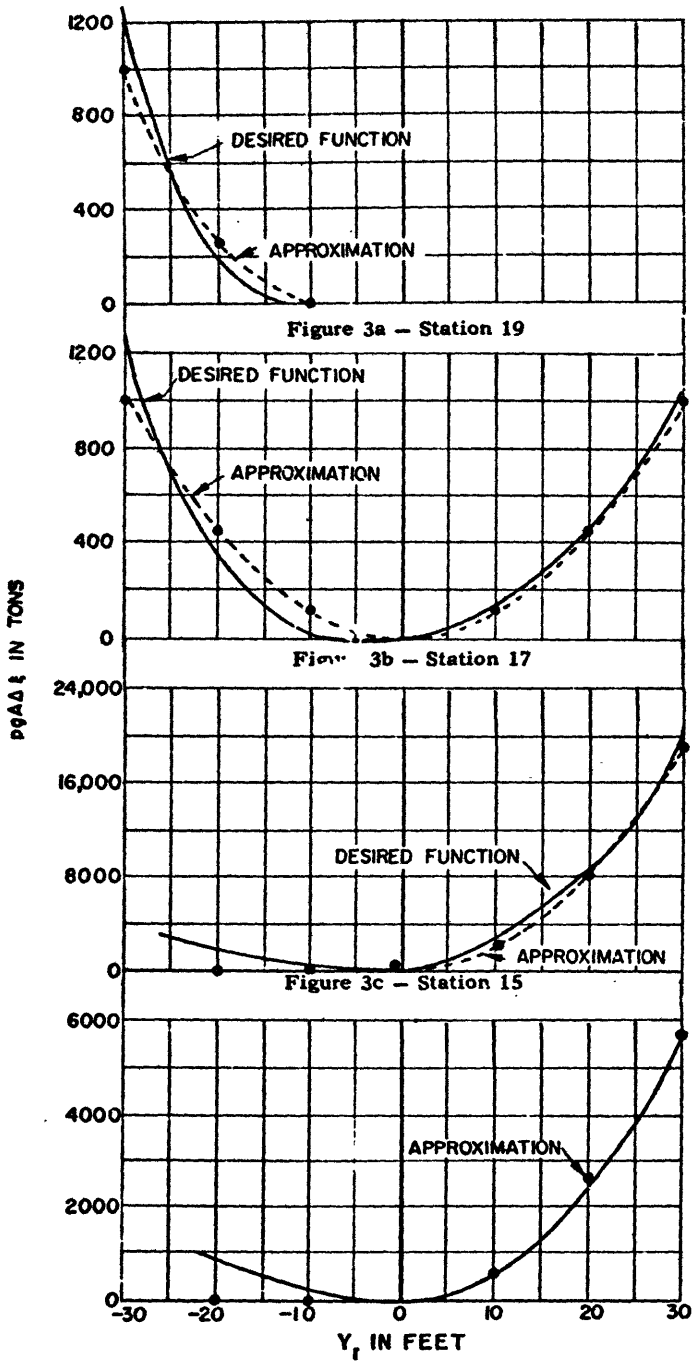

Figure 3d — Station 3

Figure 3 — Nonlinear Buoyancy Forces

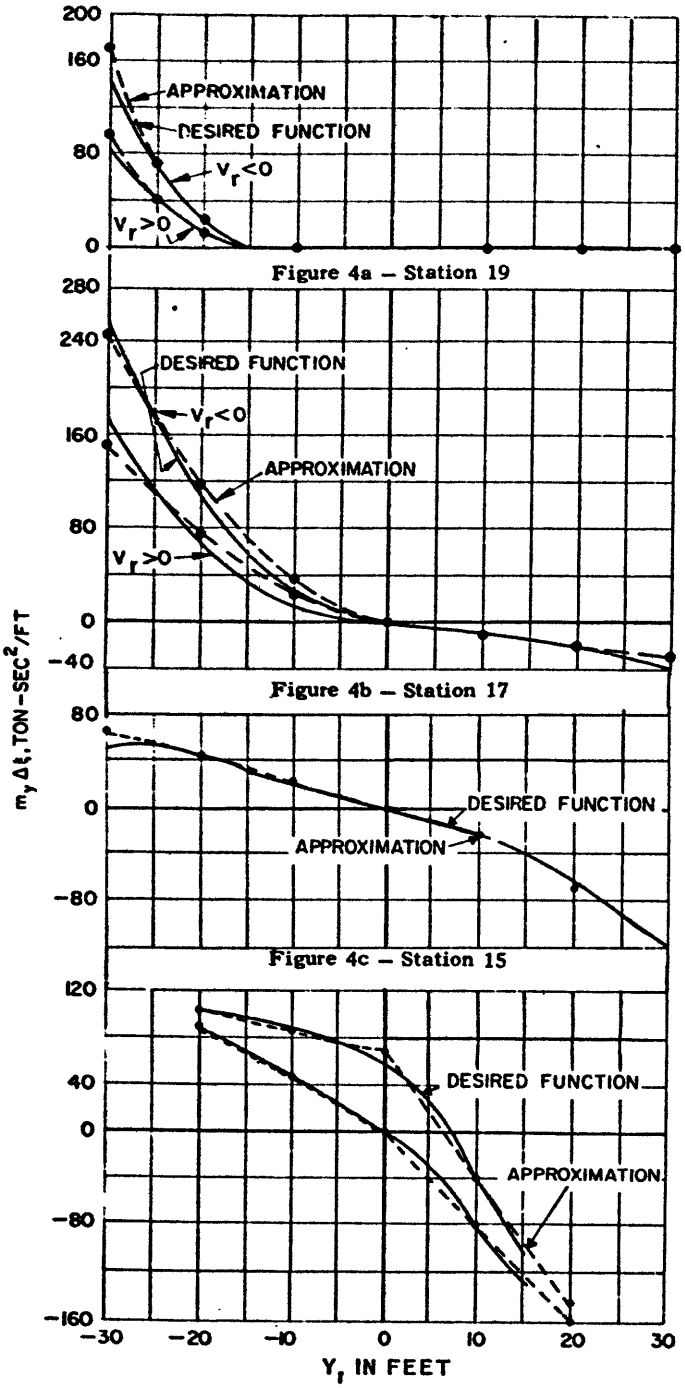

Figure 4a – Station 19

Figure 4b – Station 17

Figure 4c – Station 15

Figure 4d – Station 3

Figure 4 – Nonlinear Added Masses

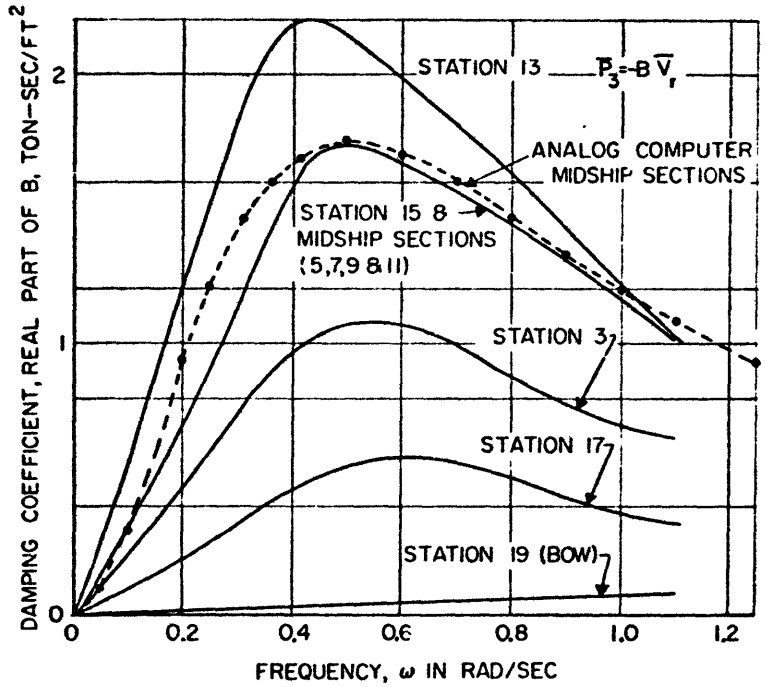

Figure 5 – Hydrodynamic Damping Coefficients

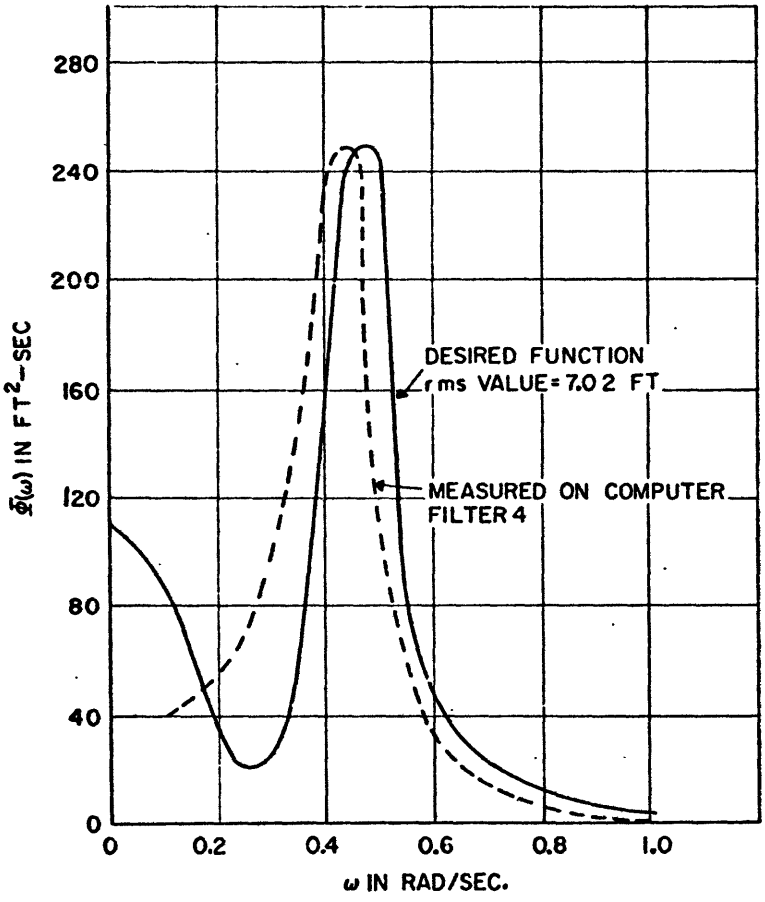

Figure 6 – Power Spectrum of Sea as Obtained from Figure 5a of Reference 5

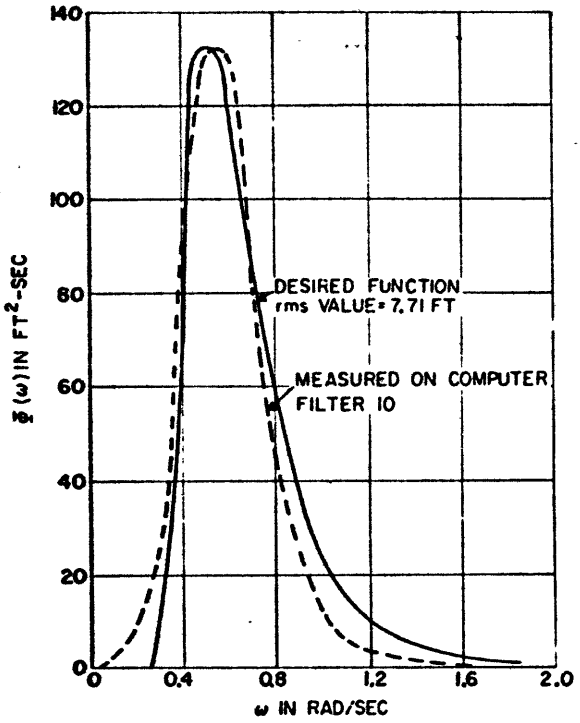

Figure 7 – Power Spectrum for 30-Knot Wind, Sea State 7

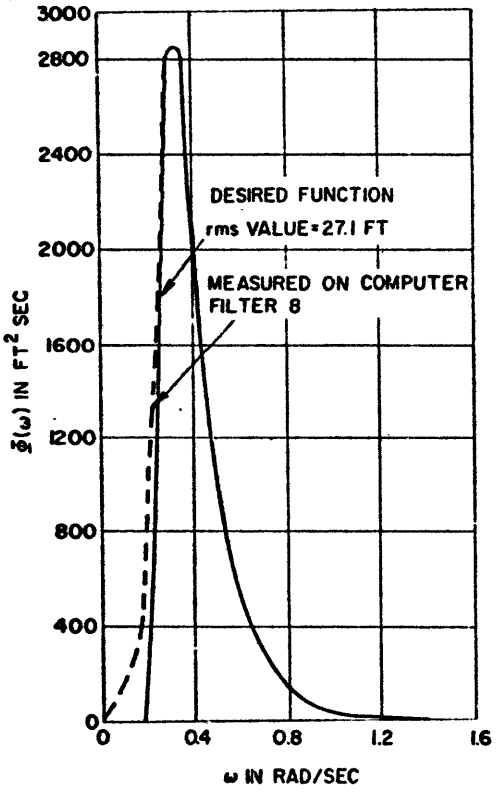

Figure 8 – Power Spectrum for 50-Knot Wind, Sea State 10

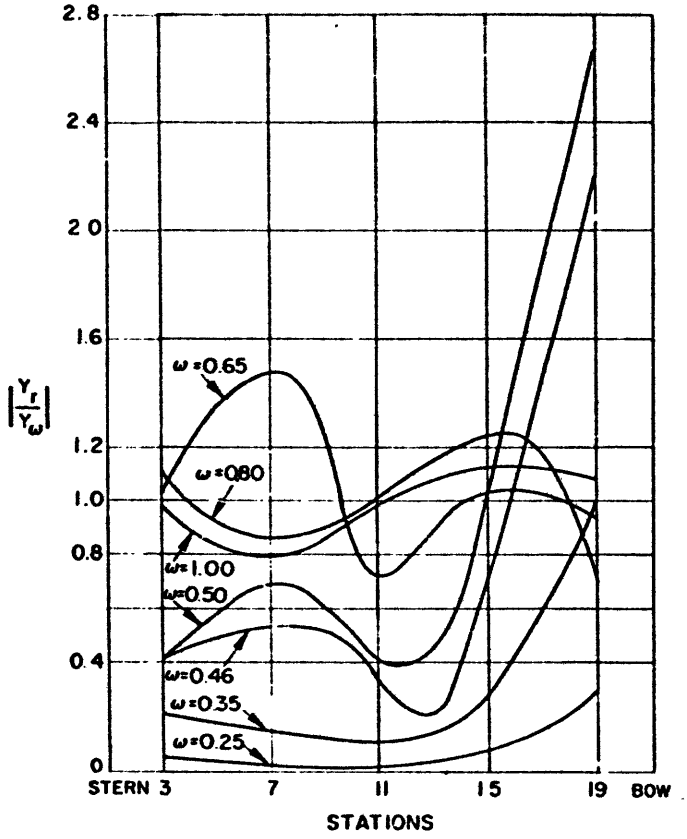

Figure 9 – Immersion Amplification Factor (16-Knot Ship Speed, Linear Analysis, Sinusoidal Waves)

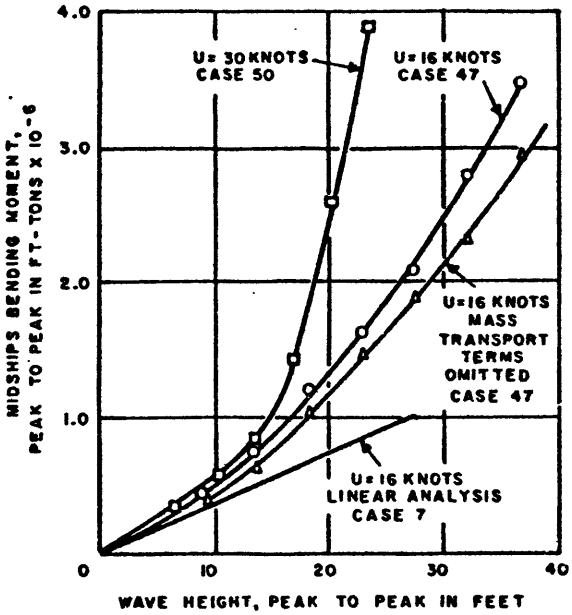

Figure 10 – Midship Bending Moment as a Function of Ship Speed and Wave Height

inusoidal wave of frequency, $\omega = 0.50$ rad/sec.

Figure 11 – Comparison of Analog with Sea Trial Results

Note: Plots shown are traced directly from actual record.

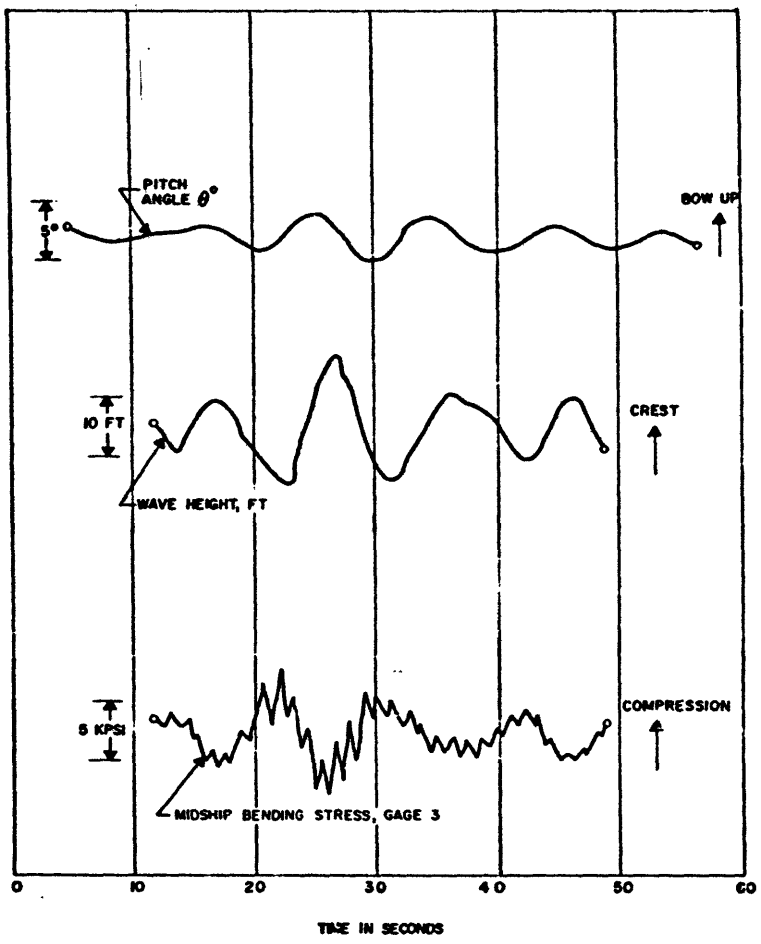

Figure 11a – Actual Records from ESSEX Sea Trials (Figure 5a, Reference 7)

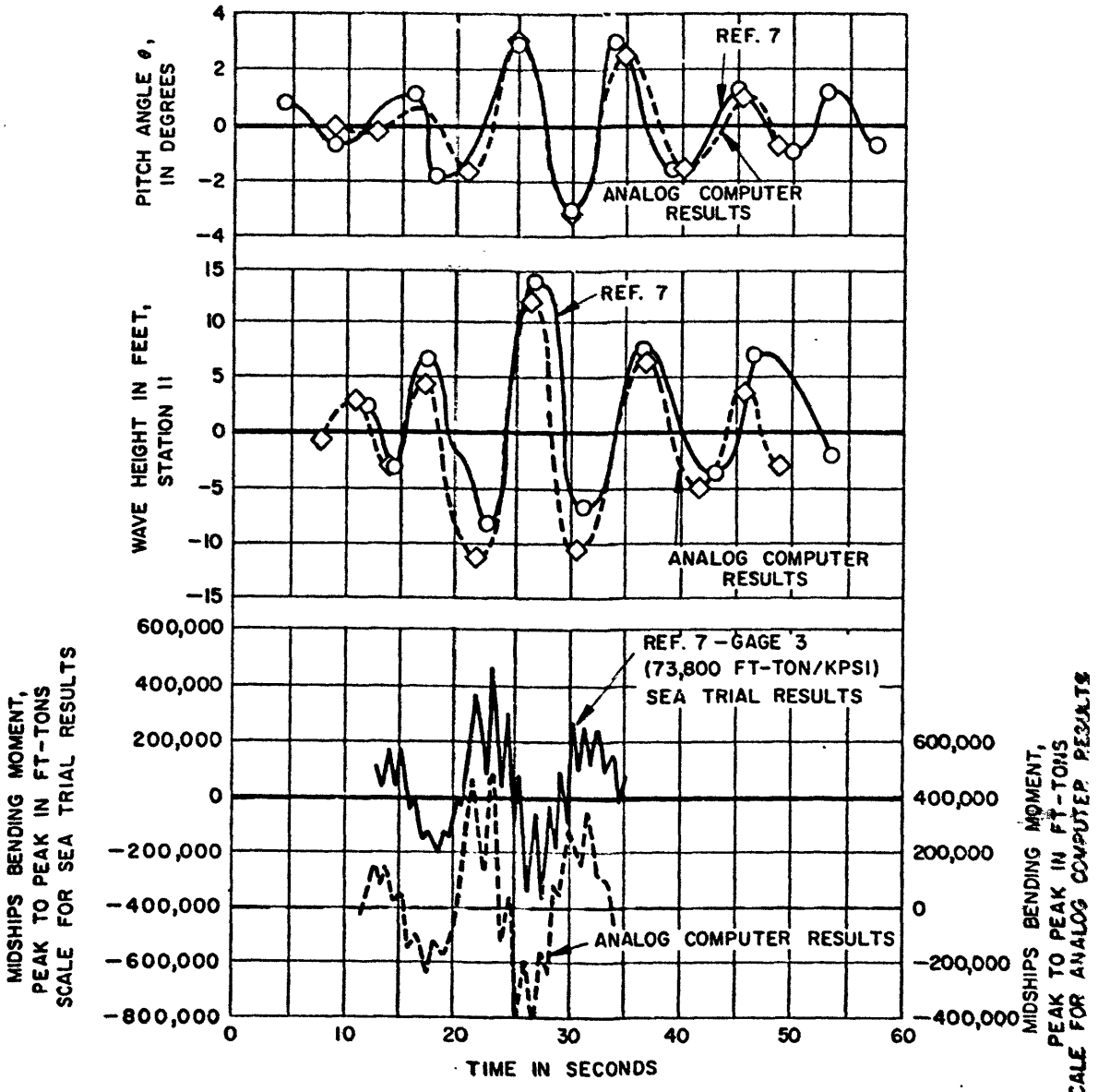

Figure 11b – Analog Results versus Sea Trial Results

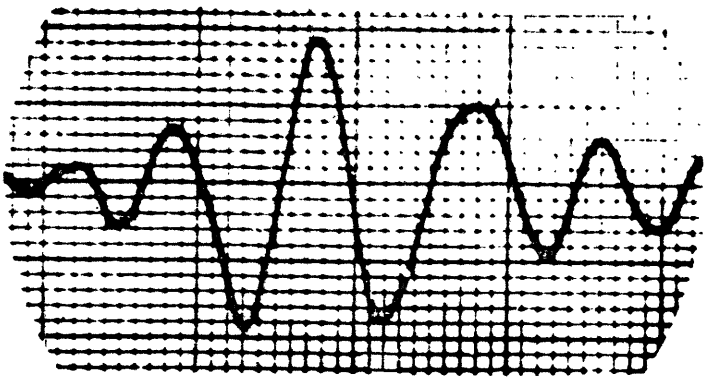

Picture No. 203
Vertical Scale: 1 division = 1.778 ft
Horizontal Scale: 1 division = 1.02 sec

Figure 12a – Wave Height, Station 11

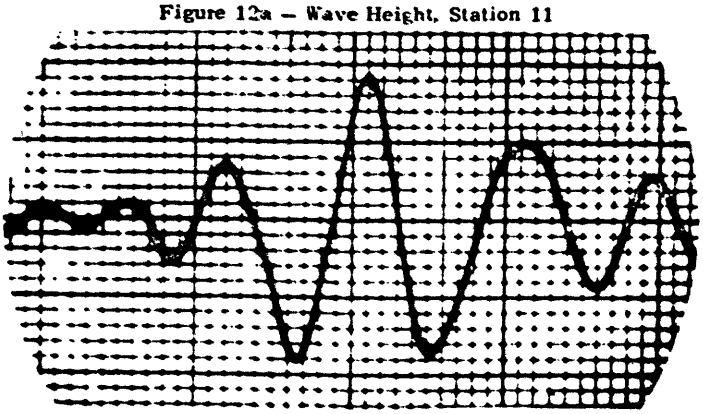

Picture No. 204
Vertical Scale: 1 division = 1.778 ft
Horizontal Scale: 1 division = 1.02 sec

Figure 12b – Wave Height, Station 3

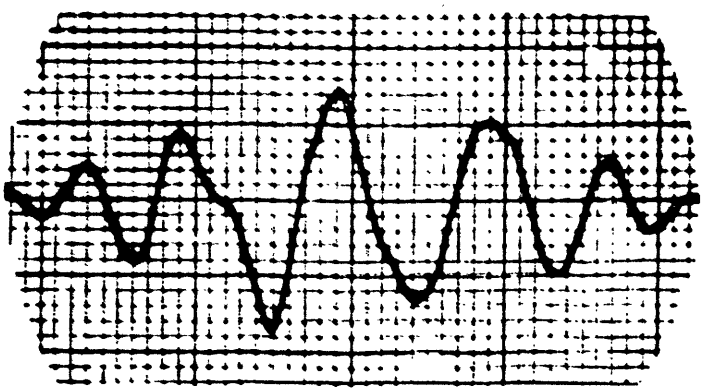

Picture No. 205
Vertical Scale: 1 division = 0.889 ft
Horizontal Scale: 1 division = 1.02 sec

Figure 12c – Emersion, Station 3

Figure 12 – Wave Height and Emersion, Case 17

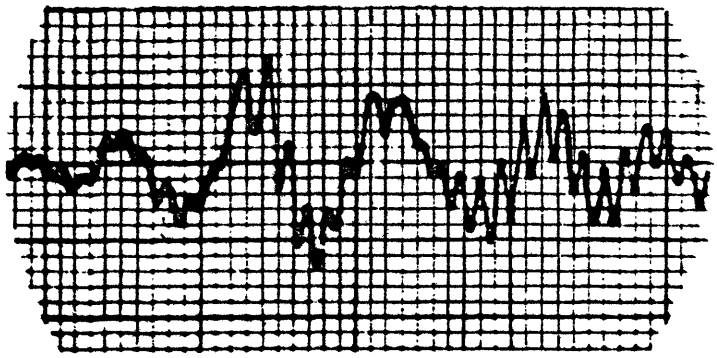

Picture No. 218
Vertical Scale: 1 division = 92,400 ft-tons
Horizontal Scale: 1 division = 1.02 sec

Figure 13a – Bending Moment, Station 8

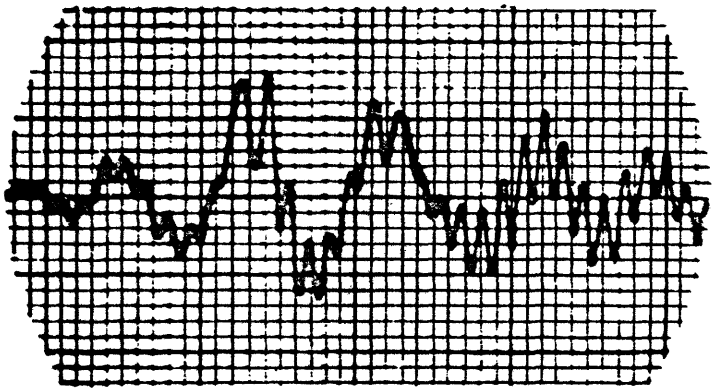

Picture No. 219
Vertical Scale: 1 division = 92,400 ft-tons
Horizontal Scale: 1 division = 1.02 sec

Figure 13b – Bending Moment, Station 10

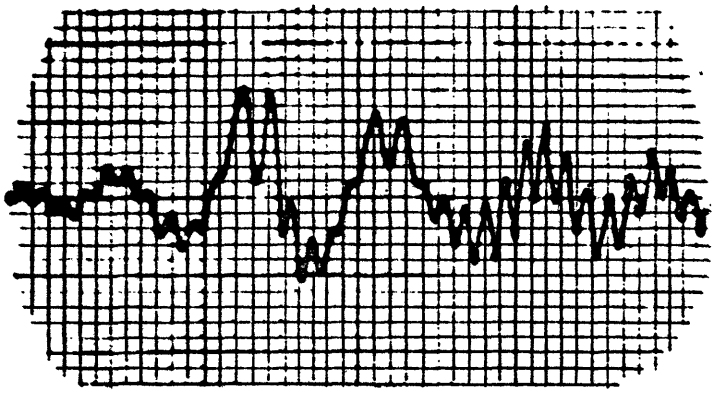

Picture No. 220
Vertical Scale: 1 division = 92,400 ft-tons
Horizontal Scale: 1 division = 1.02 sec

Figure 13c – Bending Moment, Station 12

Figure 13 – Bending Moment, Case 17

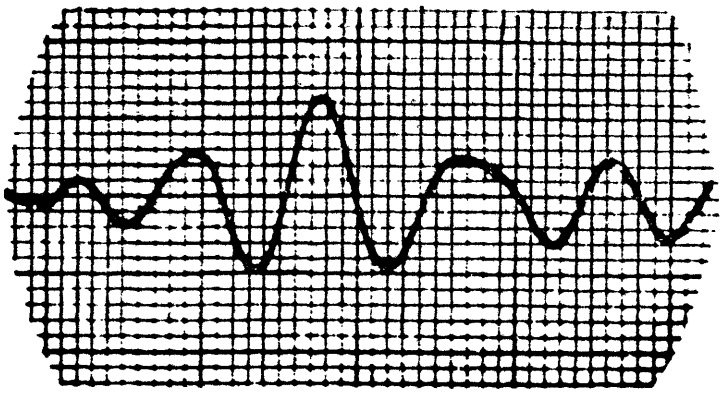

Picture No. 209
Vertical Scale: 1 division = 1.778 ft
Horizontal Scale: 1 division = 1.02 sec

Figure 14a – Emersion, Station 17

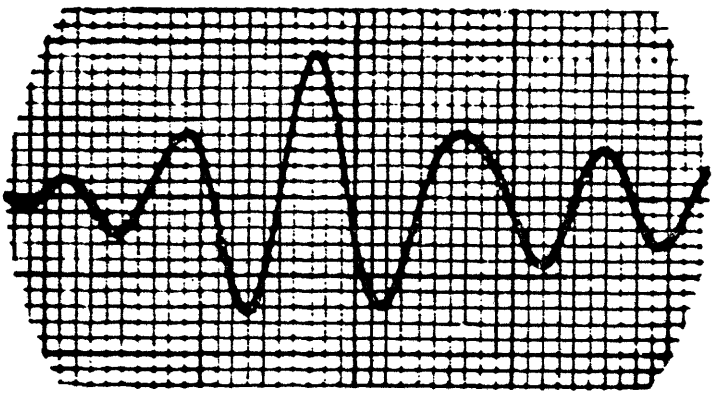

Picture No. 210
Vertical Scale: 1 division = 4.444 ft
Horizontal Scale: 1 division = 1.02 sec

Figure 14b – Emersion, Station 19

Picture No. 211
Vertical Scale: 1 division = 0.0350 g
Horizontal Scale: 1 division = 1.02 sec

Figure 14c – Acceleration, Station 11

Figure 14 – Emersion and Acceleration, Case 17

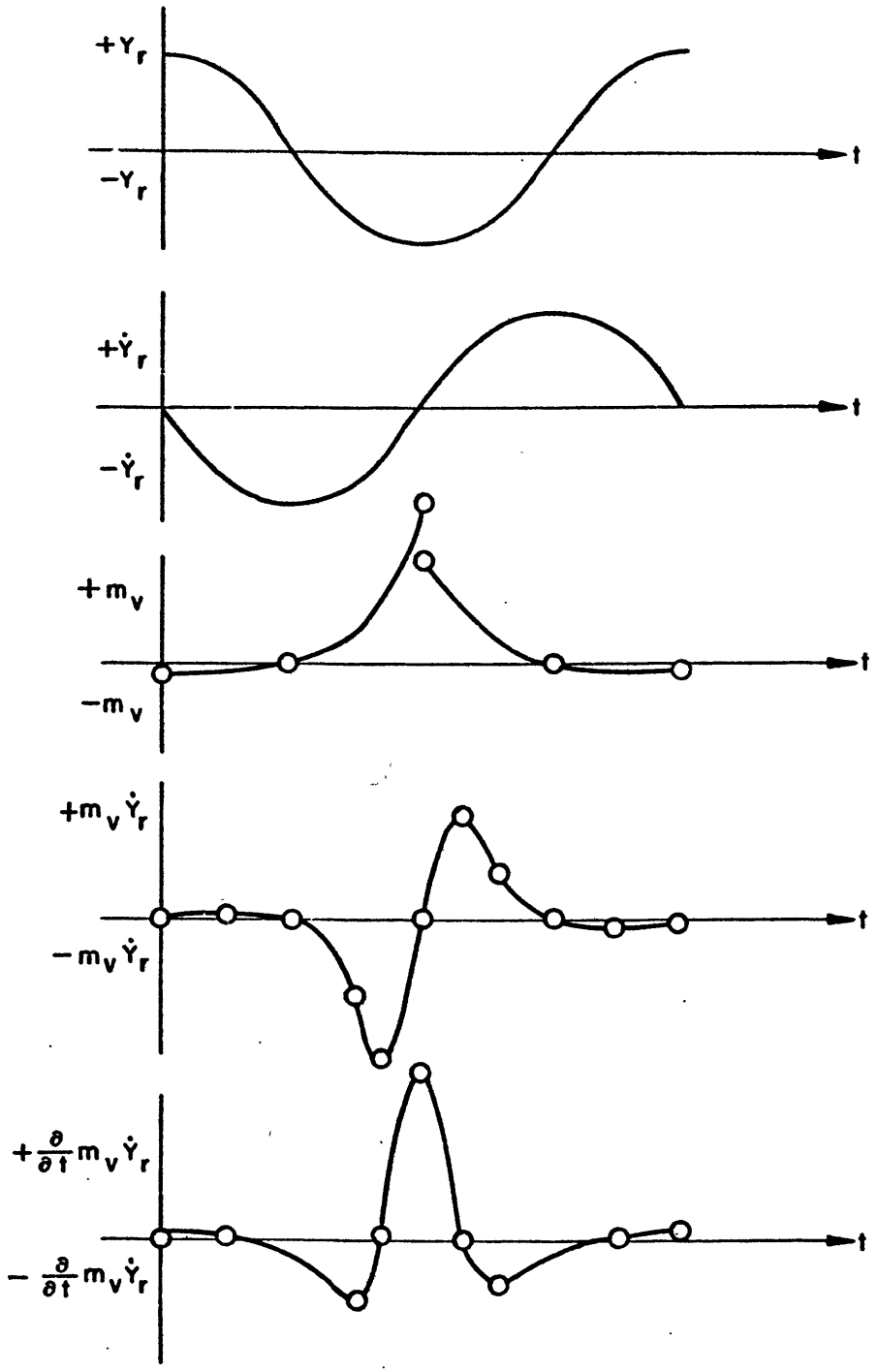

Figure 15 – Triplet Pulse Whipping Excitation (Schematic Sketch)

These curves describe the force resulting from the nonlinear portion of the added mass. When the period T of this triplet pulse is approximately equal to a natural period of hull vibration, severe "whipping" of the hull may result.

Picture No. 382
Vertical Scale: 1 division = 180,900 ft-tons
Horizontal Scale: 1 division = 1.03 sec

Figure 16a – Bending Moment, Station 8

Picture No. 383
Vertical Scale: 1 division = 180,900 ft-tons
Horizontal Scale: 1 division = 1.03 sec

Figure 16b – Bending Moment, Station 10

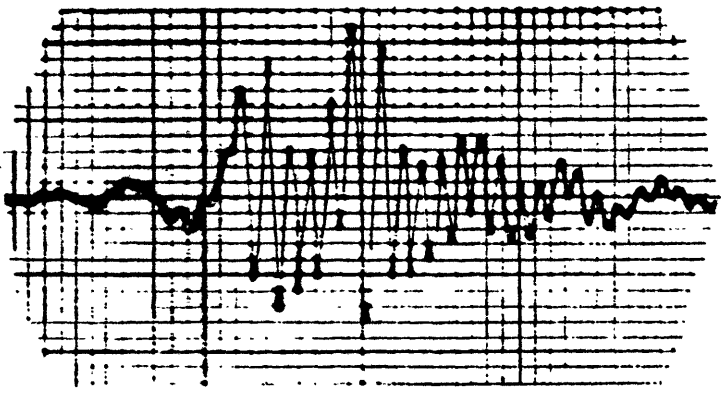

Picture No. 384
Vertical Scale: 1 division = 180,900 ft-tons
Horizontal Scale: 1 division = 1.03 sec

Figure 16c – Bending Moment, Station 12

Figure 16 – Bending Moment, Case 23

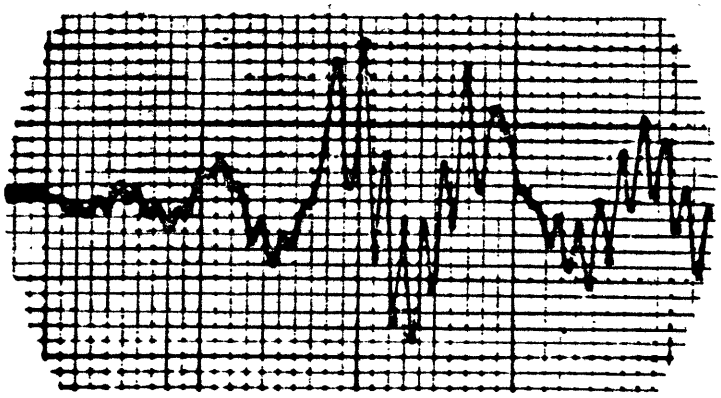

Picture No. 159
Vertical Scale: 1 division = 91,400 ft-tons
Horizontal Scale: 1 division = 1.02 sec

Figure 17a — Bending Moment, Station 8

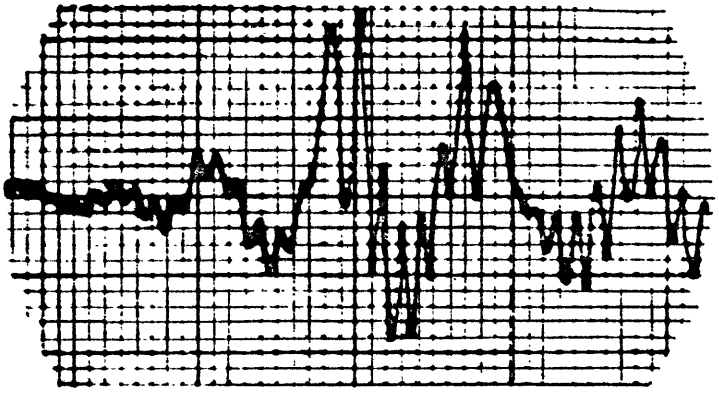

Picture No. 160
Vertical Scale: 1 division = 91,400 ft-tons
Horizontal Scale: 1 division = 1.02 sec

Figure 17b — Bending Moment, Station 10

Picture No. 161
Vertical Scale: 1 division = 91,400 ft-tons
Horizontal Scale: 1 division = 1.02 sec

Figure 17c — Bending Moment, Station 12

Figure 17 — Bending Moment, Case 14-2

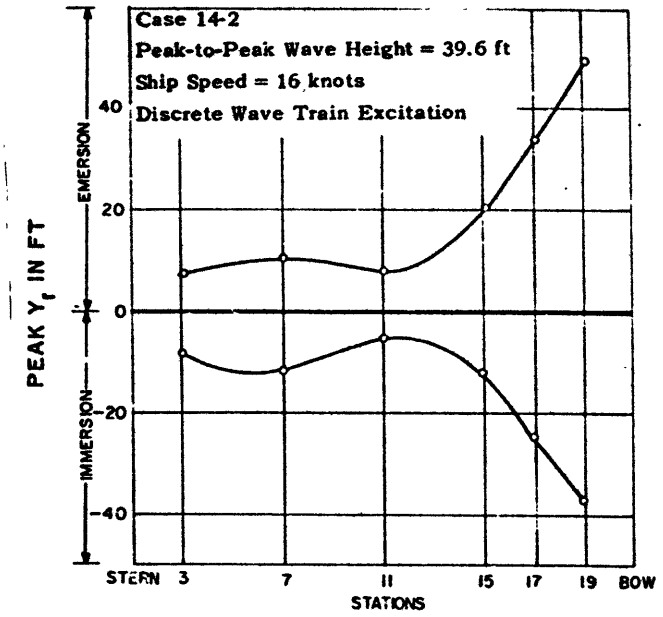

Figure 18 – Peak Relative Displacement along Ship

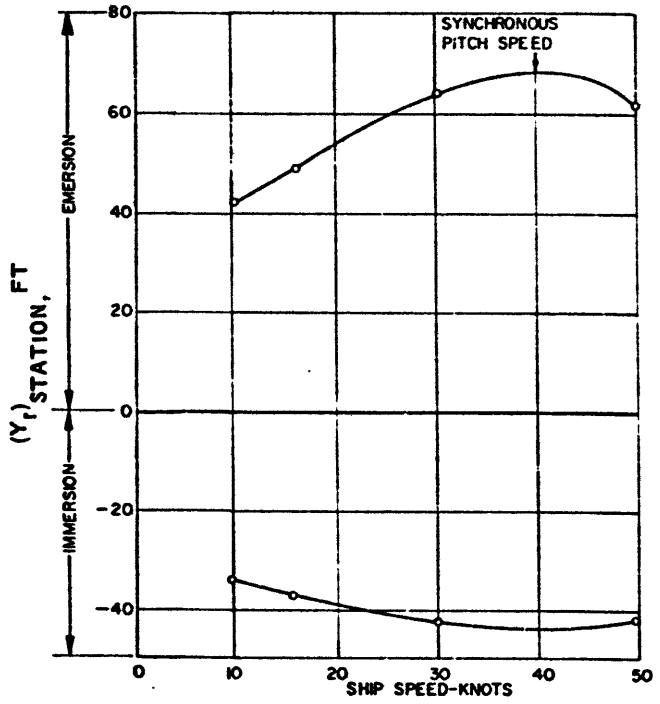

Peak-to-Peak Wave Height = 39 ft
Discrete Wave Train Excitation

Figure 19 – Peak Relative Displacement at Bow at Various Ship Speeds

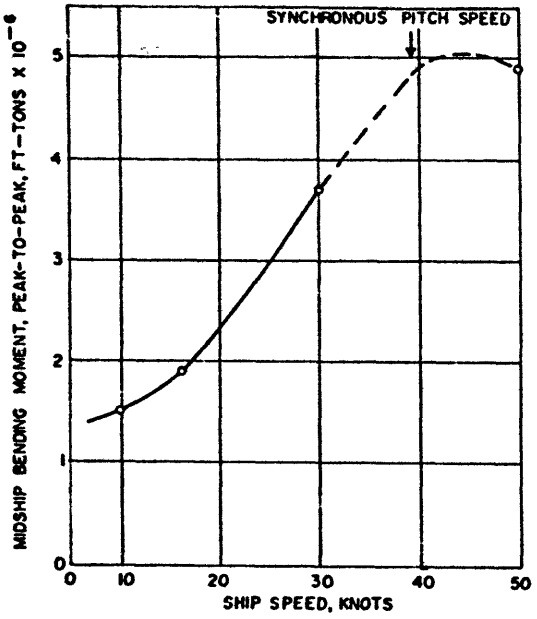

Peak-to-Peak Wave Height = 39 ft
Discrete Wave Train Excitation
Note: Dotted line was faired in because of lack of information.

Figure 20 – Midship Peak-to-Peak Bending Moment at Various Ship Speeds

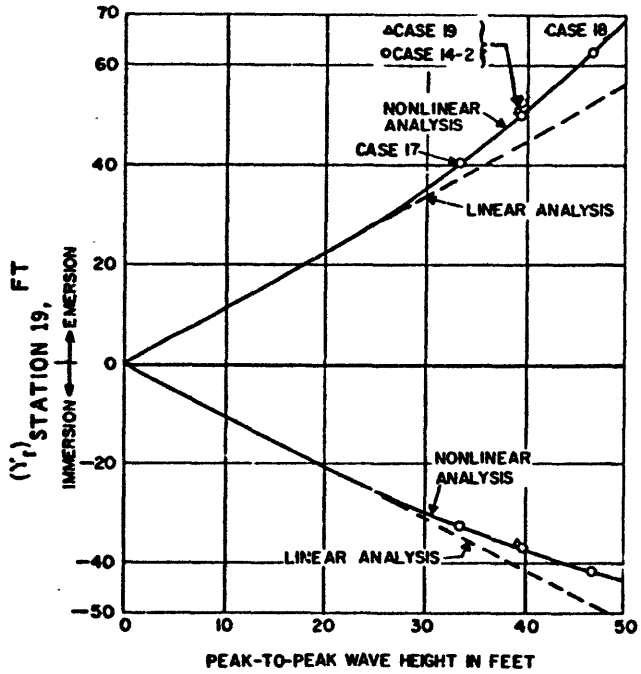

Ship Speed = 16 knots
Discrete Wave Train Excitation
Δ Rigid Body
o Elastic Body

Figure 21 – Effect of Nonlinear Hydrodynamic Forces on Peak Relative Displacement at Bow

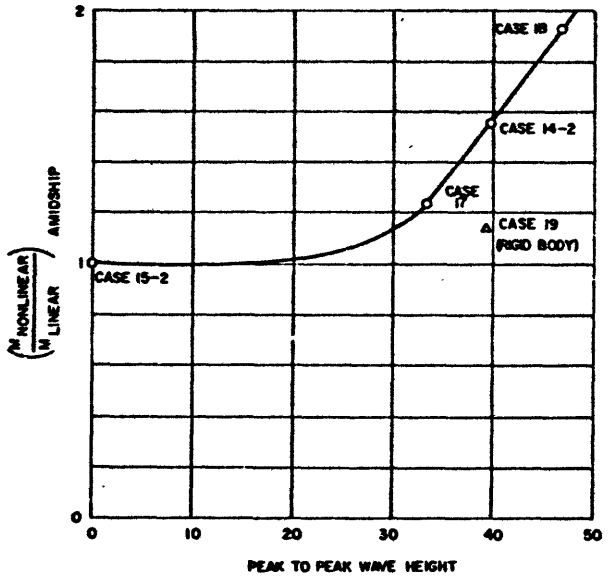

Ship Speed = 16 knots
Discrete Wave Train Excitation

Figure 22 – Peak-to-Peak Bending Moment Amplification due to Nonlinear Hydrodynamic Forces

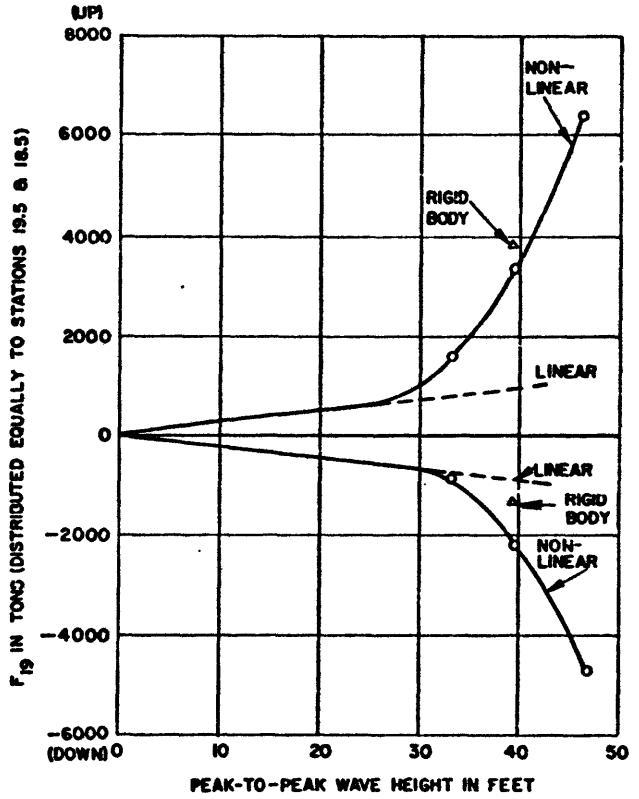

Ship Speed = 16 knots
Discrete Wave Train Excitation

Figure 23 – Peak Hydrodynamic Force at Station 19

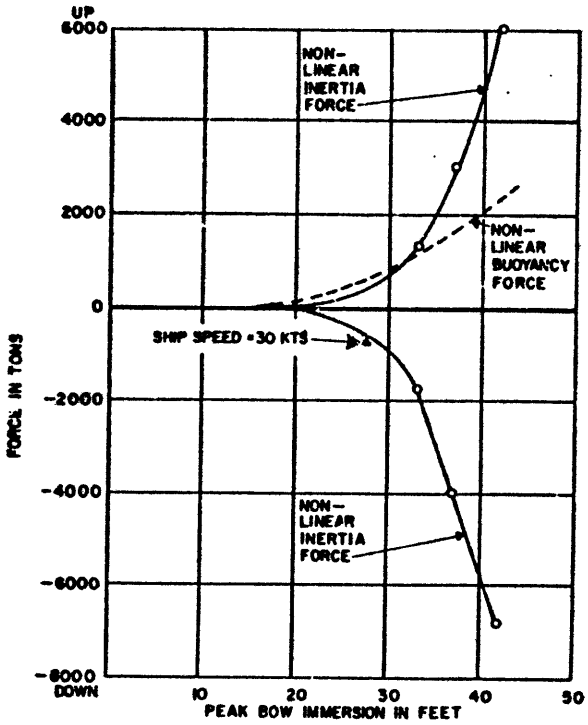

Ship Speed = 16 knots

Discrete Wave Train Excitation

Figure 24 – Peak Nonlinear Force at Station 19 versus Peak Bow Immersion

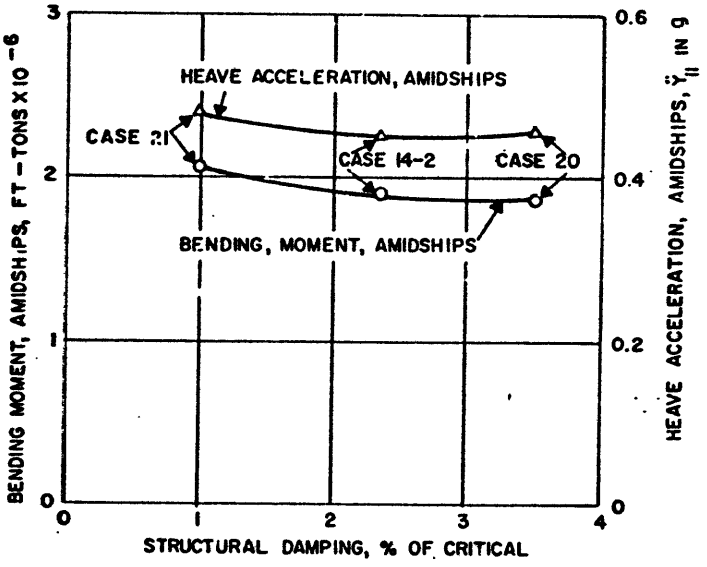

Ship Speed = 16 knots

Peak-to-Peak Wave Height = 39 ft

Discrete Wave Train Excitation

Figure 25 – Effect of Structural Damping on Bending Moment and Heave Acceleration, Amidships

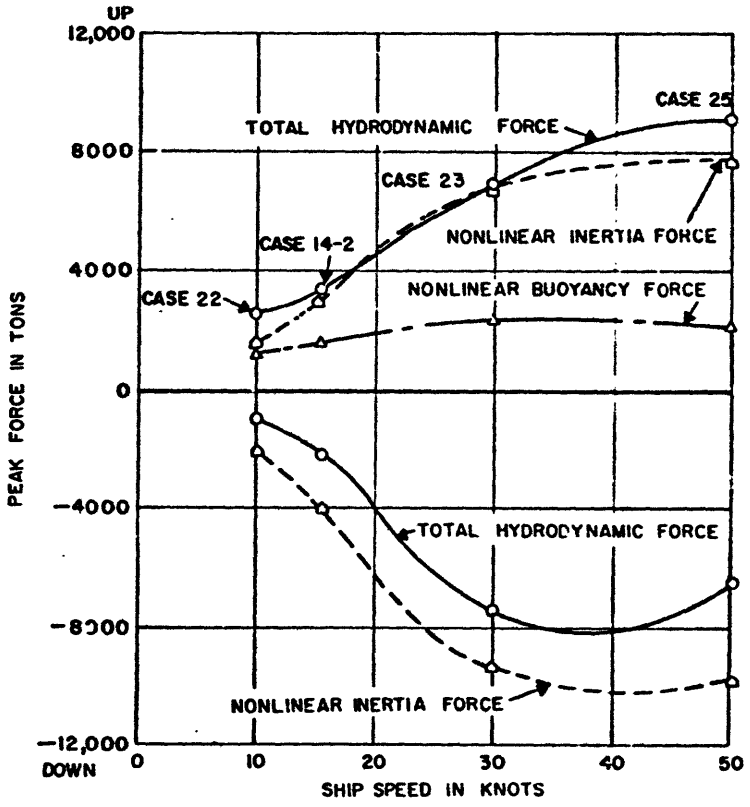

Peak-to-Peak Wave Height = 39 ft
Discrete Wave Train Excitation

Figure 26 – Effect of Ship Speed to the Peak Hydrodynamic Force at Bow

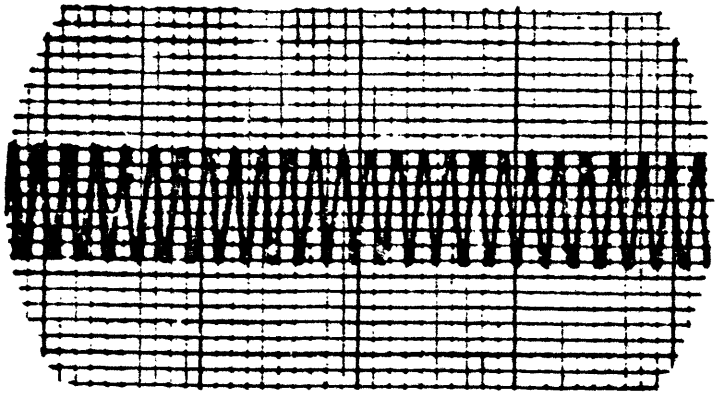

Picture No. 616
Vertical Scale: None
Horizontal Scale: 1 division = 5.72 sec
Figure 27a — Regular Wave

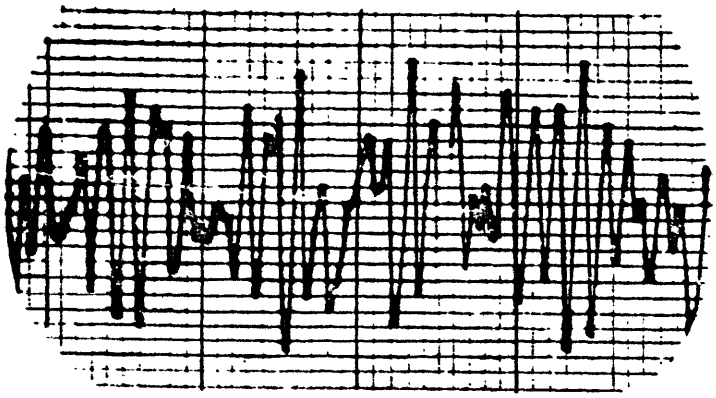

Picture No. 617
Vertical Scale: 1 division = 1.633 ft
Horizontal Scale: 1 division = 5.72 sec
Figure 27b — Irregular Wave

Figure 27 — Regular and Irregular Waves, Case 35

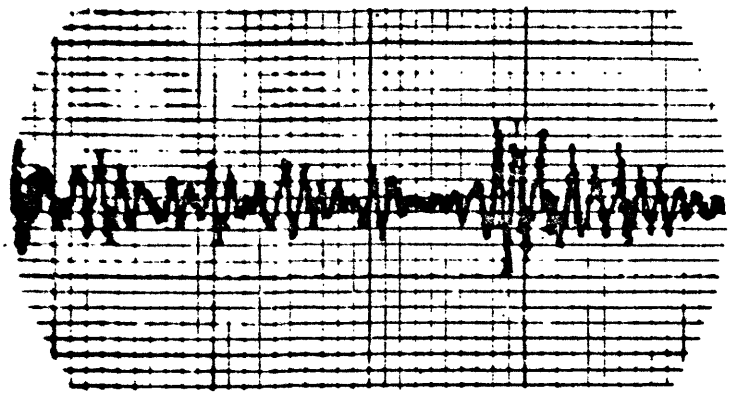

Picture No. 613a
Vertical Scale: 1 division = 169,800 ft-tons
Horizontal Scale: 1 division = 5.72 sec

Figure 28a – Bending Moment, Station 10

Picture No. 61Sb
Vertical Scale: 1 division = 169,800 ft-tons
Horizontal Scale: 1 division = 5.72 sec

Figure 28b – Bending Moment, Station 10

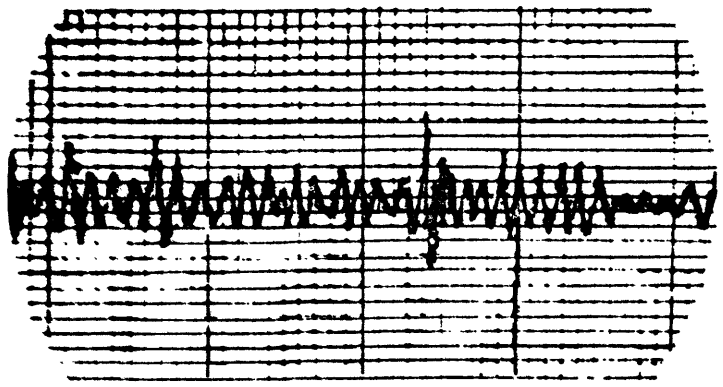

Picture No. 618c
Vertical Scale: 1 division = 169,800 ft-tons
Horizontal Scale: 1 division = 5.72 sec

Figure 28c – Bending Moment, Station 10

Figure 28 – Bending Moment, Case 35

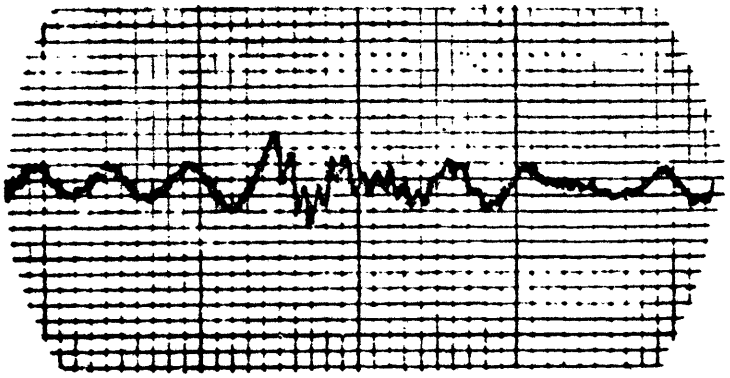

Picture No. 619a

Vertical Scale: 1 division = 169,800 ft-tons

Horizontal Scale: 1 division = 1.43 sec

Figure 29a — Bending Moment, Station 10

Picture No. 619b

Vertical Scale: 1 division = 169,800 ft-tons

Horizontal Scale: 1 division = 1.43 sec

Figure 29b — Bending Moment, Station 10

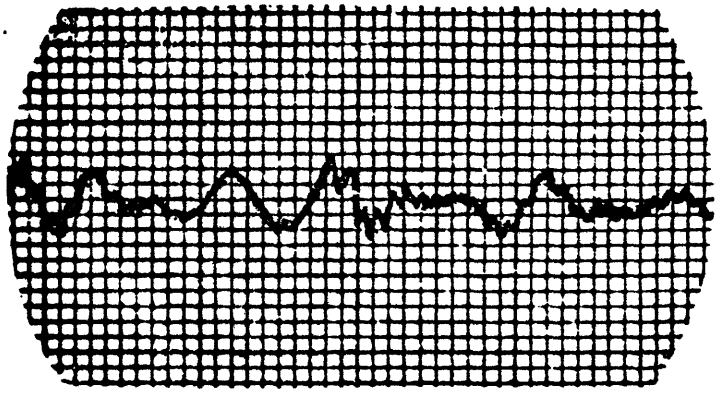

Picture No. 619c

Vertical Scale: 1 division = 169,800 ft-tons

Horizontal Scale: 1 division = 1.43 sec

Figure 29c — Bending Moment, Station 10

Figure 29 — Bending Moment, Case 35

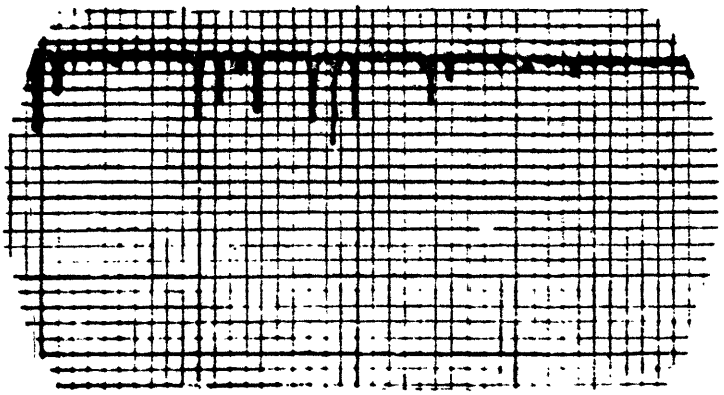

Picture No. 626a

Vertical Scale: 1 division = 223.6 tons

Horizontal Scale: 1 division = 5.72 sec

Figure 30a – Nonlinear Buoyancy Force, Station 19

Picture No. 626b

Vertical Scale: 1 division = 223.6 tons

Horizontal Scale: 1 division = 5.72 sec

Figure 30b – Nonlinear Buoyancy Force, Station 19

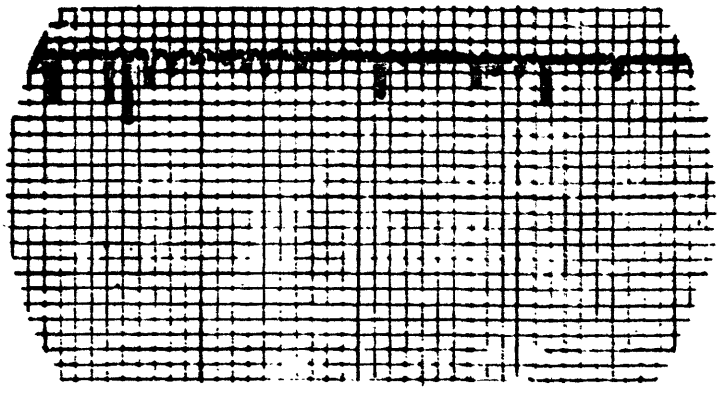

Picture No. 626c

Vertical Scale: 1 division = 223.6 tons

Horizontal Scale: 1 division = 5.72 sec

Figure 30c – Nonlinear Buoyancy Force, Station 19

Figure 30 – Nonlinear Buoyancy Force, Case 35

TABLE 1

Mass and Stiffness of Ship

Station	Mass m_s ton-sec^2/ft	Bending Stiffness $EI \times 10^{-9}$ ton-ft^2	Station	Moment of Inertia $I_{mz} \times 10^{-3}$ ton-sec^2-ft	Shear Stiffness $KAG \times 10^{-5}$ tons
0	10.17	–			
1	27.12	5.70	0.5	7.28	14.88
2	33.89	9.83	1.5	13.55	20.61
3	35.59	14.80	2.5	20.81	30.08
4	57.30	21.81	3.5	29.67	41.51
5	82.30	32.28	4.5	38.46	54.13
6	90.14	41.62	5.5	44.82	66.00
7	90.56	46.86	6.5	50.07	74.54
8	85.37	52.50	7.5	53.89	77.98
9	86.43	57.83	8.5	55.77	76.09
10	85.90	59.68	9.5	54.21	73.45
11	82.09	58.32	10.5	51.65	70.74
12	81.34	43.02	11.5	49.59	69.94
13	77.96	31.93	12.5	46.27	72.75
14	74.04	34.48	13.5	40.78	78.40
15	70.75	34.48	14.5	33.87	77.36
16	64.93	22.80	15.5	26.52	56.61
17	46.39	15.74	16.5	18.33	32.27
18	25.00	11.56	17.5	10.74	21.55
19	19.38	8.09	18.5	5.97	16.43
20	10.48	–	19.5	4.71	13.50

TABLE 2

Hull Characteristics of ESSEX

LBP	Length between perpendiculars, ft-in.	820 – 0
Δ	Displacement, long tons (salt-water)	39,503
H	Design draft, ft-in.	28 – 6
B	Breadth, ft-in	103 – 0
A_{III}	Area of midship section, sq ft	2,880
C_{III}	Midship section coefficient	0.981
C_p	Prismatic coefficient	0.586
C_b	Block coefficient	0.574
C_{WP}	Water plane coefficient	0.724

TABLE 3

Nonlinear Buoyancy and Added Mass Terms

A. Buoyancy Terms, tons		
Station 19:	$\rho g A \Delta\xi = 2.48\,(Y_r + 10)^2$	for $Y_r < -10$
	$= 0$	> -10
Station 17:	$\rho g \bar{A} \Delta\xi = 1.103\, Y_r^2$	
Station 15:	$\rho g \bar{A} \Delta\xi = 2.06\, Y_r^2$	for $Y_r > 0$
	$= 0$	< 0
Station 3:	$\rho g \bar{A} \Delta\xi = 6.37\, Y_r^2$	for $Y_r > 0$
	$= 0$	< 0
B. Added Mass Terms, ton-sec^2/ft		
Station 19:	$\bar{m}_1 \Delta\xi = 0.0121\,(Y_r + 10)^3$	for $Y_r < -10$, $V_r > 0$
	$= 0$	> -10, > 0
	$\bar{m}_2 \Delta\xi = 0.0218\,(Y_r + 10)^3$	< -10, < 0
	$= 0$	> -10, < 0
Station 17:	$\bar{m}_1 \Delta\xi = -1.08\, Y_r + 0.1286\, Y_r^2$	$Y_r < 0$, $V_r > 0$
	$= -1.08\, Y_r$	> 0, > 0
	$\bar{m}_2 \Delta\xi = -1.08\, Y_r + 0.2330\, Y_r^2$	< 0, < 0
	$= -1.08\, Y_r$	> 0, < 0
Station 15:	$\bar{m}_1 \Delta\xi = \bar{m}_2 \Delta\xi = -2.143\, Y_r - 0.0640\, Y_r$	$Y_r > 0$
	$= -2.143\, Y_r$	< 0
Station 3:	$\bar{m}_1 \Delta\xi = -4.59\, Y_r$	$Y_r < 0$, $V_r > 0$
	$= -8.40\, Y_r$	> 0, > 0
	$\bar{m}_2 \Delta\xi = 68.9 - 1.813\, Y_r$	< 0, < 0
	$= 68.9 - 11.26\, Y_r$	> 0, < 0

TABLE 4

Linear Hydrodynamic Properties

Values apply to a ship in calm water at a draft of 28.5 ft.

Station	Added Mass m_0 ton-sec^2/ft	Buoyancy Spring K_b ton/ft	Smith Correction Factor = $\frac{\rho A_0 \Delta \xi}{m_0}$
3	157.2	320.5	0.7102
5	213.1	261.1	0.7719
7	288.5	270.2	0.7509
9	324.8	270.7	0.7200
11	307.4	268.4	0.7447
13	232.3	248.7	0.8390
15	124.0	190.4	1.0528
17	40.7	101.3	1.6554
19	8.2	27.9	3.1840

TABLE 5

Summary of Inputs and Outputs used in Analog Computation

Inputs	Outputs
Mass-elastic parameters	Bending moment
Buoyancy force curves	Shear force
Added mass curves	Heave acceleration
Hydrodynamic damping coefficient curves	Angular velocity
	Pitch angle
Waveform	Immersion
	Relative displacement

Case	Type of Analysis	Speed U Knots	Wave Propogation ω rad/sec	Wave Propogation $c=\frac{g}{\omega}$ ft/sec	Nonlinear Term	Lowest Structural Mode Damping % Critical	Stiffness	RMS Wave Height ft	Sinusoidal Excitation ω rad sec	Sinusoidal Excitation $\omega' = \omega + \frac{\omega^2 U}{g}$ rad/sec	Discrete Wave Excitation Peak-to-Peak Wave Height ft	Discrete Wave Excitation Forcing Function Smoothing	Picture Number	Remark Number
1	Vibration Modes	0			Out	1.95	Basic		Several				None	1
2	↓	↓			↓	1.6	↓		↓				↓	2
3						1.9								3
4	Steady-State Wave	16	0.46	70.06	Out	2.35	Basic	10.0	0.46	0.638			None	
5	↓	↓	0.25	128.09	↓	↓	↓	↓	0.25	0.303			↓	
6			0.35	92.08					0.35	0.453				
7			0.50	64.46					0.50	0.710				
8			0.65	49.58					0.65	1.004				
9			0.80	40.29					0.80	1.337				
10			1.00	37.23					1.00	1.838				
14-2	Discrete Wave Train	16	0.46	70.06	In	2.35	Basic				39.6	C-Heavy	141-173	4
15-2	↓	↓	↓	↓	Out	↓	↓				39.5	↓	174-199	
17					In						33.4		200-232	
18					↓						46.7		233-265	
19							Rigid				39.3		266-298	
20						3.5	Basic				39.8		299-320	
21		↓				1.0					39.8		321-330	
22		10				2.35					39.1		331-363	
23		30				↓					38 8		364-396	
24		30									23.3		397-432	
25		50									37.8		433-470	
26		50									28.4		471-484	
27		16	↓	↓	↓	↓	1.25× Basic				34.6	↓	485-517	

Case	Type of Analysis	Speed U Knots	Wave Propagation ω rad/sec	Wave Propagation $c=\frac{g}{\omega}$ ft/sec	Nonlinear Terms	Lowest Structural Mode Damping % Critical	Stiffness	RMS Wave Height ft	Sinusoidal Excitation ω rad/sec	Sinusoidal Excitation ω' rad/sec	Random Excitation Sea State	Random Excitation Figure Number	Picture Number	Remark Number
29	Random Sea	16	0.46	70.06	In	2.35	Basic	7.5			Worst	6	518-545	5
30					Out								546-564	
31					In			6.0					565-586	
32						1.05		7.5					587-595	
33						3.50							596-604	
34		30				2.35		6.0					607-614	5
35													615-628	

		Knots	rad/sec	ω ft/sec		Damping % Critical		ft	ω rad/sec	ω rad/sec		Number		
29	Random Sea	16	0.46	70.06	In	2.35	Basic	7.5			Worst	6	518-545	5
30					Out								546-564	
31					In			6.0					565-586	
32						1.05		7.5					587-595	
33						3.50							596-604	
34		30				2.35		6.0					607-614	5
35													615-628	
36						1.05							629-635	
37					Out								638-645	
38		16						8.33					648-654	
39					In			7.50					657-663	
40								8.83					664-668	
41								7.50					669-673	6
42								6.00					676-678	7
43			0.35	92.08				12.0			50-kt Wind	8	681-691	
44			0.35	92.08	Out							8	694-699	
45			0.50	64.46	In			7.71			30-kt Wind	7	702-706	
46					Out							7	715-720	
47	Steady-State Sinusoidal				In			13.0	0.50	0.710	—	—	721-756	
48	Random Sea	30	0.35	92.08				10.5			50-kt Wind	8	759-768	
49	Random Sea				Out							8	769-776	
50	Steady-State Sinusoidal		0.50	64.46	In			10.0	0.50	0.894	—	—	777-805	

Case Description Remarks

Remark	Case	
1	1	No hydrodynamic forces.
2	2	Hydrodynamic buoyancy forces. No hydrodynamic damping.
3	3	Hydrodynamic buoyancy and damping forces present.
4	14-2	For this and all subsequent cases, the simulation was slightly revised to provide a greater range of immersion and a better signal-to-noise ratio.
5	29-34	Excessive excitation of lowest structural mode due to insufficient filtering of random noise generator.
6	41	Shape of nonlinear buoyancy and virtual mass functions sharpened at Sta. 19.

TABLE 7

Vibration Mode Data

Case →	1	1	1	2	2	2	2	2
Mode Number	1	2	3	1	2	3	Heave	Pitch
Frequency, cps	0.734	1.37	2.07	0.744	1.37	2.07	0.128	0.144
Damping, Percent Critical	2.0	2.0	2.2	1.6	1.7	2.3	1.2	1.1
Station ↓	Deflections							
0	+ 9.97	+ 9.99	+ 9.97	+ 9.96	+ 9.98	+ 9.97	+ 1.00	+ 9.97
1	+ 8.14	+ 7.35	+ 6.47	+ 8.13	+ 7.34	+ 6.49	+ 1.73	+ 9.09
2	+ 6.18	+ 4.44	+ 2.63	+ 6.17	+ 4.44	+ 2.65	+ 2.49	+ 8.20
3	+ 4.22	+ 1.67	− 0.585	+ 4.23	+ 1.67	− 0.581	+ 3.25	+ 7.31
4	+ 2.40	−0.624	− 2.84	+ 2.42	− 0.602	− 2.84	+ 4.02	+ 6.42
5	+ 0.821	− 2.29	− 3.78	+ 0.859	− 2.27	− 3.79	+ 4.78	+ 5.51
6	− 0.547	− 2.96	− 2.55	− 0.504	− 2.95	− 2.56	+ 5.54	+ 4.61
7	− 1.69	− 3.06	− 0.790	− 1.64	− 3.04	− 0.807	+ 6.30	+ 3.71
8	− 2.42	− 2.22	+ 1.27	− 2.39	− 2.22	+ 1.25	+ 7.04	+ 2.79
9	− 2.86	− 1.05	+ 3.01	− 2.83	− 1.07	+ 3.00	+ 7.78	+ 1.89
10	− 2.88	+ 0.483	+ 2.94	− 2.86	+ 0.454	+ 2.94	+ 8.52	+ 0.987
11	− 2.59	+ 1.93	+ 2.16	− 2.59	+ 1.89	+ 2.19	+ 9.25	+ 0.069
12	− 1.91	+ 2.85	+ 0.035	− 1.91	+ 2.82	+ 0.065	+ 9.98	− 0.851
13	− 0.883	+ 3.29	− 2.22	− 0.902	+ 3.26	− 2.19	+ 10.4	− 1.81
14	+ 0.471	+ 2.64	− 3.30	+ 0.439	+ 2.64	− 3.30	+ 11.1	− 2.73
15	+ 2.04	+ 1.41	− 3.53	+ 1.97	+ 1.43	− 3.55	+ 12.0	− 3.66
16	+ 3.80	− 0.406	− 2.60	+ 3.73	− 0.338	− 2.65	+ 12.6	− 4.39
17	+ 5.78	− 3.02	+ 0.026	+ 5.69	− 2.94	− 0.051	+ 13.4	− 5.51
18	+ 7.83	− 6.06	+ 3.99	+ 7.74	− 5.97	+ 3.89	+ 14.1	− 6.43
19	+ 9.87	− 9.22	+ 8.49	+ 9.79	− 9.10	+ 8.41	+ 14.9	− 7.36
20	+ 11.6	−12.5	+ 12.4	+ 11.5	−12.4	+ 12.2	+ 15.6	− 8.29

Case	3	3	3	3	3
Mode Number	1	2	3	Heave	Pitch
Frequency, cps	0.750	1.37	2.08	0.139	0.158
Damping, Percent Critical	1.9	1.9	2.3	21.2	22.5

TABLE 8

Results of Steady-State Sinusoidal Wave Excitation (Linear Analysis, 16 Knots of Ship Speed)

Case		4		5		6		
ω, rad/sec		0.40		0.25		0.35		
ω', rad/sec		0.6376		0.3025		0.4526		
Quantity	Station	Magnitude of Quantity	Phase Angle (Lagging) deg	Magnitude of Quantity	Phase Angle (Lagging) deg	Magnitude of Quantity	Phase Angle (Lagging) deg	Ma Qu
Y_w, ft	3	9.80	257	9.76	90	9.74	145	9
	11	9.95	125	10.0	51	9.97	80	9
	19	10.3	0	9.97	0	9.88	0	10
Y_r, ft	3	4.20	184	0.71	73	2.29	114	4
	7	4.95	355	0.33	245	1.52	283	6
	11	3.20	321	0.34	241	1.21	270	4
	15	7.46	143	0.598	57	2.58	87	9
	17	15.00	128	1.60	50	5.91	79	18
	19	22.8	116	2.77	47	9.81	74	26
$\ddot{Y}_h$, g	11	0.0905	300	0.0283	236	0.0575	260	0
$\theta°$	10.5	2.67	78	1.33	316	1.97	3	2
Hydrodynamic Force, tons	2.5	517.0	351	94.3	244	281.0	285	517
	15.5	614.0	289	72.5	224	225.0	242	786
	17.5	674.0	289	86.2	218	275.0	242	822
	19.5	273.0	276	44.6	212	135.0	239	305
Bending Moment, ft-tons	4	86.3×10^3	324	9.88×10^3	262	37.6×10^3	275	99
	8	279.	310	32.8	233	126.	263	329
	10	304.	302	35.5	226	135.	257	360
	12	260.	293	31.4	221	116.	252	307
	16	66.0×10^3	282	11.5×10^3	196	35.2×10^3	240	72

A

ed)

	7		8		9		10	
	0.50		0.65		0.80		1.00	
	0.7095		1.004		1.337		1.838	
gle ;)	Magnitude of Quantity	Phase Angle (Lagging) deg	Magnitude of Quantity	Phase Angle (Lagging) deg	Magnitude of Quantity	Phase Angle (Lagging) deg	Magnitude of Quantity	Phase Angle (Lagging) deg
	9.81	289	9.54	147	9.16	62	7.79	212
	9.97	134	9.96	246	9.96	20	9.96	276
	10.1	349	10.2	0	10.4	0	9.44	0
	4.32	200	9.99	278	10.2	220	7.64	23
	6.99	19	15.1	200	8.60	37	7.92	42
	4.11	332	7.07	79	9.97	200	9.94	95
	9.87	158	10.4	296	12.3	4	11.2	132
	18.4	141	10.2	242	11.8	291	9.66	338
	26.6	126	9.34	176	6.67	192	10.0	173
	0.0984	305	0.125	45	0.0141	132	0.0157	140
	2.62	99	0.767	45	0.680	340	0.201	106
	517.0	5	953.0	80	837.0	6	822.0	86
	786.0	303	740.0	76	532.0	129	1120.0	141
	822.0	294	439.0	34	400.0	80	177.0	338
	305.0	281	75.6	322	12.4	80	123.0	176
	99.9×10^3	338	126.0×10^3	106	97.6×10^3	23	118.0×10^3	81
	329.	320	422.	81	208.	45	284.	122
	360.	310	426.	70	265.	53	196.	122
	307.	301	315.	56	256.	47	154.	149
	72.8×10^3	284	47.9×10^3	14	62.3×10^3	20	34.5×10^3	138

APPENDIX A

MATHEMATICAL REPRESENTATIONS OF HYDRODYNAMIC FORCES

DERIVATION OF HYDRODYNAMIC FORCES

The total downward hydrodynamic force P exerted by a ship on a fluid lamina of unit thickness parallel to the axis of the ship may be written as[10]

$$P = P_1 + P_2 + P_3 \qquad \text{[A-1]}$$

where P_1 is the inertia force due to the added mass,

P_2 is the buoyancy force, and

P_3 is the hydrodynamic damping force.

P_1 may be expressed as an inertia force acting on a mass of fluid m_v that moves with the ship by[11]

$$P_1 = -\frac{d}{dt'}(m_v V_r) \qquad \text{[A-2]}$$

where V_r is the relative vertical velocity between the ship and the surface of the sea; i.e.,

$$V_r = \frac{d}{dt'}(Y_h - Y_w) = \frac{d}{dt'} Y_r \qquad \text{[A-3]}$$

where Y_h is the vertical translation of the ship,

Y_w is the vertical translation of the waves,

Y_r is the relative translation between ship and sea surface, and

t' is the time coordinate in the fluid lamina.

Since the force P_1 is expressed in a coordinate system moving longitudinally with the fluid lamina, we will express this force in a system fixed in the ship by the following coordinate transformation:

$$\zeta = (U - u)\, t + \xi; \quad \xi = \zeta - (U - u)\, t' \qquad \text{[A-4]}$$

$$t' = t; \qquad t = t' \qquad \text{[A-5]}$$

Here (ζ, t') are space and time coordinates fixed in the fluid lamina,

(ξ, t) are coordinates fixed in the ship,

U is the forward velocity of the ship, and

u is the forward velocity of the fluid lamina.

But

$$\frac{d}{dt'} f(\zeta, t') = \frac{d}{dt} f(\xi, t) = \left[\frac{\partial}{\partial t}\frac{dt}{dt'} + \frac{\partial}{\partial \xi}\frac{d\xi}{dt'}\right] f(\xi, t) \qquad \text{[A-6]}$$

where

$$\frac{dt}{dt'} = 1 \quad \text{and} \quad \frac{d\xi}{dt} = \frac{d}{dt}[\zeta - (U-u)t] = -(U-u)$$

Therefore, in operator form,

$$\frac{d}{dt} = \frac{\partial}{\partial t} - (U-u)\frac{\partial}{\partial \xi} \qquad \text{[A-7]}$$

Thus, if we operate on $Y_r(\xi, t)$ by using Equation [A-7], we have

$$V_r = \frac{dY_r}{dt'} = \frac{dY_r}{dt} = \frac{\partial Y_r}{\partial t} - (U-u)\frac{\partial Y_r}{\partial \xi} \qquad \text{[A-8]}$$

and P_1 becomes

$$P_1 = -\frac{\partial}{\partial t}(m_v V_r) + (U-u)\frac{\partial}{\partial \xi}(m_v V_r) \qquad \text{[A-9]}$$

The buoyancy force may be derived by considering Figure A-1, where the elemental volume of fluid is displaced by the ship and P_w is the pressure per unit area upon the elemental volume of fluid.

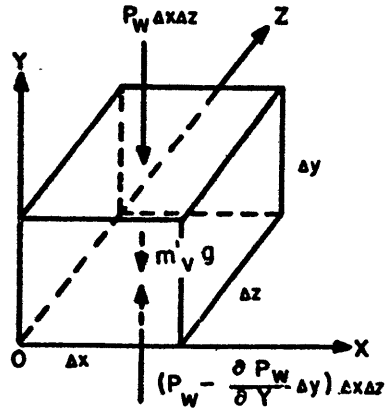

Figure A-1 – Forces Acting upon an Elemental Volume of Fluid

The application of Newton's second law of motion in the y-direction gives

$$m_v' \frac{dv}{dt'} = \left(P_w - \frac{\partial P_w}{\partial y} \Delta y \right) \Delta x \, \Delta z - P_w \, \Delta x \, \Delta z - m_v' g$$

but $m_v' = \rho \, \Delta y \, \Delta x \, \Delta z$, where ρ is the fluid density. Therefore

$$\rho \, \Delta y \, \Delta x \, \Delta z \left(g + \frac{dv}{dt'} \right) = - \frac{\partial P_w}{\partial y} \Delta y \, \Delta x \, \Delta z = - \Delta F_B' \Delta x \qquad \text{[A-10]}$$

or

$$\int_v \rho \, dy \, dx \, dz \left(g + \frac{dv}{dt'} \right) = - F_B' \int dx$$

Consider the unit length of ship,

$$\int_A \rho \, dy \, dz \left(g + \frac{dv}{dt'} \right) = - F_B'$$

but

$$\int_A dy \, dz = A$$

which is the sectional area of the displaced fluid. Thus

$$\rho A \left(g + \frac{dv}{dt'} \right) = - F_B' \qquad \text{[A-11]}$$

or, by Newton's third law,

$$\rho A \left(g + \frac{dv}{dt'} \right) = P_2'^{*} \qquad \text{[A-12]}$$

---

*This result may also be obtained simply by considering the following: If a body is resting in calm water, a buoyancy force balances out the weight of the ship; i.e., $F_B' = m_v g$. Now, if the sea is given motion, an additional force will be exerted on the ship; i.e., $F'' = m_v \frac{dv}{dt'}$. Therefore, by superposition

$$P_2' = m_v \left(g + \frac{dv}{dt'} \right) = \rho A \left(g + \frac{dv}{dt'} \right)$$

which is the buoyancy force per unit length. If the weight force is subtracted, we have

$$P_2 = \rho A \left(g + \frac{dv}{dt'}\right) - \rho g A_0 = \rho g (A - A_0) + \rho A \frac{dv}{dt'} \qquad \text{[A-13]}$$

which represents the dynamic buoyancy force deviated from still water buoyancy. The force $\rho g A_0$ represents the still water buoyancy at the ship section considered, v is the vertical velocity of the waves, and the term $\rho A \frac{dv}{dt'}$ is called the Smith correction factor.

By Equation [A-7], $\frac{dv}{dt'}$ should be transformed by

$$\frac{dv}{dt'} = \left(\frac{\partial}{\partial t} - (U - u) \frac{\partial}{\partial \xi}\right) \left(\frac{\partial Y_w}{\partial t} - (U - v) \frac{\partial Y_w}{\partial \xi}\right) \qquad \text{[A-14]}$$

The hydrodynamic damping force is expressed in the frequency domain by[12]

$$\overline{P}_3 = - B(p) \overline{V}_r \qquad \text{[A-15]}$$

where $p = j\omega$,

$\overline{P}_3$, $\overline{V}_r$ are Laplace transforms of P_3 and V_r, and

$B(p)$ can be approximated empirically.

APPROXIMATIONS IN THE HYDRODYNAMIC FORCES

Both nonlinear terms and linear terms with time-varying coefficients are found in the hydrodynamic equations. Wherever these terms have a small effect, they may be omitted. We may show that the horizontal wave velocity u is small by the following consideration:

First, we use a ship-fixed coordinate system; i.e., assume the ship to be at rest with the waves moving at a relative velocity given by $(c + U)$, where c and U are the wave propagation velocity and the ship velocity, respectively. Hence, $Y_h = 0$ and the wave height is given by

$$\begin{aligned} Y_r &= Y_h - Y_w \\ &= Y_w \\ &= - \frac{h}{2} \sin \frac{2\pi}{\lambda} [\xi + (c + U) t] \text{ --- (ship-fixed coordinates)} \end{aligned} \qquad \text{[A-16a]}$$

If the sea-fixed coordinate system is used, then

$$- Y_w = - \frac{h}{2} \sin \frac{2\pi}{\lambda} (\zeta + c t') \text{ --- (sea-fixed coordinates)} \qquad \text{[A-16b]}$$

Here we have assumed simple sinusoidal motion, where h is the peak-to-peak variation of wave height and λ is the wave length. Now, if we assume that the water particles move in circular orbits, then the maximum horizontal velocity is equal to the maximum vertical velocity; i.e., from Equation [A-16b],

$$u_{max} = \left[\frac{\partial Y_w}{\partial t'}\right]_{max} = \left[\frac{h}{2}\,\frac{2\pi c}{\lambda}\,\cos\,\frac{2\pi}{\lambda}(\zeta + ct')\right]_{max} = \frac{\pi h c}{\lambda} \qquad [A\text{-}17]$$

But $\frac{h}{\lambda} \leq 0.14$ (since the waves become unstable for larger ratios).[13] However, there are no known records of either ocean or laboratory waves attaining such extreme heights. From observations, assuming $\left[\frac{h}{\lambda}\right]_{max} = 0.05$ for long-crested waves, we have

$$u_{max} = 0.05\ \pi c = 0.157\ c \qquad [A\text{-}18]$$

Therefore, from Equation [A-16a],

$$\left[\frac{\partial Y_r}{\partial t}\right]_{max} = -\,\frac{\pi h}{\lambda}(c+U)\,\cos\,\frac{2\pi}{\lambda}[\xi + (c+U)t]_{max}$$

$$= \frac{\pi h}{\lambda}(c+U) \qquad [A\text{-}19a]$$

$$\left[\frac{\partial Y_r}{\partial \xi}\right]_{max} = -\,\frac{\pi h}{\lambda}\,\cos\,\frac{2\pi}{\lambda}[\xi + (c+U)t]_{max} = \frac{\pi h}{\lambda}$$

$$\left[U\,\frac{\partial Y_r}{\partial \xi}\right]_{max} = \frac{\pi h}{\lambda}U \qquad [A\text{-}19b]$$

and

$$u_{max}\left[\frac{\partial Y_r}{\partial \xi}\right]_{max} = \frac{\pi h}{\lambda}(0.157\ c) = (0.157)^2\ c \qquad \text{[A-20]}$$

If U and c are nearly equal to each other, the term in Equation [A-19b] is more important and even if $U \ll c$, Equation [A-20] is still small and, hence, the terms involving u may be neglected.

In the analog computer simulation of the sea, it is assumed that the sea is represented by wave trains whose frequency components travel with the same velocity c. With this assumption, and neglecting the terms proportional to u, we have from Equation [A-14],

$$\frac{dv}{dt'} = \left(\frac{\partial}{\partial t} - U\ \frac{\partial}{\partial \xi}\right)\left(\frac{\partial Y_w}{\partial t} - U\ \frac{\partial Y_w}{\partial \xi}\right) \qquad \text{[A-21]}$$

however,

$$\frac{\partial Y_w}{\partial \xi} = \frac{\pi h}{\lambda} \cos\ \frac{2\pi}{\lambda}(\xi + [c+U]t)$$

and

$$\frac{\partial Y_w}{\partial t} = \frac{\pi h}{\lambda}(c+U) \cos\ \frac{2\pi}{\lambda}(\xi + [c+U]t)$$

which are obtained from Equation [A-16a]. Therefore,

$$\frac{\partial Y_w}{\partial t} = (c+U)\ \frac{\partial Y_w}{\partial \xi} \qquad \text{[A-22]}$$

Substitution into Equation [A-21] yields

$$\frac{dv}{dt'} = \left(\frac{\partial}{\partial t} - U\,\frac{\partial}{\partial \xi}\right)\left(1 - \frac{U}{c+U}\right)\frac{\partial Y_w}{\partial t}$$

$$= \left(\frac{\partial}{\partial t} - U\,\frac{\partial}{\partial \xi}\right)\left(\frac{c}{c+U}\right)\frac{\partial Y_w}{\partial t}$$

$$= \left(\frac{\partial^2 Y_w}{\partial t^2} - U\,\frac{\partial^2 Y_w}{\partial \xi\,\partial t}\right)\left(\frac{c}{c+U}\right)$$

but from Equation [A-22], we obtain

$$\frac{dv}{dt'} = \left(\frac{\partial^2 Y_w}{\partial t^2} - \frac{U}{c+U}\,\frac{\partial^2 Y_w}{\partial t^2}\right)\left(\frac{c}{c+U}\right)$$

therefore

$$\frac{dv}{dt'} = \left(\frac{c}{c+U}\right)^2 \frac{\partial^2 Y_w}{\partial t^2} \qquad \text{[A-23]}$$

In the Smith correction term $\rho A\,\frac{dv}{dt'}$, A will be replaced by its equilibrium value A_0. Thus the buoyancy force in Equation [A-13] becomes

$$P_2 = \rho g(A - A_0) + \rho A_0\left(\frac{c}{c+U}\right)^2 \frac{\partial^2 Y_w}{\partial t^2} \qquad \text{[A-24]}$$

Actually, A_0 is a quantity that must be known anyway, but this greatly simplifies the second term in Equation [A-24], since it is a constant for a particular sea and ship velocity. To summarize, the following equations will be simulated on the analog by the force generator:

$$P = P_1 + P_2 + P_3 = P_1 + P_2 + \overline{P}_3 \qquad \text{[A-25]}$$

where

$$P_1 = -\frac{\partial}{\partial t}(m_v V_r) + U\,\frac{\partial}{\partial \xi}(m_v V_r) \qquad \text{[A-26]}$$

$$P_2 = \rho g(A - A_0) + \rho A_0 \left(\frac{c}{c+U}\right)^2 \frac{\partial^2 Y_w}{\partial t^2} \qquad \text{[A-27]}$$

$$\bar{P}_3 = -B(p)\,\bar{V}_r \qquad \text{[A-28]}$$

and

$$V_r = \frac{\partial Y_r}{\partial t} - U\,\frac{\partial Y_r}{\partial \xi} \qquad \text{[A-29]}$$

$$Y_r = Y_h - Y_w \qquad \text{[A-30]}$$

As stated previously, the term $B(p)$ will be approximated empirically.

SIMULATION OF HYDRODYNAMIC TERMS

Nonlinear terms that occur in the hydrodynamic force are the apparent mass m_v and the cross-sectional area A. The terms m_v and A are separated into linear and nonlinear parts so that they may be simulated separately on the analog. This is shown as follows:

$$m_v = m_0 + \bar{m} \qquad \text{[A-31]}$$

where m_0 is the linear part and $\bar{m}$ the nonlinear part,

$$A = A_0 - b_1 Y_r + \bar{A} \qquad \text{[A-32]}$$

where b_1 is the beam of the ship at the still waterline (see Figure A-2), Y_r is measured positive below the still waterline, and $b_1 Y_r$ is the linear part and $\bar{A}$ the nonlinear part.

In Equation [A-31], the nonlinear apparent mass $\bar{m}$ has two values, depending upon whether the ship is emerging or immerging; i.e.,

$$\bar{m} = m_1 \text{ for } V_r > 0 \qquad \text{(emersion)}$$

$$\bar{m} = m_2 \text{ for } V_r < 0 \qquad \text{(immersion)}$$

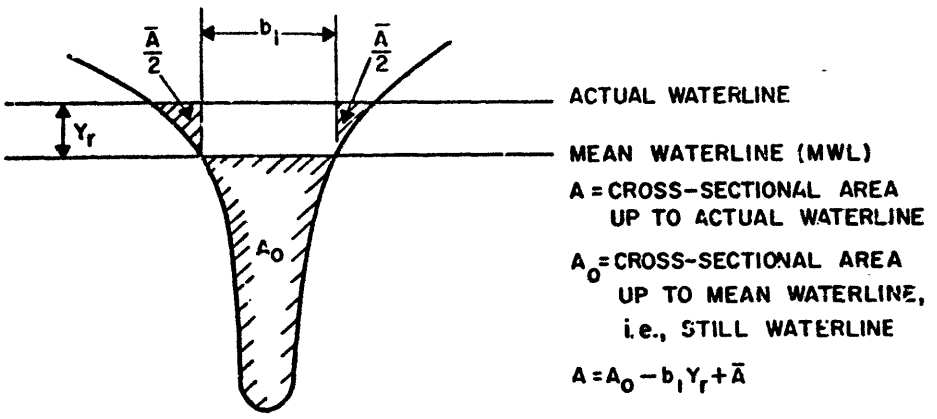

Figure A-2 – Method Used to Separate the Linear and Nonlinear Buoyancy Force

Note: Y_r is measured positive below the still waterline.

The substitution of Equation [A-31] into Equation [A-26] results in the equation

$$P_1 = -\frac{\partial}{\partial t}(m_0 + \bar{m})\, V_r + U\, \frac{\partial}{\partial \xi}(m_0 + \bar{m})\, V_r \qquad \text{[A-33]}$$

Now substituting Equation [A-29] into the first term of Equation [A-33] gives

$$P_1 = -\frac{\partial}{\partial t}(m_0 + \bar{m}) \left[\frac{\partial Y_r}{\partial t} - U\, \frac{\partial Y_r}{\partial \xi}\right] + U\, \frac{\partial}{\partial \xi}(m_0 + \bar{m})\, V_r \qquad \text{[A-34]}$$

or

$$P_1 = -m_0\, \frac{\partial^2 Y_r}{\partial t^2} + m_0 U\, \frac{\partial^2 Y_r}{\partial \xi\, \partial t} - \frac{\partial}{\partial t}(\bar{m} V_r) + U\, \frac{\partial}{\partial \xi}(m_0 V_r + \bar{m} V_r) \qquad \text{[A-35]}$$

The substitution of Equation [A-32] into Equation [A-27] gives

$$P_2 = \rho g(-b_1 Y_r + \bar{A}) + \rho A_0 \left(\frac{c}{c+U}\right)^2 \frac{\partial^2 Y_w}{\partial t^2} \qquad \text{[A-36]}$$

Next the nonlinear term $\overline{A}$ is expanded into a power series by

$$\overline{A} = b_2 Y_r^2 + b_3 Y_r^3 \qquad \text{[A-37]}$$

The nonlinear added mass terms are approximated similarly; i.e.,

$$m_1 = a_1 Y_r + a_2 Y_r^2 + a_3 Y_r^3 \qquad \text{[A-38]}$$

$$m_2 = c_1 Y_r + c_2 Y_r^2 + c_3 Y_r^3 \qquad \text{[A-39]}$$

where a_1, a_2, a_3, b_2, b_3, c_1, c_2, and c_3 are arbitrary constants to be determined.

If the Smith correction term in Equation [A-24] is added to the first term in Equation [A-35], the resulting equation is

$$P_p = -m_0 \frac{\partial^2 Y_r}{\partial t^2} + \rho A_0 \left(\frac{c}{c+U}\right)^2 \frac{\partial^2 Y_w}{\partial t^2}$$

$$= -m_0 \left[\frac{\partial^2 Y_h}{\partial t^2} - \frac{\partial^2 Y_w}{\partial t^2}\right] + \rho A_0 \left(\frac{c}{c+U}\right)^2 \frac{\partial^2 Y_w}{\partial t^2}$$

$$= -m_0 \left\{\frac{\partial^2 Y_h}{\partial t^2} - \left[1 + \frac{\rho A_0}{m_0}\left(\frac{c}{c+U}\right)^2\right] \frac{\partial^2 Y_w}{\partial t^2}\right\} \qquad \text{[A-40]}$$

This term will be generated passively by the analog computer. The remaining hydrodynamic terms, to be generated by active elements, are

$$P_a = P - P_p = m_0 U \frac{\partial^2 Y_r}{\partial \xi \partial t} - \frac{\partial}{\partial t}(\overline{m} V_r) + U \frac{\partial}{\partial \xi}(m_0 V_r + \overline{m} V_r)$$

$$+ \rho g (-b_1 Y_r + \overline{A}) - B(p) \overline{V}_r \qquad \text{[A-41]}$$

$B(p)$ is simulated by the ratio of two polynomial functions of p, selected empirically to give good fit to the real part of $B(p)$.

FINITE DIFFERENCE EQUATION OF THE HYDRODYNAMIC FORCE

In the analog computer analysis, the ship is represented as a lumped parameter system with concentrated masses and springs. Velocities are defined only at discrete points. Hydrodynamic forces for the lumped model are obtained by integrating the hydrodynamic force densities over the appropriate longitudinal intervals. Such an interval is replaced by the value of the density function, evaluated at the center of the interval, and multiplied by the interval. Thus

$$F_n = \int_{\xi_{n-1/2}}^{\xi_{n+1/2}} P(\xi)\, d\xi = (\xi_{n+1/2} - \xi_{n-1/2})\, P(\xi_n) \qquad \text{[A-42]}$$

Space derivatives are approximated by the following:

$$\left(\frac{\partial f}{\partial \xi}\right)_{\xi_n} = \frac{f(\xi_{n+1}) - f(\xi_{n-1})}{\xi_{n+1} - \xi_{n-1}} \qquad \text{[A-43]}$$

The following definitions also apply:

$$\xi_{n+1/2} - \xi_{n-1/2} = \Delta\xi \qquad \text{[A-44]}$$

$$\xi_{n+1} - \xi_{n-1} = 2\,\Delta\xi \qquad \text{[A-45]}$$

Using the above rules, Equations [A-29], [A-40], and [A-41] become

$$V_{r_n} = \dot{Y}_{r_n} - U \left\{ \frac{Y_{r_{n+1}} - Y_{r_{n-1}}}{2\,\Delta\xi} \right\} \qquad \text{[A-46]}$$

$$F_{P_n} = -\,m_{0_n}\,\Delta\xi \left\{ \frac{\partial \dot{Y}_{h_n}}{\partial t} - \left[1 + \frac{\rho A_{0_n}}{m_{0_n}} \left(\frac{c}{c+U} \right)^2 \right] \frac{\partial \dot{Y}_{w_n}}{\partial t} \right\} \qquad \text{[A-47]}$$

and

$$F_{a_n} = \Delta\xi \left\{ \frac{m_{0_n} U}{2\Delta\xi} \left(\dot{Y}_{r_{n+1}} - \dot{Y}_{r_{n-1}} \right) - \frac{\partial}{\partial t} (\bar{m} V_r)_n \right.$$

$$+ \frac{U}{2\Delta\xi} \left[(m_0 + \bar{m})_{n+1} V_{r_{n+1}} - (m_0 + \bar{m})_{n-1} V_{r_{n-1}} \right]$$

$$\left. + \rho g \left[-(b_1 Y_r)_n + \bar{A}_n \right] - (B(p) \bar{V}_r)_n \right\} \qquad \text{[A-48]}$$

At bow Station N and at stern Station 1, the above formulas are modified as

$$V_{r_N} = \dot{Y}_{r_N} - \frac{U}{\Delta\xi} \left(Y_{r_N} - Y_{r_{N-1}} \right) \qquad \text{[A-49]}$$

and

$$V_{r_1} = \dot{Y}_{r_1} - \frac{U}{\Delta\xi} \left(Y_{r_2} - Y_{r_1} \right) \qquad \text{[A-50]}$$

The term $U \frac{\partial}{\partial\xi}(m_0 + \bar{m}) V_r$ in Equation [A-41] becomes:

$$\int_{\text{Stern}}^{\text{Sta 1.5}} U \frac{\partial}{\partial\xi} [(m_0 + \bar{m}) V_r] \, d\xi = U(m_0 + \bar{m})_{1.5} V_{r_{1.5}}$$

$$\simeq \frac{U}{2} \left[(m_0 + \bar{m})_2 V_{r_2} + (m_0 + \bar{m})_1 V_{r_1} \right]$$

$$\int_{\text{Sta } N=0.5}^{\text{Bow}} U \frac{\partial}{\partial\xi} [(m_0 + \bar{m}) V_r] \, d\xi = - U(m_0 + \bar{m})_{N-0.5} V_{r_{N-0.5}}$$

$$\simeq \frac{U}{2} \left[(m_0 + \bar{m})_{N-1} V_{r_{N-1}} + (m_0 + \bar{m})_N V_{r_N} \right]$$

where $(m_0 + \bar{m})$ is zero at the stern or at the bow.

The following expressions replace Equation [A-48] at the bow and stern:

$$F_{a_N} = \Delta\xi \left\{ \frac{m_{0_N} U}{\Delta\xi} \left(\dot{Y}_{r_N} - \dot{Y}_{r_{N-1}} \right) - \frac{\partial}{\partial t} (\bar{m} V_r)_N \right\}$$

$$- \frac{U}{2} \left\{ [(m_0 + \bar{m}) V_r]_{N-1} + [(m_0 + \bar{m}) V_r]_N \right\}$$

$$+ \Delta\xi \left\{ \rho g \left([-b_1 Y_r]_N + \bar{A}_N \right) - [B(p) \bar{V}_r]_N \right\} \qquad \text{[A-51]}$$

$$F_{a_1} = \Delta\xi \left\{ \frac{\bar{m}_{0_1} U}{\Delta\xi} \left(\dot{Y}_{r_2} - \dot{Y}_{r_1} \right) - \frac{\partial}{\partial t} (\bar{m} V_r)_1 \right\}$$

$$+ \frac{U}{2} \left\{ [(m_0 + \bar{m}) V_r]_1 + [(m_0 + \bar{m}) V_r]_2 \right\}$$

$$+ \Delta\xi \left\{ \rho g \left[(-b_1 Y_r)_1 + \bar{A}_1 \right] - [B(p) \bar{V}_r]_1 \right\} \qquad \text{[A-52]}$$

The approximations for the analog simulation of hydrodynamic equations are summarized as follows:

1. u is assumed to be zero.
2. The surface wave of the sea propagates at the same velocity for all wave frequencies.
3. In the Smith correction term $\rho A \frac{dv}{dt}$, A is replaced by an equivalent value of A_0.
4. Nonlinear added mass m is a function of Y_r; i.e.,

$$\bar{m} = m_1 \cong a_1 Y_r + a_2 Y_r^2 + a_3 Y_r^3 \quad \text{for} \quad V_r > 0$$

$$= m_2 \cong c_1 Y_r + c_2 Y_r^2 + c_3 Y_r^3 \quad \text{for} \quad V_r < 0$$

5. Nonlinear cross-sectional area $\bar{A}$ is a function of Y_r also; i.e.,

$$\bar{A} = b_2 Y_r^2 + b_3 Y_r^3$$

6. In the hydrodynamic damping term $\overline{P}_3 = -B(p)\,\overline{V}_r$, $B(p)$ is simulated by the ratio of two polynomial functions of p, selected empirically to give a good fit to the real part of $B(p)$.

7. Differential operators are replaced by difference operators.

APPENDIX B

INPUT DATA FOR ESSEX

The cellular divisions used in the analysis of ESSEX are shown in Figure 2. Masses of the ship are lumped at 21 equally spaced points at intervals of 41 ft. The bending rigidity is evaluated at these same points and the shear rigidity and rotary inertia are evaluated at points midway between mass locations. These data are recorded in Table 1, page 40.

Figure 2 also shows the manner in which hydrodynamic forces are applied to the lumped model of the ship. The hydrodynamic force terms given in Equations [A-26] and [A-27] are evaluated at nine stations (3, 5, 7, 9, 11, 13, 15, 17, and 19). At four stations (3, 15, 17, and 19), nonlinear buoyancy and virtual mass effects are included. At these four stations, the buoyancy forces are equally distributed to either two or three points in the analog of the ship structure in order to obtain a more uniform force distribution.

The linear hydrodynamic properties used in the analysis are listed in Table 4. The buoyancy spring K_b is equal to $\rho g b_1 \Delta\xi$ in Equation [A-52]. Where $\Delta\xi$ is equal to 82 ft, the properties listed in Table 4 were derived from values of m_v, b_1, and A_0 recorded at the 21 equally spaced stations.

The Smith correction factor is obtained from Equation [A-47]; i.e.,

$$SCF = \frac{\rho A_{0_N} \Delta\xi}{m_{0_n}} \qquad \text{[B-1]}$$

As an example, the values listed in Table 4 for Station 5 at the design waterline of 28.5 ft are computed. The following value for m_{0_5} comes from Table B-1:

$$m_{0_5} = \left(\frac{1}{2} m'_{0_4} + m'_{0_5} + \frac{1}{2} m'_{0_6}\right) = (42.1 + 107.4 + 63.5) = 213.1 \text{ ton-sec}^2/\text{ft}$$

The buoyancy spring constant K_b is obtained as follows:

$$K_{b_5} = \rho g b_{1_5} \Delta\xi = \frac{1}{3}\left(b'_{1_4} + b'_{1_5} + b'_{1_6}\right) \rho g \Delta\xi$$

$$= \frac{1}{3}(94.8 + 100.1 + 102.4)\,(0.03205)\,(82)$$

$$\therefore K_{b_5} \simeq 261$$

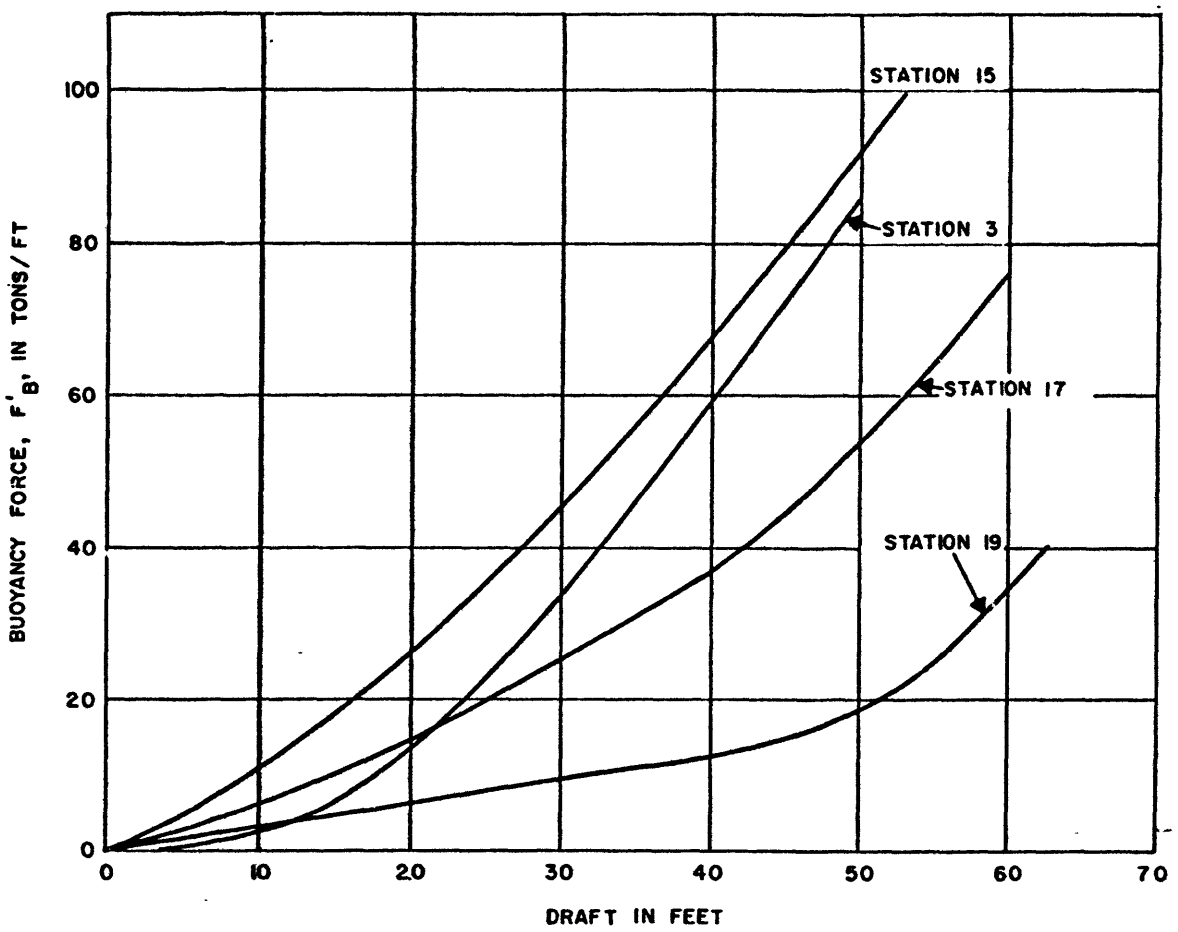

Figure B-1 – Variation of Buoyancy Force with Draft

From Equation [B-1] we have, for the Smith correction factor, the following:

$$SCF = \frac{\rho A_{0_5} \Delta\xi}{m_{0_5}} = \left(\frac{0.03205}{32.17}\right)\left(\frac{1}{2}\right)\left(\frac{1}{2}A'_{0_4} + A'_{0_5} + \frac{1}{2}A'_{0_6}\right)\frac{82}{213.1}$$

$$= 0.0003833\,(786 + 2035.4 + 1209.2) = 0.771$$

The nonlinear buoyancy forces used in the analysis are plotted in Figure 3 as functions of emersion. These curves were derived from curves of the total buoyancy force (Figure B-1) for a 1-ft section at Stations 3, 15, 17, and 19 by subtracting out the linear spring rates recorded in Table 4. A scale adjustment to the original curves was required in order to make their slopes at $Y_r = 0$ compatible with the tabulated linear spring rates. An example of the computation follows.

For various values of Y_r, we determine the actual waterline by

$$Y_r = + Y_{MWL} - Y_{AWL} \qquad [B\text{-}2]$$

where Y_{MWL} is the position of the mean waterline at a particular station. From Figure B-1, we obtain the value of buoyancy force for Y_{AWL} and Y_{MWL}. Next, from Table 4 we determine the value of the linear spring rate for Station 5. Thus,

$$\rho g\,(A - A_0)\,\Delta\xi + K_b\,Y_r = \rho g\,\bar{A}\,\Delta\xi \qquad [B\text{-}3]$$

By Equation [B-3], we obtain the value of the nonlinear buoyancy force for a particular station. The approximations to the nonlinear buoyancy forces used in the simulation are plotted in Figure 3. Algebraic expressions for these approximations are given in Table 3. These were obtained by fitting the best mathematical curve to the data points for the nonlinear buoyancy force.

The nonlinear added masses used in the analysis are plotted in Figure 4 as functions of emersion. These curves were derived from curves of total added mass for a 1-ft section (see Tables B-2 to B-5) by subtracting out the constant added masses recorded in Table 4. A scale adjustment to the original curves was required in order to make the values at $Y_r = 0$ compatible. The approximations are plotted in Figure 4. Algebraic expressions for these approximations are given in Table 3. An example of the computation follows: First choose any Y_{AWL} for a particular section that is the actual waterline of the section. Then

$$Y_r = Y_{MWL} - Y_{AWL} \qquad [B\text{-}4]$$

where Y_{MWL} is the mean waterline and is equal to 28.5 ft. Then from Tables B-2 to B-5, we find the corresponding value of the total added mass m_v. Next, we subtract out the value of constant added mass m_0 listed in Table 4. This result gives the nonlinear virtual mass $\bar{m}$.

Curves of the hydrodynamic damping coefficient for a 1-ft section are shown in Figure 5. The damping coefficient is related to the transfer function as follows: In general,

$$\bar{P}_3 = -B(p)\,\bar{V}_r \qquad \text{[B-5]}$$

For $p = i\omega$,

$$\bar{P}_3 = -B(j\omega)\,\bar{V}_r = -[C(\omega) + jD(\omega)]\,\bar{V}_r \qquad \text{[B-6]}$$

where $C(\omega)$ is the hydrodynamic damping coefficient. In the electrical analogy, $B(p)$ is approximated by a function with the following form; see Appendix C:

$$B(p) = \frac{\tau_2 p\, B_0}{\tau_2 p + (1 + \tau_1 p)^2} \qquad \text{[B-7]}$$

from which the damping coefficient is

$$C(\omega) = \frac{B_0\, R}{1 + \left(\frac{R\tau_1}{\tau_2}\right)^2 \left(\frac{\omega_0}{\omega} - \frac{\omega}{\omega_0}\right)^2} \qquad \text{[B-8]}$$

where $R = \dfrac{\tau_2}{\tau_2 + 2\tau_1}$ and $\omega_0 = \dfrac{1}{\tau_1}$; see Appendix C. The maximum value of $C(\omega)$ occurs at $\omega = \omega_0$. Then

$$C(\omega)_{max} = B_0\, R$$

The power spectrum of the three sea states used in the analysis are plotted in Figures 6, 7, and 8. The rms value of wave height is also given in these figures. This rms value of wave height is computed from the formula

$$\bar{Y}_w = \sqrt{\int_0^\infty \Phi(\omega)\, d\omega} \qquad \text{[B-9]}$$

where $\Phi(\omega)$ is the power spectral density function. The mean value of peak-to-peak wave height is approximately equal to 2.8 times the rms value. For the sea state shown in Figure 6, the contribution to the integral for values of ω below 0.25 was ignored.

Approximations to the power spectral density functions used in the analysis are plotted in Figures 6, 7, and 8. These curves were obtained from the response of electrical filters used in the simulation of random sea states.

The velocity of wave propagation of sea surface is an important parameter in the analysis, and it has been established that

$$c(\text{fps}) = \frac{g}{\omega} \qquad \text{[B-10]}$$

The value of c obtained from Equation [B-10] was used to design the delay line and to compute the Smith correction in Equation [A-47]. The wave velocity relative to the ship is equal to $c + U$. When sea-fixed power spectral distribution function is expressed in terms of ship-fixed coordinates, the magnitude of the function is decreased by the factor $1/\left(1 + \frac{U}{c}\right)$ and the frequency scale is increased by the factor $\left(1 + \frac{U}{c}\right)$. The wave velocity for a particular sea state is chosen to correspond to the frequency at the peak of the power spectral density function.

TABLE B-1

Added Mass as a Function of Design Waterline of 28.5 Feet

Station n	Added Mass m'_{0_n} ton-sec^2/ft	Station n	Added Mass m'_{0_n} ton-sec^2/ft	Station n	Added Mass m'_{0_n} ton-sec^2, ft
0	0.23	7	146.06	14	99.87
1	18.12	8	157.76	15	60.58
2	37.34	9	164.27	16	36.97
3	59.43	10	163.27	17	18.19
4	84.20	11	155.58	18	7.96
5	107.44	12	140.39	19	3.48
6	127.03	13	117.14	20	0.71

Note: The values for add mass are lumped extending over the ship length from Station $(n - \frac{1}{2})$ to Station $(n + \frac{1}{2})$.

TABLE B-2

Added Mass as a Function of Immersion or Emersion, Station 3

A. Immersion

Immersion y ft	Half Breadth b ft	Added Mass per Unit Length m_1 ton-sec^2 ft^2	Immersion y ft	Half Breadth b ft	Added Mass per Unit Length m_1 ton-sec^2 ft^2	Immersion y ft	Half Breadth b ft	Added Mass per Unit Length m_1 ton-sec^2 ft^2
12	12.60	0.36	25	36.45	2.44	38	42.65	2.75
13	15.10	0.51	26	37.20	2.45	39	42.95	2.75
14	17.70	0.69	27	37.95	2.45	40	43.20	2.76
15	19.90	0.86	28	38.55	2.46	41	43.50	2.78
16	22.30	1.06	29	39.10	2.51	42	43.75	2.80
17	24.60	1.27	30	39.60	2.54	43	43.95	2.84
18	26.75	1.48	31	40.15	2.61	44	44.20	2.86
19	28.55	1.65	32	40.55	2.64	45	44.45	2.89
20	30.20	1.82	33	40.95	2.68	46	44.70	2.92
21	31.70	1.97	34	41.30	2.70	47	44.95	2.93
22	33.05	2.12	35	41.70	2.74	48	45.10	2.93
23	34.30	2.25	36	42.00	2.74			
24	35.55	2.39	37	42.35	2.75			

B. Emersion

Emersion y ft	Half Breadth b ft	Added Mass per Unit Length m_2 ton-sec^2 ft^2	Emersion y ft	Half Breadth b ft	Added Mass per Unit Length m_2 ton-sec^2 ft^2	Emersion y ft	Half Breadth b ft	Added Mass per Unit Length m_2 ton-sec^2 ft^2
12	12.60	0.19	25	36.45	1.58	38	42.65	2.33
13	15.10	0.28	26	37.20	1.64	39	42.95	2.37
14	17.70	0.38	27	37.95	1.67	40	43.20	2.41
15	19.90	0.47	28	38.55	1.70	41	43.50	2.45
16	22.30	0.59	29	39.10	1.76	42	43.75	2.51
17	24.60	0.73	30	39.60	1.84	43	43.95	2.54
18	26.75	0.87	31	40.15	1.92	44	44.20	2.57
19	28.55	0.99	32	40.55	2.04	45	44.45	2.62
20	30.20	1.11	33	40.95	2.13	46	44.70	2.62
21	31.70	1.23	34	41.30	2.17	47	44.95	2.62
22	33.05	1.34	35	41.70	2.22	48	45.10	2.62
23	34.30	1.43	36	42.00	2.26			
24	35.55	1.53	37	42.35	2.30			

TABLE B-3

Added Mass as a Function of Immersion or Emersion, Station 15

Immersion or Emersion y ft	Half Breadth b ft	Added Mass per Unit Length m_1 or m_2 ton-sec^2 ft^2	Immersion or Emersion y ft	Half Breadth b ft	Added Mass per Unit Length m_1 or m_2 ton-sec^2 ft^2	Immersion or Emersion y ft	Half Breadth b ft	Added Mass per Unit Length m_1 or m_2 ton-sec^2 ft^2
0	0	0	19.84	31.4	1.22	37.39	37.2	1.64
1	7.00	0.09	20.28	31.6	1.24	38	37.45	1.67
2	11.60	0.22	20.80	31.8	1.26	39	37.90	1.69
3	14.70	0.33	21.41	32.0	1.27	40	38.25	1.72
4	17.30	0.41	22.10	32.2	1.29	41	38.85	1.76
5	19.10	0.48	22.85	32.6	1.31	42	39.35	1.78
6	20.90	0.55	23.67	32.8	1.35	43	39.85	1.82
7	22.20	0.61	24.53	33.0	1.37	44	40.40	1.86
8	23.55	0.67	25.45	33.3	1.39	45	40.95	1.90
9	24.60	0.72	26.40	33.6	1.42	46	41.50	1.95
10	25.55	0.76	27.37	33.9	1.44	47	42.00	1.99
11	26.35	0.82	28.35	34.2	1.47	48	42.60	2.03
12	27.15	0.87	29.32	34.4	1.49	49	43.05	2.07
13	27.80	0.91	30.27	34.6	1.49	50	43.65	2.12
14	28.50	0.96	31.22	34.9	1.51	51	44.15	2.16
15	29.15	1.02	32.17	35.2	1.54	52	44.70	2.21
16	29.70	1.06	32.96	35.5	1.57	53	45.20	2.26
17	30.15	1.11	33.76	35.8	1.57	54	45.75	2.32
18	30.65	1.16	34.50	36.0	1.59			
18.98	31.00	1.19	35.15	36.3	1.60			
19.23	31.10	1.20	35.75	35.6	1.61			
19.50	31.20	1.21	36.65	36.9	1.64			

TABLE B-4

Added Mass as a Function of Immersion or Emersion, Station 17

A. IMMERSION

Immersion y ft	Half Breadth b ft	Added Mass per Unit Length m_1 ton-sec^2/ft^2	Immersion y ft	Half Breadth b ft	Added Mass per Unit Length m_1 ton-sec^2/ft^2	Immersion y ft	Half Breadth b ft	Added Mass per Unit Length m_1 ton-sec^2/ft^2
0	0	0	72.03	17.3	0.37	48	31.30	1.54
1	5.30	0.05	73.86	17.8	0.39	49	32.65	1.68
2	7.30	0.06	75.74	18.2	0.41	50	33.90	1.81
3	8.60	0.10	27.62	18.7	0.43	51	35.30	1.96
4	9.70	0.13	29.52	19.2	0.46	52	36.70	2.13
5	10.50	0.15	31.37	19.7	0.48	53	37.80	2.26
6	11.20	0.16	33.20	20.1	0.50	54	39.25	2.44
7	11.80	0.18	34.95	20.7	0.54	55	40.55	2.61
8	12.50	0.2[illegible]	36.63	21.3	0.64	56	42.10	2.82
9	12.95	0.21	38.21	22.1	0.71	57	43.35	2.99
9.49	13.2	0.22	39.70	22.9	0.78	58	44.70	3.17
10.07	13.4	0.23	41.06	23.9	0.87	59	46.00	3.36
10.84	13.8	0.24	42.30	24.8	0.94	60	47.75	3.62
11.76	14.1	0.25	43.38	25.9	1.04	61	49.20	3.85
12.83	14.5	0.26	44.34	26.8	1.11	62	50.60	4.07
14.07	15.0	0.28	45.14	27.6	1.19	63	52.10	4.31
15.43	15.4	0.29	45.80	27.5	1.22			
16.95	15.9	0.31	46.30	28.4	1.26			
18.55	16.3	0.33	46.67	29.5	1.36			
20.26	16.8	0.34	47.00	29.95	1.41			

B. Emersion

Emersion y ft	Half Breadth b ft	Added Mass per Unit Length m_2 ton-sec^2/ft^2	Emersion y ft	Half Breadth b ft	Added Mass per Unit Length m_2 ton-sec^2/ft^2	Emersion y ft	Half Breadth b ft	Added Mass per Unit Length m_2 ton-sec^2/ft^2
0	0	0	20.95	17.00	0.36	45.31	27.90	0.82
1	5.30	0.05	22.31	17.40	0.38	45.87	28.60	0.91
2	7.30	0.08	22.70	17.70	0.39	46.32	29.10	0.95
3	8.60	0.10	25.11	18.10	0.41	47	29.95	1.00
4	9.70	0.13	26.54	18.50	0.43	48	31.30	1.09
5	10.50	0.15	27.97	18.80	0.44	49	32.55	1.18
6	11.20	0.16	29.40	19.20	0.45	50	33.90	1.27
7	11.80	0.18	30.81	19.50	0.46	51	35.30	1.38
8	12.50	0.20	32.23	19.90	0.47	52	36.70	1.49
9	12.95	0.21	33.60	20.30	0.49	53	37.80	1.58
10.76	13.80	0.24	34.94	20.70	0.50	54	39.25	1.71
11.31	14.00	0.25	36.26	21.20	0.52	55	40.55	1.82
12.43	14.40	0.26	37.53	21.80	0.54	56	42.10	1.96
13.18	14.70	0.27	38.75	22.50	0.58	57	43.35	2.08
14.02	15.00	0.28	39.91	23.20	0.61	58	44.70	2.21
14.99	15.30	0.29	41.02	23.90	0.65	59	46.00	2.34
16.03	15.60	0.30	42.03	24.70	0.68	60	47.75	2.53
17.17	16.00	0.32	42.98	25.50	0.73	61	49.20	2.69
18.36	16.30	0.33	43.84	26.30	0.77	62	50.60	2.84
19.64	16.60	0.34	44.61	27.10	0.82	63	52.10	3.01

TABLE B-5
Added Mass as a Function of Immersion or Emersion, Station 19 (Bow)

A. Immersion

Immersion y ft	Half Breadth b ft	Added Mass per Unit Length m_1 ton-sec^2 ft^2	Immersion y ft	Half Breadth b ft	Added Mass per Unit Length m_1 ton-sec^2 ft^2	Immersion y ft	Half Breadth b ft	Added Mass per Unit Length m_1 ton-sec^2 ft^2
0.43	2.8	0.01	52.76	28.6	0.77	56.75	28.6	1.57
1.62	4.4	0.03	54.07	28.1	0.99	57.20	29.2	1.61
3.07	5.3	0.04	55.17	28.3	1.21	57.48	29.8	1.61
4.76	5.9	0.05	56.05	28.9	1.41			
6.65	6.2	0.05						
8.75	6.3	0.06						
11.05	6.3	0.07						
13.51	6.1	0.07						
16.08	5.8	0.08						
18.78	5.5	0.08						
21.53	5.3	0.08						
24.37	5.0	0.08						
27.19	4.9	0.08						
30.03	4.9	0.08						
32.82	4.9	0.08						
35.57	5.1	0.08						
38.23	5.7	0.09						
40.78	6.9	0.10						
43.19	8.3	0.13						
45.47	10.3	0.17						
47.56	12.4	0.23						
49.49	14.8	0.39						
51.23	17.3	0.56						

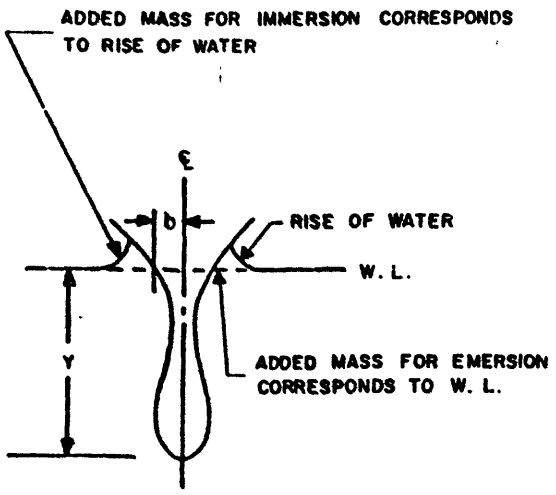

B. Emersion

Emersion y ft	Half Breadth b ft	Added Mass per Unit Length m_2 ton-sec^2 ft^2	Emersion y ft	Half Breadth b ft	Added Mass per Unit Length m_2 ton-sec^2 ft^2	Emersion y ft	Half Breadth b ft	Added Mass per Unit Length m_2 ton-sec^2 ft^2
0.23	2.0	0	14.77	5.9	0.08	42.03	7.6	0.10
0.29	2.4	0.01	16.95	5.7	0.08	44.04	9.1	0.12
0.61	3.0	0.01	19.21	5.5	0.08	45.94	10.7	0.15
1.17	3.9	0.02	21.50	5.3	0.08	47.73	12.6	0.19
1.94	4.6	0.03	23.85	5.0	0.08	49.41	14.7	0.25
2.94	5.2	0.04	26.20	4.9	0.08	50.95	17.2	0.33
4.14	5.7	0.04	28.56	4.9	0.08	52.36	19.8	0.42
5.54	6.1	0.05	30.92	4.8	0.08	53.61	22.1	0.54
7.10	6.3	0.06	33.24	4.9	0.08	54.71	24.3	0.66
8.82	6.3	0.06	35.54	5.1	0.08	55.62	26.0	0.76
10.69	6.3	0.07	37.77	5.7	0.09	56.32	27.7	0.85
12.68	6.1	0.07	39.95	6.5	0.09	57.30	29.3	0.96

APPENDIX C

SIMULATION OF HYDRODYNAMIC FORCES IN ANALOG COMPUTATIONS

Figure C-1 shows a schematic of the circuit employed in simulating Equation [A-47]. To verify that this circuit does simulate the force F_{P_n}, consider the voltage drop $e_1 - e_3$, thus

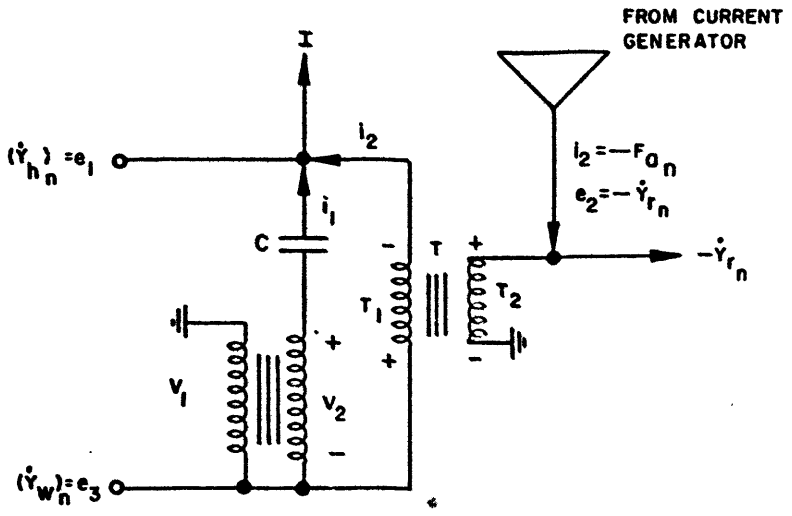

Figure C-1 – Circuit for Simulating F_{P_n}

$$e_1 - e_3 = -\frac{1}{C}\int i_1\,dt + V_2 \qquad \text{[C-1]}$$

but

$$e_3 - \frac{1}{K}V_2 = V_1 \qquad \text{[C-2]}$$

Now, substituting Equation [C-1] into [C-2] gives

$$e_1 - V_1 - KV_1 + \frac{1}{C}\int i_1\,dt = 0$$

or

$$-C\left[\dot{e}_1 - \dot{V}_1\,(1+K)\right] - i_1 \qquad \text{[C-3]}$$

Comparison with Equation [A-47] shows that

$$C = m_{0_n}\,\Delta\xi$$

$$i_1 = F_{p_n}$$

$$e_1 = \dot{Y}_{h_n}$$

$$e_3 = V_1 - \dot{Y}_{w_n}$$

and

$$K = \left(\frac{\rho A_0}{m_0}\right)_n \left(\frac{c}{c+U}\right)^2$$

Thus substituting these quantities into Equation [C-3] yields

$$F_{p_n} = -m_{0_n}\,\Delta\xi \left\{ \left(\frac{\partial \dot{Y}_h}{\partial t}\right)_n - \left[1 + \left(\frac{\rho A_0}{m_0}\right)_n \left(\frac{c}{c+U}\right)^2\right] \left(\frac{\partial \dot{Y}_w}{\partial t}\right)_n \right\}$$

which agrees with Equation [A-47]. The transformer T is used to inject the force $(F_a)_n - i_2$, which is generated by the current generator, into the circuit shown in Figure C-1. The total hydrodynamic force is then injected into the circuit representing the ship structure in Figure D-1, page 91, shown as the current I. The current generator circuit employed to simulate the force $(F_a)_n$ represented by Equation [A-48] is shown in Figure C-2.

From Figure C-2 we note that

$$e' = -\left(K' e_0 + K_1 e_1 + \ldots . K_7 e_7\right) = -K' e_0 - \sum_{n=1}^{7} K_n e_n \qquad \text{[C-4]}$$

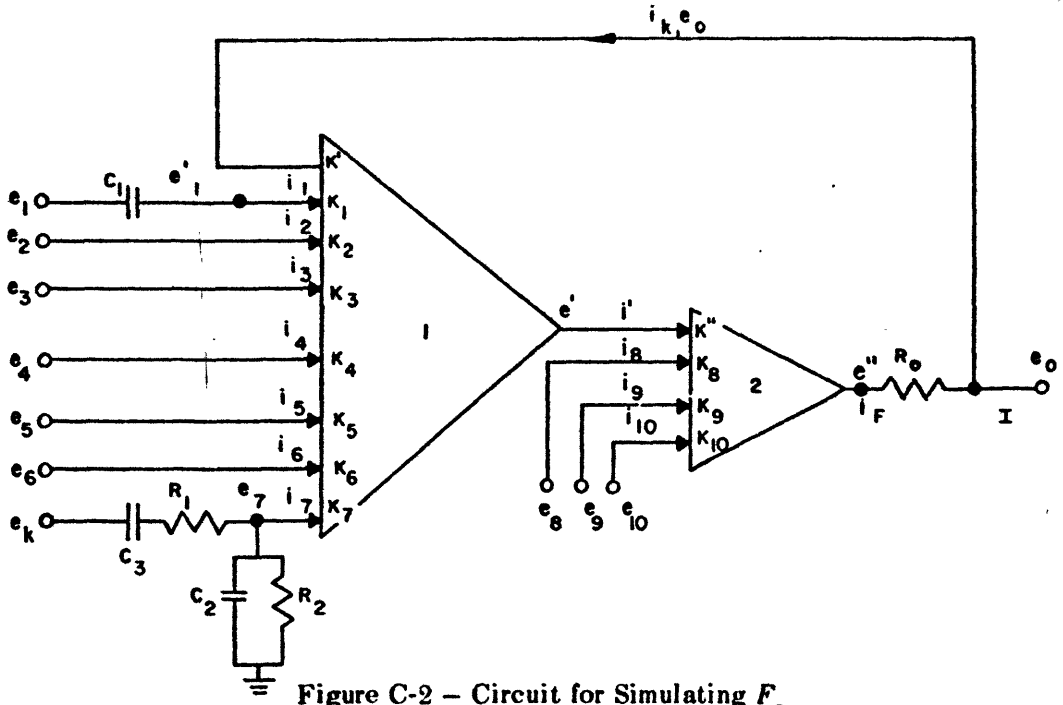

Figure C-2 – Circuit for Simulating F_{a_n}

also that

$$e'' = -K'' e' - \sum_{n=8}^{10} K_n e_n \qquad \text{[C-5]}$$

Substituting Equation [C-4] into Equation [C-5] yields

$$e'' = -K'' \left(-K' e_0 - \sum_{n=1}^{7} K_n e_n \right) - \sum_{n=8}^{10} K_n e_n \qquad \text{[C-6]}$$

but the voltage drop across the resistance R_0 is

$$e'' - e_0 = i_F R_0 \qquad \text{[C-7]}$$

Now substituting Equation [C-6] into [C-7] gives

$$K'' K' e_0 + K'' \sum_{n=1}^{7} K_n e_n - \sum_{n=8}^{10} K_n e_n - e_0 = i_F R_0$$

or

$$(K''K' - 1)\, e_0 + K'' \sum_{n=1}^{7} K_n e_n - \sum_{n=8}^{10} K_n e_n = i_F R_0 \qquad [C\text{-}8]$$

If the gain from the feedback loop K' and the gain K'' are adjusted so that their product is one, we get from Equation [C-8];

$$\frac{K''}{R_0} \sum_{n=1}^{7} K_n e_n - \frac{1}{R_0} \sum_{n=8}^{10} K_n e_n = i_F \qquad [C\text{-}9]$$

which shows that the current through the resistance R_0 is proportional to the sum of the input voltages to the circuit and also independent of the value of the output voltage e_0. The sum of the currents from amplifier 2 in Figure C-2 is

$$i_F = \sum_{n=8}^{10} i_n + i' \qquad [C\text{-}10]$$

since

$$i' \sum_{n=1}^{7} i_n + i_k \qquad [C\text{-}11]$$

Combining Equations [C-10] and [C-11] yields

$$i_F = \sum_{n=1}^{10} i_n + i_k \qquad [C\text{-}12]$$

From Figure C-2, we have

$$i_k = i_F - I \qquad [C\text{-}13]$$

Substituting Equation [C-13] into [C-12] results in

$$i_F = \sum_{n=1}^{10} i_n + i_F - I$$

or

$$I = \sum_{n=1}^{10} i_n \qquad \text{[C-14]}$$

which shows that the sum of the currents into the amplifiers less the feedback current i_k is equal to the output current I of the circuit. Now if the output impedance of the circuit is adjusted so that it is infinite, then $i_k = 0$ and, hence, Equation [C-12] results in

$$i_F = \sum_{n=1}^{10} i_n \qquad \text{[C-15]}$$

and Equation [C-13] becomes

$$I = i_F \qquad \text{[C-16]}$$

Thus Equations [C-9] and [C-16] produce

$$I = \frac{K''}{R_0} \sum_{n=1}^{7} K_n e_n - \frac{1}{R_0} \sum_{n=8}^{10} K_n e_n \qquad \text{[C-17]}$$

Now expansion of Equation [C-17] gives

$$I = \frac{1}{R_0} [K'' \{K_1 e_1' + K_2 e_2 + K_3 e_3 + K_4 e_4 + K_5 e_5 + K_6 e_6 + K_7 e_7\}$$

$$- \{K_8 e_8 + K_9 e_9 + K_{10} e_{10}\}] \qquad \text{[C-18]}$$

Comparing Equation [C-18] with Equation [A-48] shows that

$$e_2 = -\overline{A}_n, \qquad K_2 K'' = \rho g$$

$$e_3 = +(\overline{m}\, V_r)_{n-1}, \qquad K_3 K'' = U/2\,\Delta\xi$$

$$e_4 = +Y_{r_n}, \qquad K_4 K'' = \rho g b_{1_n}$$

$$e_5 = +V_{r_{n-1}}, \qquad K_5 K'' = U(m_0)_{n-1}/2\,\Delta\xi$$

$$e_6 = -\dot{Y}_{r_{n+1}}, \qquad K_6 K'' = m_{0_n}\, U/2\,\Delta\xi$$

$$e_8 = +(\overline{m}\, V_r)_{n+1}, \qquad K_8 = U/2\,\Delta\xi$$

$$e_9 = +V_{r_{n+1}}, \qquad K_9 = U(m_0)_{n+1}/2\,\Delta\xi$$

$$e_{10} = -\dot{Y}_{r_{n-1}}, \qquad K_{10} = m_{0_n}\, U/2\,\Delta\xi$$

$$1/R_0 = \Delta\xi, \qquad I = (F_a)_n$$

Substituting these values in Equation [C-18] results in the following:

$$-(F_a)_n = \Delta\xi \left[-K'' K_1 e_1' + \rho g \overline{A}_n - \frac{U}{2\,\Delta\xi}(\overline{m}\, V_r)_{n-1} - \rho g b_{1_n}\, Y_{r_n} \right.$$

$$- \frac{U}{2\,\Delta\xi}(m_0)_{n-1}\, V_{r_{n-1}} + \frac{U}{2\,\Delta\xi}\, m_{0_n}\, \dot{Y}_{r_{n+1}} - K'' K_7 e_7$$

$$\left. + \frac{U}{2\,\Delta\xi}(\overline{m}\, V_r)_{n+1} + \frac{U}{2\,\Delta\xi}(m_0)_{n+1}\, V_{r_{n+1}} - \frac{U}{2\,\Delta\xi}\, m_{0_n}\, \dot{Y}_{r_{n-1}} \right]$$

or

$$-(F_a)_n = \Delta\xi \left[\frac{m_{0_n}\, U}{2\,\Delta\xi} \left(\dot{Y}_{r_{n+1}} - \dot{Y}_{r_{n-1}} \right) - K'' K_1 e_1' + \frac{U}{2\,\Delta\xi} \left\{ (m_0 + \overline{m})_{n+1}\, V_{r_{n+1}} \right. \right.$$

$$\left. \left. - (m_0 + \overline{m})_{n-1}\, V_{r_{n-1}} \right\} + \rho g \left\{ \overline{A}_n - b_{1_n}\, Y_{r_n} \right\} - K'' K_7 e_7 \right] \qquad \text{[C-19]}$$

The terms $K'' K_1 e_1$ and $K'' K_7 e_7$ will be developed separately. First, consider in more detail the circuit containing the capacitor C_1, as shown in Figure C-3.

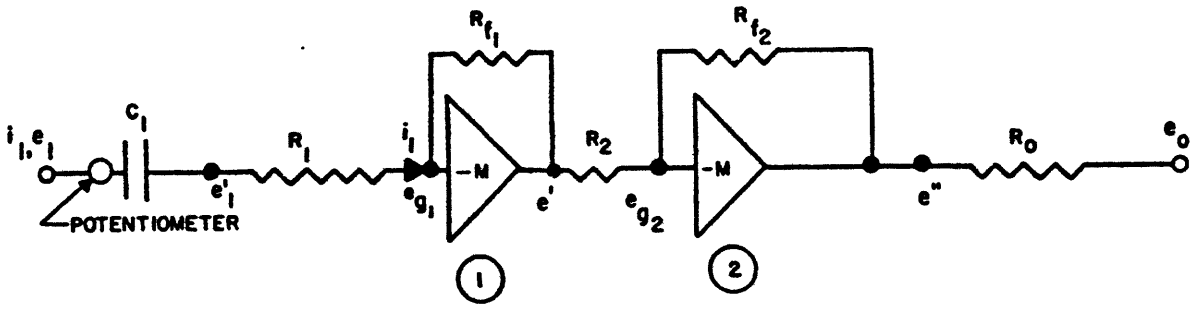

Figure C-3 – Circuit for Simulating the Inertia Force

We may write

$$e_1 - e_1' = \frac{i}{p C_1} \qquad \text{[C-20]}$$

$$e_1' = i R_1 \qquad \text{[C-21]}$$

Eliminating i gives

$$e_1 = e_1' + \frac{e_1}{p R_1 C_1}$$

or

$$e_1 = e_1' \left(1 + \frac{1}{p R_1 C_1}\right) \qquad \text{[C-22]}$$

or solving for e_1 gives

$$e_1' = \left(\frac{p R_1 C_1}{1 + p R_1 C_1}\right) e_1 \qquad \text{[C-23]}$$

however,

$$e' = -i R_{f_1} \qquad \text{[C-24]}$$

Eliminating i from Equation [C-21] gives

$$e_1' = \frac{e'}{R_{f_1}} R_1$$

or

$$e' = -\frac{R_{f_1}}{R_1} e_1' = -K_1 e_1' \qquad \text{[C-25]}$$

Similarly,

$$e'' = -\frac{R_{f_2}}{R_2} e' = -K'' e' \qquad \text{[C-26]}$$

Substituting for e' in Equation [C-26] from [C-25] results in

$$e'' = K'' K_1 e_1' \qquad \text{[C-27]}$$

The substitution of e_1' from Equation [C-23] into Equation [C-27] yields

$$\text{gain} = \frac{e''}{e_1} = K'' K_1 \left(\frac{p R_1 C_1}{1 + p R_1 C_1} \right) \qquad \text{[C-28]}$$

Since

$$i_0 = i = C_1 \frac{\partial e_1}{\partial t} = \frac{1}{R_0} K'' K_1 e_1'$$

set potentiometer such that $C_1 = \frac{1}{R_0}$, then

$$\frac{1}{R_0} \frac{\partial e_1}{\partial t} = \frac{1}{R_0} K'' K_1 e_1'$$

If we set $e_1 = (\bar{m} V_r)$ and $\frac{1}{R_0} = \Delta\xi$, we have

$$-\Delta\xi \frac{\partial}{\partial t} (\bar{m} V_r)_n = -\frac{1}{R_0} K'' K_1 e_1' \qquad \text{[C-29]}$$

which is the second term in Equation [C-19].

Now consider the term $K'' K_7 e_7$ in Equation [C-19]. This term represents the damping coefficient which is related to the hydrodynamic force $\bar{P}_3$ as

$$\bar{P}_3 = -B(p) \bar{V}_r = -K'' K_7 e_7 \Delta\xi \qquad \text{[C-30]}$$

For $p = j\omega$, we get

$$\bar{P}_3 = -B(j\omega) \bar{V}_r = -[C(\omega) + jD(\omega)] \bar{V}_r \qquad \text{[C-31]}$$

from which the real part $C(\omega)$ is used to represent the dampjng coefficient. $B(p)$ is simulated by a function of the form

$$B(p) = \frac{\tau_2 p B_0}{\tau_2 \rho + (1 + \tau_1 p)^2} \qquad \text{[C-32]}$$

where

$$C(\omega) = \frac{B_0 R}{1 + \left(\frac{R\tau_1}{\tau_2}\right)^2 \left(\frac{\omega_0}{\omega} - \frac{\omega}{\omega_0}\right)^2} \qquad \text{[C-33]}$$

where $\frac{\tau_2}{\tau_2 + 2\tau_1} = R$ and $\omega_0 = \frac{1}{\tau_1}$.

This relationship may be shown as follows:

Put $p = j\omega$ into Equation [C-32]. Therefore,

$$B(j\omega) = \frac{j\omega \tau_2 B_0}{j\omega \tau_2 + (1 + \tau_1 j\omega)^2} \qquad [C\text{-}34]$$

or let

$$B(j\omega) = \frac{ja}{c + jb} \qquad [C\text{-}35]$$

where $a = \omega \tau_2 B_0$, $b = \omega (\tau_2 + 2\tau_1)$, and $c = 1 - \tau_1^2 \omega^2$. Multiplying Equation [C-35] by $(c-jb)/(c-jb)$ gives

$$B(j\omega) = \frac{ja(c-jb)}{c^2 + b^2} = \frac{jac + ab}{c^2 + b^2} \qquad [C\text{-}36]$$

Now the real part of Equation [C-36] is $C(\omega)$; thus

$$C(\omega) = \frac{ab}{c^2 + b^2} \qquad [C\text{-}37]$$

or

$$C(\omega) = \frac{\omega^2 \tau_2 B_0 (\tau_2 + 2\tau_1)}{\omega^2(\tau_2 + 2\tau_1)^2 + (1 - \tau_1^2 \omega^2)^2} \qquad [C\text{-}38]$$

or

$$C(\omega) = \frac{B_0 R}{1 + \frac{1}{\omega^2}\left(\frac{1 - \tau_1^2 \omega^2}{\tau_2 + 2\tau_1}\right)^2}$$

or

$$C(\omega) = \frac{B_0 R}{1 + \left(\frac{R\tau_1}{\tau_2}\right)^2 \left(\frac{\omega_0^2 - \omega^2}{\omega_0 \omega}\right)^2} = \frac{B_0 R}{1 + \left(\frac{R\tau_1}{\tau_2}\right)^2 \left(\frac{\omega_0}{\omega} - \frac{\omega}{\omega_0}\right)^2} \qquad [C\text{-}39]$$

The circuit that simulates this function is shown in Figures C-2 and C-4 for convenience.

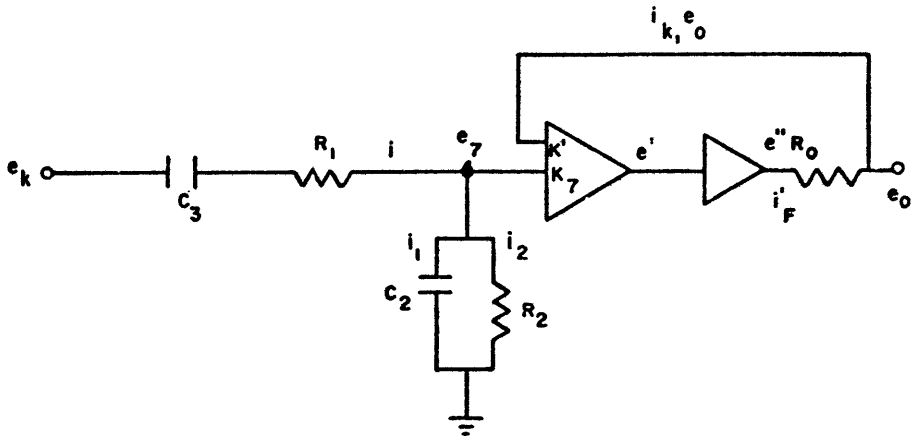

Figure C-4 – Circuit for Simulating the Hydrodynamic Damping Force

From Kirchoff's law, we have

$$i = i_1 + i_2 \qquad \text{[C-40]}$$

and for the voltage drops

$$e_k - e_7 = iR_1 + \frac{1}{C_3}\int idt = iR_1 + \frac{i}{pC_3}$$

$$e_7 = \frac{1}{C_2}\int i_1 dt = i_2 R_2 \qquad \text{[C-41]}$$

or

$$e_7 = \frac{i_1}{pC_2} = i_2 R_2 \qquad \text{[C-42]}$$

Solving for the currents and substituting into Equation [C-40] yields

$$\frac{e_k - e_7}{R_1 + \frac{1}{pC_3}} - pC_2 e_7 + \frac{e_7}{R_2}$$

or

$$e_7 = \frac{e_k}{\left(\frac{1}{R_1 + \frac{1}{pC_3}} + pC_2 + \frac{1}{R_2}\right)\left(R_1 + \frac{1}{pC_3}\right)} \qquad [C\text{-}43]$$

or

$$e_7 = \frac{pC_3R_2e_k}{(pC_3R_1 + 1)(1 + pC_2R_2) + pR_2C_3} \qquad [C\text{-}44]$$

Let

$$C_3R_1 = C_2R_2 = \tau_1 \text{ and } R_2C_3 = \tau_3 \qquad [C\text{-}45]$$

Therefore

$$e_7 = \frac{p\tau_2 e_k}{p\tau_2 + (1 + p\tau_1)^2} \qquad [C\text{-}46]$$

From Figure C-4, we have

$$e' = -K_7 e_7 - K' e_0$$

$$e'' = -e'K''$$

$$e'' - e_0 = i_F' R_0$$

ubstitution of the first two equations into the third equation gives

$$K''K_7 e_7 + K''K' e_0 - e_0 = i_F' R_0$$

r

$$K''K_7 e_7 + (K''K' - 1) e_0 = i_F' R_0 \qquad \text{[C-47]}$$

et

$$K''K' = 1$$

hus Equation [C-47] becomes

$$K''K_7 e_7 = i_F' R_0 \qquad \text{[C-48]}$$

ow substitute Equation [C-46] into [C-48]; thus

$$K''K_7 \frac{pT_2 e_k}{pT_2 + (1 + pT_1)^2} = i_F' R_0$$

r

$$i_F' = \frac{1}{R_0} \frac{B_0 pT_2}{pT_2 + (1 + pT_1)^2} e_k \qquad \text{[C-49]}$$

here $B_0 = K''K'$. If

$$\frac{1}{R} = \Delta\xi$$

$$e_k = \bar{V}_{r_n}$$

nd, from Equation [C-34],

$$B(p) = \frac{B_0 pT_2}{pT_2 + (1 + pT_1)^2}$$

Then upon substitution into Equation [C-49], we get

$$-(i_F)_n = -B(p)\,\bar{V}_{r_n}\,\Delta\xi = \bar{P}_3\,\Delta\xi \qquad \text{[C-50]}$$

which is identical to Equation [A-15] in finite difference equation form.

As a result, with the substitution of Equations [C-29] and [C-50] into Equation [C-19], the complete simulation of the negative of the force represented by Equation [A-48] is obtained. This current $(F_a)_n = i_2$ is then injected into the circuit shown in Figure C-1 by means of a one-to-one transformer with the secondary polarity opposite of the primary polarity. Therefore, the total hydrodynamic force is then in turn inserted into the ship structure as the current I shown in Figure D-1.

Next we will see how Equation [A-46] may be simulated on the analog. Figure C-5 shows the circuitry employed for one station.

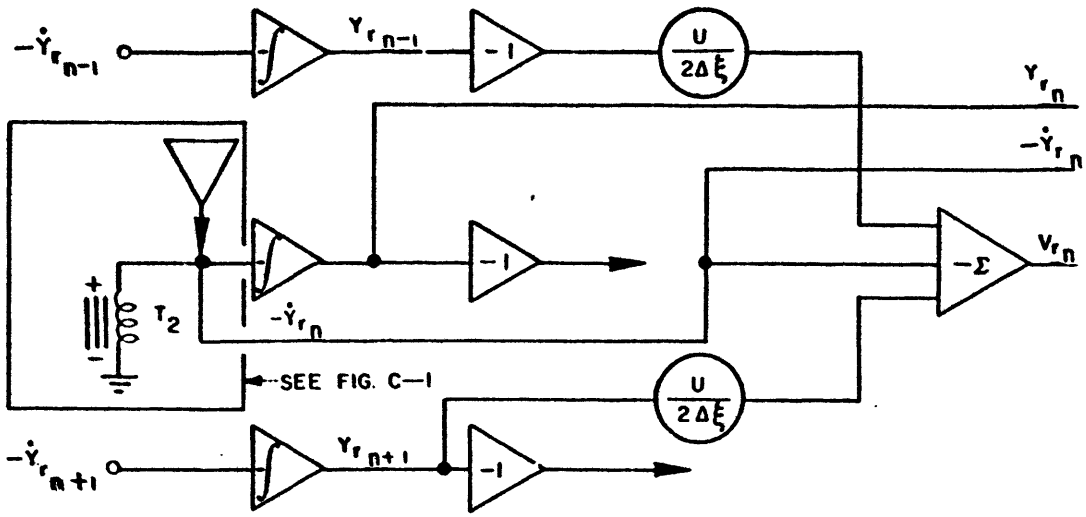

Figure C-5 – Circuit for Simulation of the Relative Velocity V_r

Here the hydrodynamic force $-(F_a)_n$ generated by the circuit shown in Figure C-2 is injected as a current into the circuit of Figure C-1. The voltage e_0 of Figure C-2 is $-\dot{Y}_{r_n}$, which is generated by the circuit of Figure C-1; i.e.,

$$e_1 - e_3 = T_1 = \dot{Y}_{h_n} - \dot{Y}_{w_n} = \dot{Y}_{r_n} \qquad \text{[C-51]}$$

ut

$$T_1 = -T_2 \qquad \text{[C-52]}$$

hus

$$T_2 = -\dot{Y}_{r_n} \qquad \text{[C-53]}$$

The voltage $-\dot{Y}_{r_n}$ is then used as an input to the circuit of Figure C-5. By performing he indicated operations for the three inputs shown in Figure C-5, we get

$$(1) \quad -\frac{U}{2\Delta\xi} \int \dot{Y}_{r_{n-1}}\, dt = -\frac{U}{2\Delta\xi}\, Y_{r_{n-1}}$$

$$(2) \quad -\dot{Y}_{r_n}$$

$$(3) \quad \frac{U}{2\Delta\xi} \int \dot{Y}_{r_{n-1}}\, dt = \frac{U}{2\Delta\xi}\, Y_{r_{n+1}}$$

If we add these three quantities by means of the summing amplifier, we obtain

$$\dot{Y}_{r_n} + \frac{U}{2\Delta\xi}\, Y_{r_{n-1}} - \frac{U}{2\Delta\xi}\, Y_{r_{n+1}} = V_{r_n}$$

or

$$V_{r_n} = \dot{Y}_{r_n} - \frac{U}{2\Delta\xi}\left(Y_{r_{n+1}} - Y_{r_{n-1}}\right) \qquad \text{[C-54]}$$

which agrees with Equation [A-46].

Finally, consider the generation of the inputs to the circuit of Figure C-2. The added mass term $\bar{m}$ and the terms proportional to the buoyancy $\bar{A}$ are the two terms that have not been accounted for. The two inputs are supplied in terms of curves which are approximated by polynomials. For the buoyancy force,

$$\rho g \Delta\xi \bar{A}_n = N(Y_r + b)^2 \qquad \text{[C-55]}$$

Thus,

$$\bar{A}_n = \frac{N}{\rho g \Delta \xi} \cdot \left(Y_{r_n} + b \right)^2 \qquad \text{[C-56]}$$

As an example, consider Station 17 on ESSEX. Here $b = 0$ and $N = \frac{1.103}{\rho g \Delta \xi}$; as a result, Equation [C-56] becomes

$$\bar{A}_{17} = \frac{1.103}{\rho g \Delta \xi} Y_{r_{17}}^2 \qquad \text{[C-57]}$$

The circuit for simulating $\bar{A}_{17}$ is shown in the upper portion of Figure C-6. The boxes in Figure C-6 represent multipliers. A consideration of the circuit shows that the output voltage e_{o_1} is equal to

$$e_{o_1} = -K e_{i_1}^2 \qquad \text{[C-58]}$$

where e_{i_1} is assumed to be positive; i.e., $e_{i_1} > 0$. Then, comparison with Equation [C-57] shows

$$K \equiv 1.103/\rho g \Delta \xi \qquad \text{[C-59]}$$

$$e_{i_1} = Y_{r_{17}} \qquad \text{[C-60]}$$

Hence

$$e_{o_1} = -\frac{1.103}{\rho g \Delta \xi} Y_{r_{17}}^2 = -\bar{A}_{17} \qquad \text{[C-61]}$$

which is one of the inputs used in the circuit of Figure C-2.

Now consider the generation of the term $\bar{m} V_{r_{17}}$. The circuit employed to obtain $\bar{m} V_{r_{17}}$ is shown in the lower portion of Figure C-6. The momentum term for Station 17 is determined as an example. As previously stated, a polynomial is used to approximate the added mass term. Since the added mass is different for the emergent and immergent phases of the ship's motion, we have basically two different polynomials that must be simulated by the analog. Depending upon whether $Y_r > 0$ or $Y_r < 0$, the added mass term is further broken up into two additional segments for analog simulation. The governing polynomials are listed for Station 17:

For $Y_{r_{17}} < 0$ and $V_{r_{17}} > 0$,

$$V_{r_{17}} (m_1 \Delta\xi)_{17} = \left(-1.08\, Y_{r_{17}} + 0.1286\, Y_{r_{17}}^2\right)\ V_{r_{17}} \qquad \text{[C-62]}$$

For $Y_{r_{17}} > 0$ and $V_{r_{17}} > 0$,

$$V_{r_{17}} (m_1 \Delta\xi)_{17} = \left(-1.08\, Y_{r_{17}}\right)\ V_{r_{17}} \qquad \text{[C-63]}$$

For $Y_{r_{17}} < 0$ and $V_{r_{17}} < 0$,

$$V_{r_{17}} (m_2 \Delta\xi)_{17} = \left(-1.08\, Y_{r_{17}} + 0.2330\, Y_{r_{17}}^2\right)\ V_{r_{17}} \qquad \text{[C-64]}$$

For $Y_{r_{17}} > 0$ and $V_{r_{17}} < 0$,

$$V_{r_{17}} (m_2 \Delta\xi)_{17} = \left(-1.08\, Y_{r_{17}}\right)\ V_{r_{17}} \qquad \text{[C-65]}$$

Now again consider Figure C-6 and assume that the input voltages $e_{i_1} < 0$ and $e_{i_2} > 0$. Thus, Diodes 1 and 2 conduct while Diode 3 does not conduct.* Hence, the output of summers 1 and 2 are, respectively,

$$e_1'' = K_2 \left(e_{i_1}\right)^2 - K_1\, e_{i_1} \qquad \text{[C-66]}$$

$$e_2'' = K_4 \left(e_{i_1}\right)^2 - K_3\, e_{i_1} \qquad \text{[C-67]}$$

The output voltages of multipliers M_3 and M_4 are, respectively,

$$e_1' = e_1''\, e_{i_2} \qquad \text{[C-68]}$$

$$e_2' = 0 \qquad \text{[C-69]}$$

*Diode has the property of permitting an appreciable current flow in only one direction.

When Equation [C-66] is substituted into [C-68], the result is

$$e_1' = e_{i_2} \left[K_2 \left(e_{i_1} \right)^2 - K_1 \, e_{i_1} \right] \qquad \text{[C-70]}$$

The output e_{0_2} is related to e_1' by

$$e_{0_2} = \frac{R_f}{R_4} \, e_1' \qquad \text{[C-71]}$$

Substitution of Equation [C-70] into [C-71] yields

$$e_{0_2} = \frac{R_f}{R_4} \left(e_{i_2} \right) \left[K_2 \left(e_{i_1} \right)^2 - K_1 \, e_{i_1} \right] \qquad \text{[C-72]}$$

But from Equation [C-60],

$$e_{0_2} = \frac{R_f}{R_4} \left(e_{i_2} \right) \left[K_2 \left(Y_{r_{17}} \right)^2 - K_1 \, Y_{r_{17}} \right] \qquad \text{[C-73]}$$

therefore

$$e_{0_2} = \left[\frac{R_f}{R_4} \, K_2 \left(Y_{r_{17}} \right)^2 - \frac{R_f}{R_4} \, K_1 \, Y_{r_{17}} \right] e_{i_2} \qquad \text{[C-74]}$$

Comparison with Equation [C-62] shows that

$$\frac{R_f}{R_4} \, K_2 \equiv \frac{0.1286}{\Delta \xi} \qquad \text{[C-75]}$$

$$\frac{R_f}{R_4} \, K_1 = \frac{1.08}{\Delta \xi} \qquad \text{[C-76]}$$

and

$$e_{i_2} \equiv V_{r_{17}}$$

where

$$R_f/R_4 = 1/\Delta\xi \qquad \text{[C-77]}$$

$$e_{0_2} = \frac{1}{\Delta\xi}\left(1.08\,Y_{r_{17}} + 0.1286\,Y_{r_{17}}^2\right) V_{r_{17}} = (m_1 V_r)_{17} \qquad \text{[C-78]}$$

Now for

$$e_{i_1} \equiv Y_{r_{17}} > 0 \qquad \text{[C-79]}$$

$$e_{i_2} \equiv V_r > 0 \qquad \text{[C-80]}$$

Then Diodes 1 and 3 do not conduct but Diode 2 does, and we may write

$$e_1'' = -K_1\, e_{i_1} \qquad \text{[C-81]}$$

$$e_2'' = -K_3\, e_{i_1} \qquad \text{[C-82]}$$

and

$$e_1' = e_1''\, e_{i_2} \qquad \text{[C-83]}$$

$$e_2' = e_2''\, e_{i_1} = 0 \qquad \text{[C-84]}$$

Consequently,

$$e_1' = -e_{i_2}\, K_1\, e_{i_1} \qquad \text{[C-85]}$$

Now

$$e_{0_2} = \frac{R_f}{R_4}\, e_1' \qquad \text{[C-86]}$$

Substituting Equation [C-85] into [C-86] results in

$$e_{o_2} = -\frac{R_f}{R_4}\, e_{i_2}\, K_1\, e_{i_1} \qquad \text{[C-87]}$$

or, as previously determined from Equations [C-76] and [C-78],

$$e_{o_2} = -\frac{R_f}{R_4}\, K_1\, Y_{r_{17}}\, V_{r_{17}} = -1.08\, Y_{r_{17}}\, V_{r_{17}}\, \frac{1}{\Delta\xi} \qquad \text{[C-88]}$$

or

$$(m_1 V_r)_{17} = -1.08\, Y_{r_{17}}\, V_{r_{17}}\, \frac{1}{\Delta\xi} \qquad \text{[C-89]}$$

which agrees with Equation [C-63].

To establish the remaining equations for this station and those for other stations, continue in a similar fashion.

Thus we have derived the necessary inputs and have shown how they may be simulated via analog computer for the force generator black box.

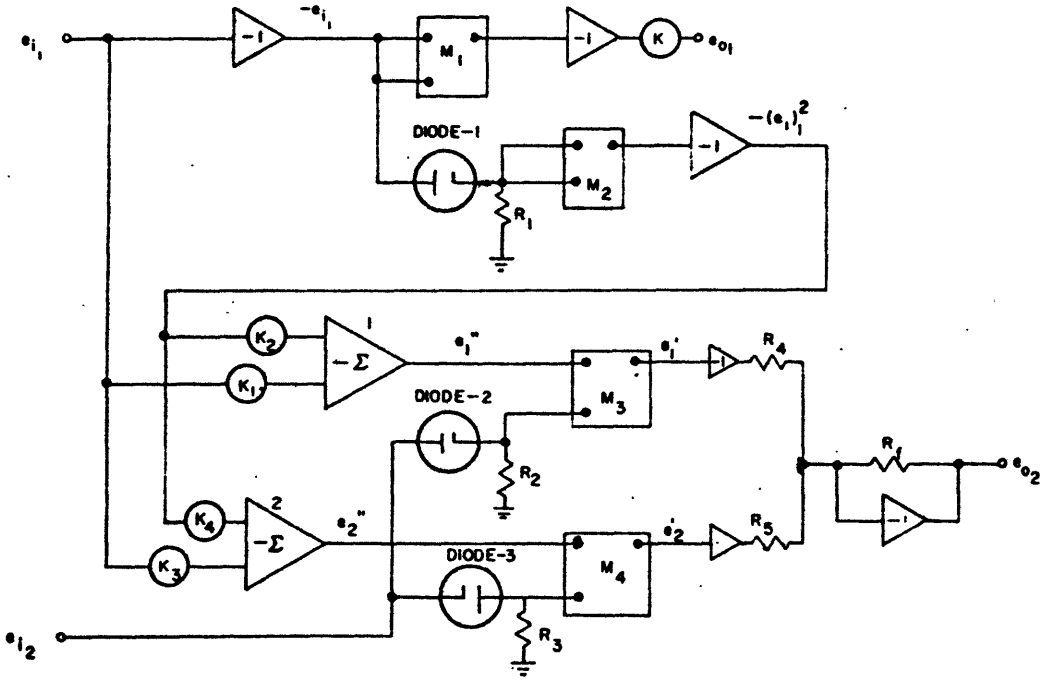

Figure C-6 – Generation of $\bar{A}$ and $\bar{m}\, V_r$

APPENDIX D

SIMULATION OF SHIP PARAMETERS AND SHIP RESPONSE

The equations employed in the simulation of the ship structure are

$$\frac{\partial \dot{Y}_h}{\partial \xi} + \frac{1}{\text{KAG}} \frac{\partial V}{\partial t} - \dot{\gamma} = 0 \qquad \text{[D-1]}$$

$$\frac{\partial M}{\partial \xi} - I_\mu \frac{\partial \dot{\gamma}}{\partial t} - V = 0 \qquad \text{[D-2]}$$

$$\frac{\partial M}{\partial t} - EI \frac{\partial \dot{\gamma}}{\partial \xi} = 0 \qquad \text{[D-3]}$$

and the equation of motion is

$$m \frac{\partial^2 Y_h}{\partial t^2} + C \frac{\partial Y_h}{\partial t} + \frac{\partial V}{\partial \xi} = P = P_a + P_p \qquad \text{[D-4]}$$

The symbols in these equations are defined as

Y_h	Vertical displacement of the ship measured from the still waterline (Including elastic and rigid body motion of ship)[3]
KAG	Shear rigidity
V	Shear force
γ	Angle through which a ship section is rotated about a transverse axis
M	Bending moment
I_μ	Mass moment of inertia about a transverse axis
EI	Bending rigidity
m	Ship mass per unit length
C	Structural damping coefficient
P	Force per unit length

Equations [A-46] through [A-48] and [D-1] through [D-4] are now put into difference forms as follows:

$$(F_p)_n = -m_{0_n} \Delta\xi \left[\left(\frac{\partial \dot{Y}_h}{\partial t}\right)_n - \left\{1 + \left(\frac{\rho A_0}{m_0}\right)_n \left(\frac{c}{c+U}\right)^2\right\} \left(\frac{\partial \dot{Y}_w}{\partial t}\right)_n\right] \quad \text{[D-5]}$$

$$(F_a)_n = \Delta\xi \left[\frac{m_{0_n} U}{2\Delta\xi} \left(\dot{Y}_{r_{n+1}} - \dot{Y}_{r_{n-1}}\right) - \frac{\partial}{\partial t} (\bar{m} V_r)_n\right.$$

$$+ \frac{U}{2\Delta\xi} \left\{(m_0 + \bar{m})_{n+1} V_{r_{n+1}} - (m_0 + \bar{m})_{n-1} V_{r_{n-1}}\right\}$$

$$\left. + \rho g \left\{-b_{1_n} Y_{r_n} + \bar{A}_n\right\} - B_{n_{(p)}} \bar{V}_{r_n}\right] \quad \text{[D-6]}$$

$$V_{r_n} = \dot{Y}_{r_n} - U\left[\frac{Y_{r_{n+1}} - Y_{r_{n-1}}}{2\Delta\xi}\right] \quad \text{[D-7]}$$

$$\dot{Y}_{h_{n+1}} - \dot{Y}_{h_{n-1}} + \left(\frac{\Delta\xi}{KAG}\right)_n \left(\frac{dV}{dt}\right)_n - \Delta\xi\, \dot{\gamma}_n = 0 \quad \text{[D-8]}$$

$$(M_{n+1/2} - M_{n-1/2}) - (I_\mu \Delta\xi)_n \left(\frac{d\dot{\gamma}}{dt}\right)_n - \Delta\xi\, V_n = 0 \quad \text{[D-9]}$$

$$\left(\frac{\Delta\xi}{EI}\right)_{n+1/2} \left(\frac{dM}{dt}\right)_{n+1/2} - (\dot{\gamma}_{n+1} - \dot{\gamma}) = 0 \quad \text{[D-10]}$$

$$(m\Delta\xi)_{n+1/2} \left(\frac{d\dot{Y}_h}{dt}\right)_{n+1/2} + (c\Delta\xi)_{n+1/2} (\dot{Y}_h)_{n+1/2} + (V_{n+1} - V_n)$$

$$= \Delta\xi P_{n+1/2} = F_{n+1/2} = (F_\rho)_{n+1/2} + (F_a)_{n+1/2} \quad \text{[D-11]}$$

These foregoing equations are to be simulated on the analog computer.

To accomplish the simulation, a circuit for the ship structure, such as is shown in Figure D-1, is devised to represent electrically the mathematical relations expressed by Equations [D-8] through [D-11]. (The ship structure is divided into 20 equally spaced sections, and the hydrodynamic forces are represented by 9 segments with forces applied at 14 positions along the ship length. Figure D-1 shows the circuit for representing a single segment of the ship structure.)

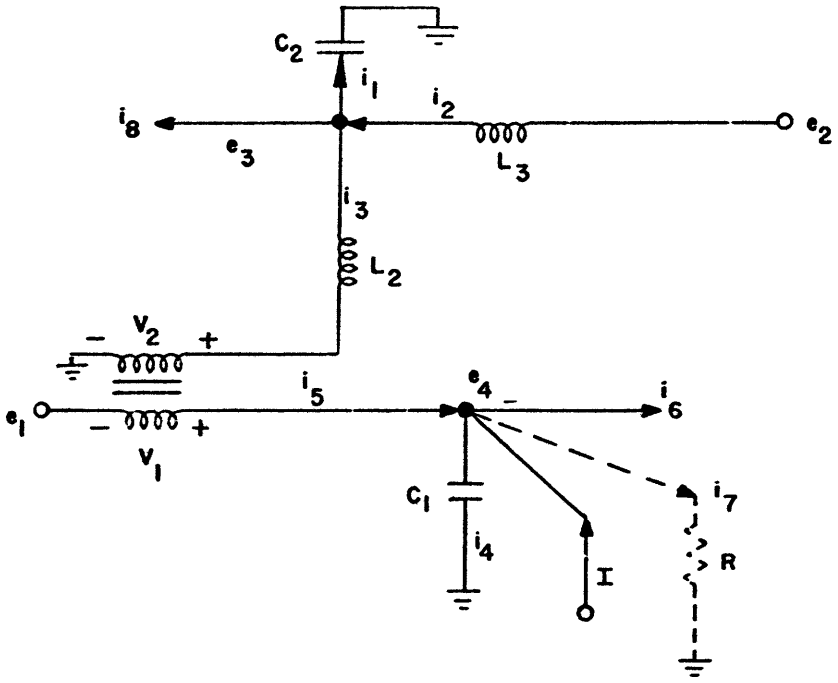

Figure D-1 – Circuit Representing Ship Structure

The lower portion of the circuit, shows that

$$i_5 + I = i_4 + i_6 + i_7 \qquad \text{[D-12]}$$

Since

$$i_4 = C_1 \dot{e}_4$$

Equation [D-12] may be rewritten as

$$C_1 \dot{e}_4 + i_7 + i_6 - i_5 = I \qquad \text{[D-13]}$$

Using the relation

$$i_7 = \frac{e_4}{R}$$

and substituting into Equation [D-13] yields a useful expression for I,

$$C_1 \dot{e}_4 + \frac{e_4}{R} + i_6 - i_5 = I \qquad \text{[D-14]}$$

A comparison of Equation [D-14] with Equation [D-11] shows that they have the same form; in fact, when

$$C_1 = (m\Delta\xi)_{n+1/2}$$

$$e_4 = \dot{Y}_{h_{n+1/2}}$$

$$\frac{1}{R} = (c\Delta\xi)_{n+1/2}$$

$$i_6 = V_{n+1}$$

$$i_5 = V_n$$

and

$$I = F_{n+1/2}$$

and then substituting into Equation [D-14], we obtain

$$(m\Delta\xi)_{n+1/2} \left(\frac{d\dot{Y}_h}{dt}\right)_{n+1/2} + (c\Delta\xi)_{n+1/2} \dot{Y}_{h_{n+1/2}} + V_{n+1} - V_n = F_{n+1/2}$$

which agrees with Equation [D-11]. The resistor in Figure D-1 is dashed in because in reality it is not used for the reason that the inherent resistance in the circuitry itself is used to simulate the structural damping.

Now consider the upper portion of the circuit in Figure D-1. For the sum of the currents at the node, we have

$$i_2 = i_1 + i_3 + i_8 \qquad \text{[D-15]}$$

but

$$i_1 = C_2 \dot{e}_3 \qquad \text{[D-16]}$$

so that substituting Equation [D-16] into [D-15] gives

$$i_2 = C_2 \dot{e}_3 + i_3 + i_8 \qquad \text{[D-17]}$$

However, the current i_3 in the primary of the transformer is equal to V_n; hence, the current in the secondary i_3 is related to that of the primary through the turns ratio of the transformer. Thus we get

$$i_3 = K i_5 = K V_n \qquad \text{[D-18]}$$

When Equation [D-18] is substituted into [D-17] and rearranged

$$(i_2 - i_8) - C_2 \dot{e}_3 - K V_n = 0 \qquad \text{[D-19]}$$

A comparison of Equation [D-19] with [D-9] shows that they are of the same form. Hence, if

$$i_2 = M_{n+1/2}$$

$$i_8 = M_{n+1/2}$$

$$C_2 = (I_\mu \Delta\xi)_n$$

$$e_3 = \dot{\gamma}_n$$

$$K = \Delta\xi$$

we have

$$(M_{n+1/2} - M_{n+1/2}) - (I_\mu \Delta\xi)_n \frac{d\dot{\gamma}_n}{dt} - \Delta\xi V_n = 0$$

which agrees with Equation [D-9].

Next consider the voltage drop across inductor L_3. Thus

$$e_3 - e_2 = -L_3 \frac{di_2}{dt} \qquad \text{[D-20]}$$

or

$$L_3 \frac{di_2}{dt} - (e_2 - e_3) = 0 \qquad \text{[D-21]}$$

A comparison with Equation [D-10] shows that

$$L_3 = \left(\frac{\Delta\xi}{EI}\right)_{n+1/2}$$

$$i_2 = M_{n+1/2}$$

$$e_3 = \dot{\gamma}_n$$

$$e_2 = \dot{\gamma}_{n+1}$$

Therefore

$$\left(\frac{\Delta\xi}{EI}\right)_{n+1/2} \left(\frac{dM_{n+1/2}}{dt}\right) - (\dot{\gamma}_{n+1} - \dot{\gamma}_n) = 0$$

which agrees with Equation [D-10].

Finally, consider the voltage drop across the primary of the transformer and inductor L_2. Thus

$$e_3 = L_2 \frac{di_3}{dt} + V_2 \qquad \text{[D-22]}$$

but

$$e_1 - e_4 = -V_1 = -K\bar{V}_2 \qquad \text{[D-23]}$$

Now substituting Equation [D-23] into [D-22] and rearranging gives

$$e_4 - e_1 + L_2 K \frac{di_3}{dt} - K e_3 = 0 \qquad \text{[D-24]}$$

or, from previous considerations and $e_1 = \dot{Y}_{h_{n-1/2}}$,

$$\dot{Y}_{h_{n+1/2}} - \dot{Y}_{h_{n-1/2}} + L_2 \overline{\Delta\xi}^2 \left(\frac{dV}{dt}\right)_n - \Delta\xi \dot{\gamma}_n = 0$$

As a result, if

$$L_2 = \left(\frac{1}{\Delta\xi \, \mathrm{KAG}}\right)_n$$

we get

$$\dot{Y}_{h_{n+1/2}} - \dot{Y}_{h_{n-1/2}} + \left(\frac{\Delta\xi}{\mathrm{KAG}}\right)_n \left(\frac{dV}{dt}\right)_n - \Delta\xi \dot{\gamma}_n = 0 \qquad \text{[D-25]}$$

which agrees with Equation [D-8].

Thus Equations [D-8] through [D-10] are the equations which simulate the elastic ship structure.

APPENDIX E

SIMULATION OF SEAWAY

There now remains to show how the wave generator is used to simulate the sea. This will give us the final input into the force generator. This input is the vertical velocity of the waves $\dot{Y}_w$ shown in Figure C-1. Essentially three types of seas may be simulated on an analog computer. These are sinusoidal, random, and discrete seas: see Figure E-1.

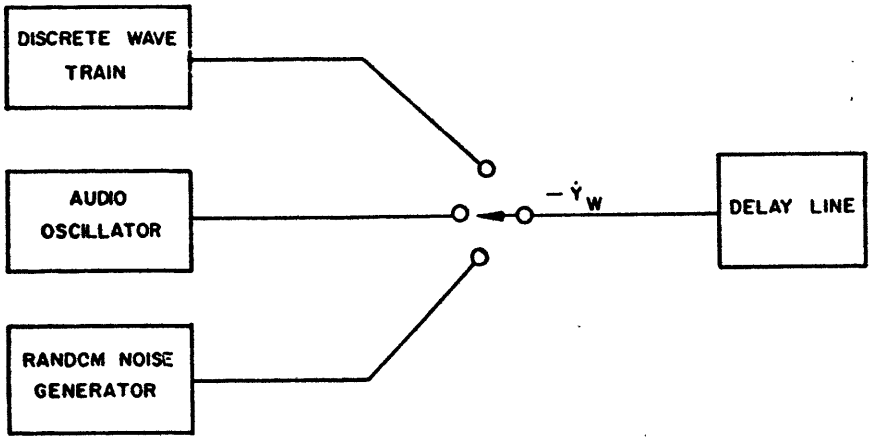

Figure E-1 – Wave Generator Detail

The delay line is employed so that when a particular wave velocity is applied to a station on the ship, this same velocity will appear sometime later at another station, depending upon ship and wave speed. Thus the time delay depends upon the relative velocity V_h of ship and sea wave in the horizontal direction. Therefore,

$$V_h = c + U \cos \chi \qquad \text{[E-1]}$$

where χ is the angle between ship heading and wave propagation. For head seas $\chi = 0$,

$$V_h = c + U \qquad \text{[E-2]}$$

Consequently, the time for the same crest to reach another position or station on the ship depends upon the distance between stations; i.e.,

$$T_d = \frac{\Delta\xi}{V_h} = \frac{\Delta\xi}{c+U} \qquad \text{[E-3]}$$

The circuit employed to simulate the time delay is shown in Figure E-2. This circuit serves to transmit a wave signal without attenuation but with a phase shift $\phi = 2\pi f T_d$, where T_d is the delay time of the line and f is the wave frequency.

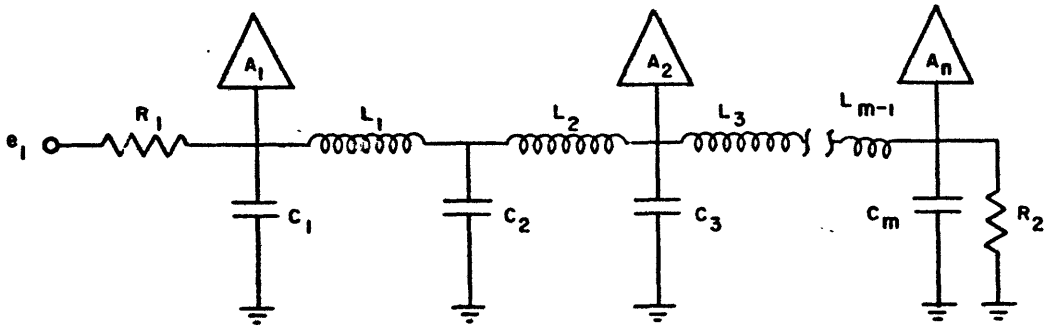

Figure E-2 – Time-Delay Line

The time delay per section is from Figure E-2,

$$T_d = \sqrt{LC} = \frac{\Delta\xi}{c+U} \qquad \text{[E-4]}$$

where

$$L = \frac{\Delta\xi}{c+U} \quad R \qquad \text{[E-5]}$$

and

$$C = \frac{\Delta\xi}{c+U} \quad \frac{1}{R} \qquad \text{[E-6]}$$

The resistors in the circuit are employed so that any reflections due to the inductors are attenuated. The value of the resistors is from Equations [E-5] and [E-6]:

$$\frac{L}{C} = R^2$$

or

$$R = \sqrt{\frac{L}{C}} \qquad \text{[E-7]}$$

Thus the input signal Y_w applied to the delay line will be transmitted along the line in a manner similar to that of the simulated wave.

An oscillator, which generates a sinusoidal function with the proper frequency and magnitude, is employed to generate sinusoidal waves.

The generation of a discrete (time history) wave train is accomplished by the use of a photoformer. A mask of the wave train is prepared and a photosensitive transducer is used to generate a voltage signal by tracing the form on the mask.

A noise generator, which produces a voltage signal with a constant power spectral density, is employed to generate random seas. The required power spectrum is obtained by connecting the noise generator to an electrical filter. Then the power spectral density of the output of the filter is related to that of the input by

$$\Phi_0(\omega) = |A(p)|^2 \, \Phi_i(\omega) \qquad \text{[E-8]}$$

where $|A(p)|^2$ is the absolute value of the filter transfer function and $p = j\omega$. The peak response of the filter occurs near $\omega = \frac{1}{\sqrt{LC}}$, and the bandwidth between half-power points is $\omega = R\sqrt{\frac{C}{L}}$. The input spectral density is constant; hence, the design of the filter is given by

$$A(p)|^2 = K \sqrt{\Phi_0(\omega)} \qquad \text{[E-9]}$$

Now the analog simulation of the ship response to an arbitrary sea condition is complete. Thus, for a definite sea condition, we may obtain the bending moment the ship encounters and, hence, the section modulus for design purposes. The specific advantage in analog computation is that a ship may be designed first on paper and then, before its construction, simulated on the analog to determine its response either statistically or deterministically. The analog described herein will give only the information on the main hull-girder flexures and ship motions.

REFERENCES

1. Jasper, N.H. and Birmingham, J.T., "Strains and Motions of USS ESSEX (CVA 9) during Storms near Cape Horn," David Taylor Model Basin Report 1216 (Aug 1958).

2. Andrews, J.N., "A Method for Computing the Response of a Ship to a Transient Force," David Taylor Model Basin Report 1544 (Nov 1963).

3. MacNeal, R.H., "Analog Computer Analysis of the Bow Slamming Problem for the USS ESSEX," Computer Engineering Associates Report on Project ESD172 (Jan 1961).

4. Jasper, N.H., et al., "Response to Wave Loads," David Taylor Model Basin Report 1537 (Jun 1961).

5. Schwendler, R.G., "Improved Analog Computer Analysis of the Bow Slamming Problem," Computer Engineering Associates Report on Project ES178 (Apr 1962).

6. Jasper, N.H. and Church, J.W., "Structural Seaworthiness Studies," Transactions, Society of Naval Architects and Marine Engineers, Vol. 71 (1963).

7. Rayleigh, L., "Theory of Sound," Dover Publications, New York, Vol. I, pp. 256 and 257, Equations (1) and (2) (1945).

8. Lewis, E.V., "Ship Speeds in Irregular Seas," Transactions, Society of Naval Architects and Marine Engineers, Vol. 63 (1955).

9. Lewis, E.V., "Increasing the Sea Speed of Merchant Ships," Davidson Laboratory Report 744 (Apr 1959).

10. "Simulation of the Sea and Analog Computation of the Forces on a Ship in Waves," Reed Research, Inc., Project RR-1458-N (Nov 1959).

11. Lamb, H., "Hydrodynamics," Sixth Edition, Dover Publications, New York, (1932), p. 168.

12. Golovato, P., "A Study of the Transient Pitching Oscillations of a Ship," Journal of Ship Research, Vol. 2, No. 4 (Mar 1959).

13. Michell, J.H., "On the Highest Waves in Water," Philosophical Magazine, Vol. 36 (1893), p. 430.